博　士　論　文

A Physical-layer Investigation on Concurrent Transmission for Wireless Networks

(同時送信型無線ネットワークの物理層に関する研究)

平成 29 年 6 月 1 日

指導教員　　森川 博之 教授

東京大学大学院工学系研究科
電気系工学専攻

37-147260

廖 椿豪
リャウ シュンハウ
Chun-Hao Liao

Abstract

Multi-hop networks are expected to play an important role in the upcoming Internet-of-Thing (IoT) era. Concurrent transmission (CT) is a revolutionary multi-hop protocol that significantly improves the MAC- and network-layer efficiency by allowing synchronized packet collisions. Although its superiority has been empirically verified, there is still a lack of comprehensive physical-layer investigation on how the receiver survives such packet collisions, particularly in the presence of the carrier frequency offsets (CFO) between the transmitters. In this work, we undertake this task. The main contributions are threefold.

Analyses of the CT characteristics: By utilizing the similarity between the CT and the wireless multi-path fading channel, we present an equivalent channel model of the one-hop behavior of CT. Next, we provide actual measurement numbers to show that the CFO is the dominating factor in the CT channel, and the *beating* effect resulting from the CFO affects the receiver performance significantly. In view of the importance of the beating signal, we further theoretically derive the closed form of the average fading duration (AFD) of the beating in terms of the transmitter number and the standard deviation of the CFO, and prove that the derived AFD is an effective indicator to quantify the receiver performance degradation resulting from the beating. Our derivation theoretically shows that the AFD can be reduced by increasing the deviations of CFO and the number of transmitters that joins the CT. Finally, we estimate the AFD in real systems by measuring the CFO of a large amount sensor nodes.

Evaluations of CT on IoT standards: We evaluate the results for IEEE 802.15.4, IEEE 802.15.4g, and a recently popular low-power-wide-are (LPWA) standard - the LoRa system. We distinguish our evaluation from the previous ones by the extensive CT effect modeling, discerning metrics, and accurate and reproducible evaluation platform. The main findings from our evaluations are as follows. For the IEEE 802.15.4 system, we show that the adopted direct

sequence spread spectrum (DSSS) scheme plays the key role in combating the beating effect. However, due to the limited length of DSSS, the receiver still suffers from the beating if the fading duration is too long. On the other hand, we also show that the basic M-ary FSK mode of IEEE 802.15.4g is vulnerable to CT due to the lack of error correcting mechanism. We also prove that is a proper error correcting mechanism is implemented, CT can still be applied to the IEEE 802.15.4g system. For the LoRa system, we find that, due to the time-domain and frequency-domain energy spreading effect, LoRa is robust to the packet collisions resulting from CT. We further show that the receiver performance under CT can be further improved by introducing timing offsets between the relaying packets.

Proposal of novel CT-enabled applications: The third contribution is the proposal of two novel CT-enabled applications using the insight obtained from the theoretical analysis and comprehensive evaluations. The first proposal is the multiple-building-area networks (MBAN), which is a wireless network consisting of only indoor low-power devices while providing a wide coverage over several buildings. In view of that the 2.4 GHz multi-hop networks suffer from the weak penetration power, we strive to construct a CT-based sub-GHz LoRa network (CT-LoRa). Thanks to the analyses and evaluations in the previous chapters, we have learned that introducing timing offsets can improve the reliability of LoRa receiver under CT. Toward this, we propose a timing delay insertion method, the offset-CT method, that adds random timing delay before the packets while preventing the timing offset from diverging over the multi-hop network. Moreover, we conduct proof-of-concept experiments to demonstrate the feasibility of CT-LoRa. Secondly, we propose to apply CT to the distributed antenna system (DAS). Specifically, in the conventional DAS, sophisticated cooperations are adopted to prevent fading. However, such cooperation also significantly restrict the real-time capability. On the other hand, CT can realize real-time DAS but with the risk of introducing fading. Since we have learned that the fading duration can be improved by having more antennas and higher CFO deviation, we proposed to adopt the CT in the DAS system with massive antenna as well as large random frequency offset to guarantee both real-time capability and reliability.

Contents

List of Figures

List of Tables

Chapter 1

Introduction

This chapter provides an overview of this thesis. We will first sequentially discuss the research background, subject, and goal. Next, the main contributions of this thesis will be highlighted. Finally, the structure of this thesis will be elaborated in the end of this chapter.

1.1 Research background

We are marching toward the new era of the Internet of Things (IoT) - the world that everything is smartly connected and coordinated with each other to better sever human beings. The concept of IoT was first proposed in 1995 by Bill Gates in his famous book "The Road Ahead" [1], where he depicted a future where networks are ubiquitously available and could be accessed *anytime*, *anywhere*, by *anyone* and *anything* (4A). He also envisioned the network would be evolving from the current *Human-to-Human (H2H)* oriented (where the service over the internet is passively demanded by human beings and mainly for the purpose of text, audio, and video,) to Human-to-Machine (H2M) based, (where all the things are connected, accessed and controlled by human beings through internet,) and finally to *Machine-to-Machine (M2M)* based. In the IoT era, things can ubiquitously sense the physical world, the sensed data are then delivered by robust networks for processing and analysis over the cloud, and finally, things can promptly and spontaneously respond, as if they have the intelligence to feel, talk, think, and react. The blooming of IoT is expected to significantly improve our life quality in an all-round manner, and the potential IoT applications cover broadly from home living, energy management, health care, transportation, to even agriculture.

The importance of IoT has raised great attentions from all over the world. Many countries have proposed their nation-level projects for IoT. To give specific examples, as early as the year of 2009, Japanese government proposed the u-Japan project [2], and the EU kicked off the action plan on IoT [3]. Moreover, the IoT is also identified as the killer applications for the next generation cellular mobile system (5G) [4, 5]. The Ericsson forecast report predicts that there will be more than 18 billion of devices connected to IoT by the year of 2021 [6] and Cisco also predicts that IoT can generate more than 19 trillion US dollars of value globally by connecting the unconnected devices via IoT [7]. It is also predicted that the M2M-type communications will overwhelm the H2H-type ones by the order of 10 to 100 times in the near future.

However, the emerging IoT applications impose brand new challenges for the current wireless networks. While the main focus of the current wireless networks is to accommodate H2H devices with higher throughput rate, IoT requires a *long-life* and *ubiquitous* wireless network that can accommodate tremendous M2M devices with typical lighter and less frequent traffic. Particularly, although the single-hop star topology that the current wireless networks (e.g. LTE or WiFi [8]) mostly adopts can indeed provide a more efficient spectrum usage, it is not the optimal design from the long-life and ubiquitous point of view. In the single-hop star topology, all the devices are directly connected and to central base stations, and hence the coverage is determined by the density of the base stations and the one-hop communication ranges. Therefore, in order to achieve ubiquitously available networks, it is either the base stations that needs to be densely deployed or the transmission power that needs to be greatly enhanced. Moreover, the single-hop star topology are not able to provide satisfactory coverage in many indoor scenarios since the devices might be deployed in highly shielded locations such as the basement.

On the other hand, a multi-hop mesh topology, where the devices could autonomously help to relay the packets to the destiny, is a more suitable solution for constructing a wide-covering and low-power network. Specifically, the coverage can be very easily extended to even highly shielded locations by simply deploying more low-cost terminal devices. Moreover, the transmission power of each device can also be reduced since the required communication range is much shorter. To this end, many IoT-oriented solutions adopt the multi-hop mesh topologies, such as ZigBee [9], SmartMesh developed by the Linear Technology [10], and Thread [11] by over 50 companies including Google.

In view of the great potentiality for the multi-hop mesh network to play a key role in the upcoming IoT era, in this thesis, we present a series of studies on the multi-hop mesh protocols. Specifically, our main focus is a revolutionary multi-hop protocol named *concurrent transmission* (CT). In the following subsections, we will briefly introduce the background and the problem of the CT protocol.

1.1.1 Research subject - the concurrent transmission protocol

For a very long time, wireless communication system designers intuitively believe that packet collisions are problematic and try their best to avoid them. Many protocols and system designs are deeply rooted in this intuition, and the multi-hop protocols are no

exception. Currently, the most commonly adopted multi-hop protocols are basically *collision-avoidance-based*, and one famous example is the MAC-layer design of the IEEE 802.15.4 [12] families. Specifically, in a typical collision-avoidance-based protocol, when a device attempts to access the channel, it needs to perform the so-called *carrier sensing* to check if there is other devices also using the same channel. If the channel is occupied, the device needs to wait for a specifically back-off time (typically determined by some random mechanism) before the next attempt of accessing the channel. Such a procedure is commonly referred to as carrier sense multiple access with collision avoidance (CSMA/CA). In a more crowded scenario where the collision problems further escalate, people would adopt more sophisticated collision-avoidance schemes, such as the RTS/CTS handshaking for the hidden node problem.

However, those collision avoidance mechanisms significant degrade the efficiency of the channel utilization. Use the CSMA/CA as an example, the carrier sensing time becomes a constant overhead for every packet transmission. Moreover, in order to reduce the collision rate, the back-off time is typically designed to be longer than the packet length, which further increases the transmission delay.

In order to improve the efficiency, people start to consider the possibility of taking the risk of packet collisions. In the year of 2008, Dutta et al. [13] first experimentally showed that the acknowledgment message (ACK) of the IEEE 802.15.4 system can be received with a very high successful rate under a synchronized packet collision. Inspired by this works, Ferrari et al. published the paper "Efficient Network Flooding and Time Synchronization with Glossy" [14] in the year of 2011, which becomes the first proposal of a full framework of the concurrent transmission.

Concurrent transmission (CT) is a multi-hop protocol that recently revolutionized the design of IEEE-802.15.4-based wireless sensor networks (WSN). As the name suggests, CT allows multiple nodes to transmit packets that carry the same content simultaneously instead of trying to avoid packet collisions. By allowing such packet collisions, CT enables very fast back-to-back packet relaying and greatly enhances the efficiency of both the MAC and network layer of multi-hop networks. From the aspect of MAC layer, CT removes any collision-avoidance mechanisms, including carrier sensing and back-off time, which greatly reduce the latency of the packet relaying. From the network-layer point of view, CT realizes fast topology-independent flooding which spares the multi-hop network

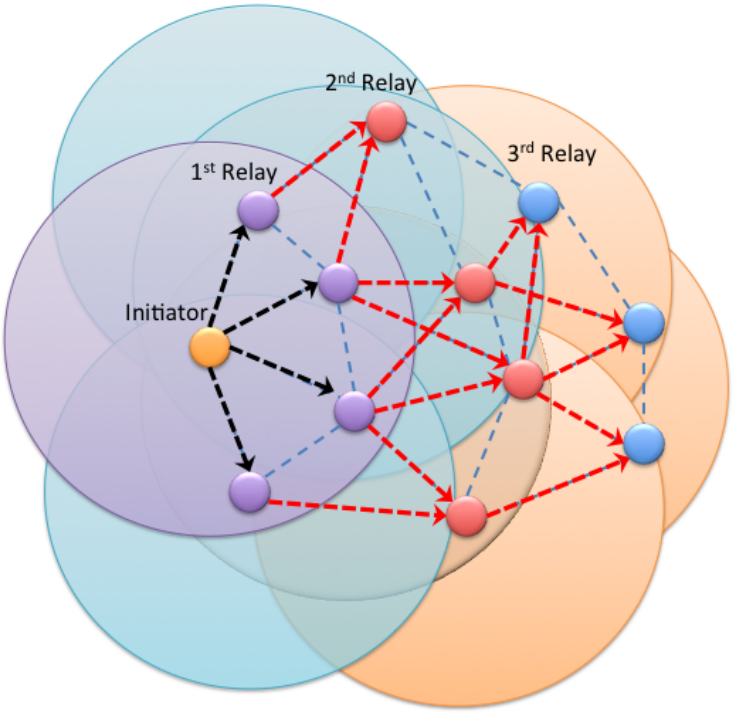

Fig. 1.1 The illustration of a multi-hop using the CT flooding.

from complicated routing procedures, such as topology discovery, path searches, and loop detection. Fig. 1.1 illustrates an example of the CT flooding over a multi-hop network.

Nowadays, CT has become a quickly emerging research field in the area of multi-hop protocols. Based on the first proposal in [14], there are many follow-up works trying to further improve the performance [15–17]. Moreover, there are also attempts to combine the CT with other techniques, like channel pipelining [18, 19]. Finally, there are studies about extensively performance comparisons between the CT-based flooding protocol and the conventional ones. Specifically, [20] and [21] confirmed that no matter from energy consumption, reliability, or latency point of view, CT can provide a better or comparable performance. (More detail about the comparison can be found in Chap. 2.)

1.1.2 Problem - insufficient physical-layer investigations

The fundamental design concept of CT is to expose the physical-layer under the risk of harmful packet collisions in order to trade for higher efficiency in the upper layer.

Although CT indeed facilitates the construction of highly efficient multi-hop networks, it is not generally applicable to any wireless standards due to the packet collision it introduces. Specifically, even though the colliding packets all carry identical contents, there are still several non-ideal physical-layer effects (including the channel effects and the inevitable offset between the transmitters) that can severely degrade the reliability of the receivers. Moreover, the physical-layer receiver performance under such packet collisions is vastly different from standard to standard. Therefore, the essential prerequisite for CT to success is to ensure that in the physical layer, the packet receptions is still reliable under the identical-content synchronized packet collisions.

A careful physical-layer investigation on the conditions that enable reliable receptions under the packet collisions is an essential step for constructing a reliable CT-based network. However, in the current CT researches, there is still lacking a systematic and comprehensive the investigation on the physical-layer receiver performance under CT. Specifically, we list three main problems regarding the current CT researches as follows.

- The physical-layer CT effects are not considered comprehensively. CT introduces various non-ideal effects in the physical-layer, but currently, only a parts of the effects, i.e., the capture effect and the synchronization error are well investigated.
- The current physical-layer receiver performance investigations are most empirical, and the evaluations are mostly based on limited experiment.
- The current CT researches mainly focus on the IEEE 802.15.4 systems, but the applicability of CT to other standards is still unclear.

1.2 Research goal

In view of the incompleteness of the current researches, the research goal of this work is to provide a systematic and comprehensive study on the physical-layer behavior of CT that clarifying the mechanisms and conditions allowing reliable Rx for CT. Specifically, this study differs from the previous one by taking the following aspects into considerations.

（1） We comprehensively evaluate the receiver performance under all the relevant non-ideal effect resulting from CT. Particularly, we put special emphasis on the effect of carrier frequency offset (CFO) which is overlooked in the previous works.

（2） In contrast to the previous experimentally evaluation that simply treats CT as individual non-idea effects, we theoretically analysis the complete characteristic of CT as a wireless channel.

（3） Besides the analysis, we also conduct extensive software simulations, and hardware emulations and experiments to verify our analysis.

（4） Unlike the previous works which focus on only individual standards, we provide extensive investigation and comparisons over various IoT-oriented standards.

With this study, people can understand not only the physical-layer characteristic of CT but also how CT affects the receiver performance. With this insight, people can then understand the actual reasons why CT succeeds on the IEEE 802.15.4 standard as well as the applicability to other technologies. Finally, with the insight provided by this research, not only the performance of CT can be further improved, but more importantly, the possibility for new CT-enabled applications can be discovered.

1.3 Main contributions

In this section, we overview the main achievement of this thesis. The main contributions are threefold.

Analysis of the CT characteristics: Our first contribution is that we model the one-hop CT behavior as a wireless multi-path fading channel, and analyze the CT characteristics. Based on the channel characteristics, we identify the systems that are compatible to CT. Moreover, we theoretically derive important characteristics, such as the level crossing rate (LCR) and average fading duration (AFD), of the fading signal under the CT. We theoretically prove that the AFD is affected by two main factors, i.e., the deviations of CFO and the number of transmitters that join the CT. In addition, we prove that the AFD is one important factor that affects the receiver performance by Monte-Carlo simulation.

Evaluations of CT on IoT standards: Next, we provide by far the most comprehensive evaluation of the receiver performance under CT. We distinguish our evaluation from the others' by the following aspects. First, we focus on clarifying the sufficient conditions for receivers to survive the beating effect. Second, we evaluate the receiver performance in terms of a newly defined metric, *sensitivity gain*, in order to discerningly reflect the gain and loss caused by CT. Moreover, our evaluations are based on not only simulations

but also real-chip emulations that provide reproducible and fine-grained control against all the transmitter offsets. Most importantly, we evaluate and compare several important IoT-oriented wireless standards, including the IEEE 802.15.4 and IEEE 802.15.4g, and LoRa.

Proposal of novel CT-enabled applications: Our third contribution is the proposal of new CT-enabled applications using the insight obtained from the theoretical analysis and comprehensive evaluation. Specifically, we proposed a CT-enabled multi-hop LoRa network (CT-LoRa) for constructing a multiple-building area network, and the CT-enabled distributed antenna system (CT-DAS) for real-time factory automation.

1.4 Thesis structure

In this section, we overview the structure of this thesis.

Chapter 2: We will first give a detail introduce of related works of CT in this chapter. Specifically, we will introduce the detail operation, the pros and cons, the physical-layer non-ideal effects, and the related previous physical-layer investigations.

Chapter 3: This chapter introduces our first main contribution - the analysis of the CT characteristics. Specifically, we will analog the CT as a wireless fading channel, and analysis its fading characteristics.

Chapter 4: This chapter presents the second main contribution - the comprehensive receiver performance evaluation under CT for various different IoT-oriented standard. Specifically, the evaluation result for the IEEE 802.15.4, IEEE 802.15.4g, and LoRa system would be presented.

Chapter 5: This chapter elaborate the third main contributions - the developed novel applications enabled by CT. Specifically, we will introduce the CT-LoRa and CT-DAS technology.

Chapter 6: This chapter concludes this thesis and point out potential future research directions.

Chapter 2

Related Works

In this chapter, we overview the related works of concurrent transmission (CT). We will first introduce the operation of CT, and its pros and cons when comparing to the conventional multi-hop protocols in detail We will also discuss the recent blooming of the CT-based protocols. Next, we will examine the non-ideal physical-layer effect of CT which prevents the conventional wireless communication systems to used CT. We will also elaborate countermeasure that conventional wireless communication systems took to avoid CT. Finally, we discuss the recent studies on the physical-layer receiver performance under CT.

2.1 CT-based protocols

In this section, we overview the basic operation and the merits of CT. The family of CT-based protocols will be also presented.

2.1.1 Basic operation principle of the CT flooding

CT enables ultra-fast packet flooding over the network. Fig. 2.1 illustrates the basic operation of the CT flooding protocol for multi-hop networks. As the conventional ones, for each flooding, there is one and only one node serving as the initiator who starts the first packet transmission. The essential difference between the CT flooding protocol and the conventional ones is the timing of the retransmission. While conventional ones perform carrier sense and random timing back-off to avoid packet collisions during relaying, in the CT flooding, any receiver who successfully decodes the packet, shall perform retransmission *as soon as possible* such that the relay packets can be transmitted at almost the same time. This simple mechanism effectively synchronizes the packet transmissions of each hop and is referred to as the *radio-driven* synchronization (RDS) in this work. The same procedure continues until the packets flood through the whole network. With the CT flooding, an efficient low-latency one-to-any broadcast protocol can be easily realized.

In the CT flooding, every node in the network is requested to join and dedicate to the current flooding. This means that simultaneous multiple information flows are prohibited. The next packet flooding (no matter from the same or different initiator) can only be started after the previous flooding finishes. To accommodate multiple packet transmissions from multiple nodes and achieve any-to-any transmissions, a super scheduler is needed to

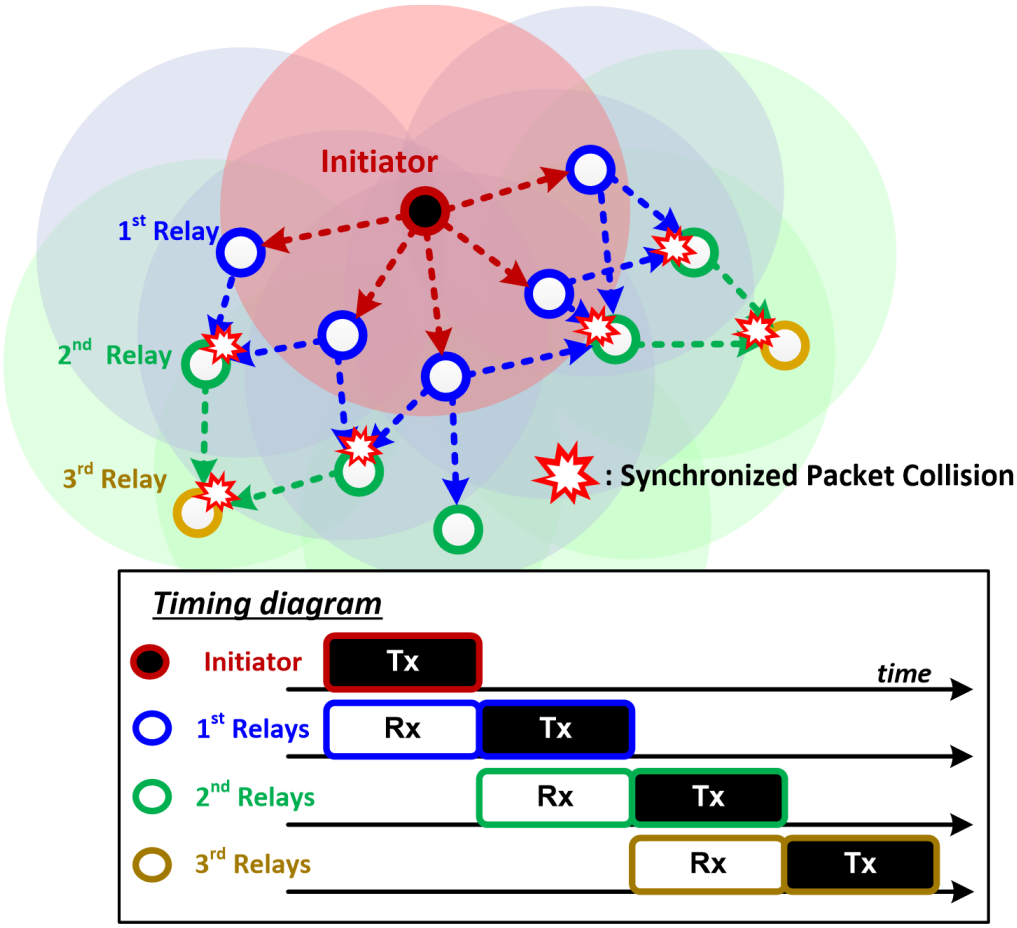

Fig. 2.1 The operation of the CT flooding protocol.

coordinate the order and the timing of the nodes to serve as the initiator sequentially [20, 21].

As a good interpretation, the final realization of the CT flooding network can be imagined as a wireless bus shared by all the nodes, where only one node can access the bus at a time, and each access is very short. Moreover, the nodes are naturally synchronized in each flooding by the radio driven synchronization (RDS). To be more specific, since each node performs immediate retransmission, the node can accurately estimate the absolute transmission timing of the initiator by subtracting the receiving time by multiplication of the packet length and the hop count. Therefore, all the nodes can perform the synchronization once whenever the super scheduler starts a flooding.

Thanks to this mechanism, the super scheduler can easily coordinate the access in a

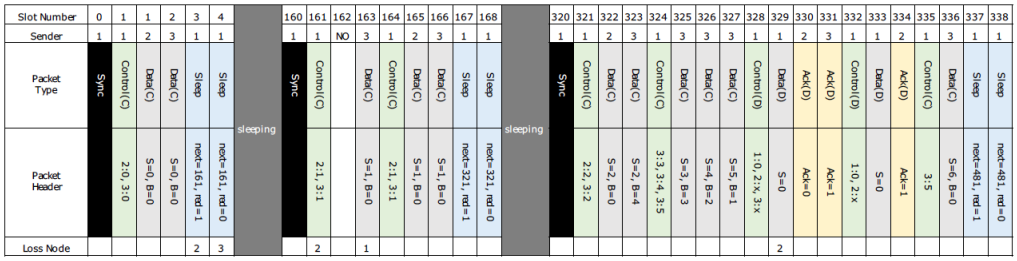

Fig. 2.2 An timing scheduling example of the CT-based protocols [21].

well-scheduled TDMA manner. Specifically, the timeline is divided into equal-length slots and assigned to the nodes. Each node acts as the initiator only in its assigned slots and serves as the relay in the other slots. Fig. 2.2 illustrate an example of the TDMA scheduling given in [21], including the time slot for the synchronization, control, data, and sleep trigger packet. Moreover, details about how the scheduler collects the traffic demands from the nodes and performs scheduling adaptively can be found in [20, 21].

2.1.2 Pros and cons of the CT flooding

Next, we compare the advantages and disadvantages of the CT flooding protocol against the conventional collision-avoidance (CA) routing ones from the aspects of latency, energy consumption, and reliability. Note that, in typical WSN researches, the total throughput is usually a control variable. That is, the nodes generate the packets under a given traffic model (could be deterministic or random, heavy or light) so that the expectation of the total traffic is fixed in each evaluation. Then, the performance is evaluated by the latency, energy consumption, and reliability.

Many works [20, 21] have shown that the CT flooding can provide comparable latency performance, better reliability, and much lower energy consumption when comparing to the conventional collision-avoidance-based routing protocols. Specifically, although the CT flooding dedicates the whole network capacity to serve only one packet flooding at a time, the quick flooding time compensates the loss in the network capacity. In addition, in the flooding, a packet could be heard several times by a node, which greatly increases the successful rate of packet reception. Moreover, due to the well-scheduled TDMA property,

the CT flooding enables accurate duty cycling and greatly reduces the receiver listening time as well as the energy consumption. In the following, we will provide detailed discussions from each aspect.

Latency: From the latency point of view, for both the CT flooding and the CA routing have merits and limitations. As the reviewer pointed out, although the relay timing of the CT flooding is short, only one packet is allowed to be transmitted at a time. This increases the total latency when the traffic is heavy and there are many nodes queuing in the line. On the other hand, the routing protocol might seem to be more efficient, since it can accommodate multiple information flows simultaneously. However, the CA mechanism makes the relay time much longer. Moreover, the CA also prohibits the nodes close to each other from sending a packet at the same time, which greatly reduces the possibility of simultaneous multiple information flows.

In short, the metrics of CA routing is more observable in a large scale network, while CT flooding is beneficial in a middle or small scale network. As for the typical WSN scenario, the evaluation results in [20] show that the CT flooding and the CA routing achieve similar latency performance.

Energy consumption: The very fast relay greatly helps to reduce the energy consumption. Comparing to the slow and unpredictable relay time in CA, the relay time in CT is not only an order smaller but deterministic, which allows the realization of the aforementioned well-scheduled TDMA system. As a result, a very accurate duty cycling can be achieved - every node can wake up accurately at the same time, finishes the packet flooding in a short period, and goes back to sleep promptly. This advantage not only reverses the disadvantage of the flooding but also makes the energy consumption significantly better than the CA routing.

Reliable: From the reliability point of view, the CT flooding surprisingly outperforms the CA routing. The CT flooding indeed suffers from the packet collision, which is exactly the problem we would like to tackle in this work. However, the CT flooding enjoys the multiple reception diversity. Specifically, a packet could be heard several times by a node during the flooding, which greatly increases the successful rate of packet reception. On the other hand, a routing-based relay fails when any node on the shortest path fails. Moreover, the well-known hidden node issue, i.e. multiple transmitters fail to sense the presences of each other and send independent packets to one receiver, could further degrade the reliability.

Other aspects: In addition, the CT flooding inherits many great advantages from the flooding. For example, it is much simpler and more robust in mobile applications since it requires no topology information and routing tables; it realizes more efficient one-to-any broadcasts, while the routing achieves only one-to-one communications; and the traffic is uniformly distributed to every node so that the energy consumption is fair.

2.1.3 CT-based protocols family

Back to the year of 2008, there were already some works pointed out that the packet collisions are not necessarily harmful and could be used for increasing the network efficiency. Specifically, Dutta et al. [13] proposed the Backcast, which allows all nodes that match the destination respond to a unicast, multicast, or broadcast transmit the acknowledgment packets simultaneously. Based on the idea of Backcast, a complete MAC protocol, A-MAC, was later proposed by the same authors in [22].

The preliminary idea of CT flooding is first presented in [23], which allows the nodes that joint the flooding to transmit the packet concurrently. However, the timing concurrency problem in [23] is still not properly solved, so the receiver mainly survives the CT due to capture effect. It is not until Ferrari et al. presented a sophisticated interrupt and transmitter/receiver buffer handling mechanism in [14] that the receivers are allowed to fast and stably perform retransmission. Yuan et al. [24] experimentally verified that the achieved standard deviation is as small as 0.14 us. Therefore, we consider the Glossy protocol in [14] the first mature proposal of the CT flooding.

Very soon after the proposal, there have been many follow-up works trying to further improve the efficiency of the CT-based flooding. Particularly, many of those works are trying to reduce the number of the node that joins the flooding. To give some examples, Wang et al. [15] proposed to building a spare backbone network for CT to alleviate the timing accumulation problem. Yuan et al. [25] proposed the Sparkle protocol, which limits the nodes that join the CT flooding by topology control, and Brachmann et al. [17] proposed the LaneFlood which actually does not perform flooding but creates a lane consisting of multiple nodes on the shortest path for packet relaying. Finally, Rao et al. [16] proposed to introduce intentional power offset to increase the probability of capture effect and hence the packet reception rate. There are also works trying to combine CT with

other technique to further overall network utility. For example, Doddavenkatappa et al. proposed to combine CT with the channel pipeline to create seamless CT flooding [18, 19].

There are also many attempts to apply CT to other technologies, such as SourceSync with 802.11 [26] and CXFS with 802.15.4g [27]. However, unlike IEEE 802.15.4 where CT can be applied straightforwardly, pre-coding or extra error correcting mechanisms are found to be necessary for reliable connections. For example, the STBC is applied in SourceSync, and Hamming code is adopted in CXFS.

2.2 Physical-layer effects of CT

In this section, we discuss the physical-layer effects of CT. We will first present an overview of the effects, and then discuss each individual ones. We will also briefly discuss the techniques that adapts in conventional wireless communication systems to avoid CT.

During the packet flooding, only the first-hop transmission (the red area in Fig. 2.1) is collision-free. Starting from the second-hop relay, it is possible for multiple transmitters to concurrently transmit packets to one receiver so that the synchronized packet collisions occur. Although all the packet carries the same contents, they are inevitably and independently affected by many physical-layer effects since the transmitters are all independent from each other. Specifically, the received power and phase of the packets could be different since the channel the each packet passes through are independent. Moreover, due to the hardware/software processing variations and the propagation delay difference, the arrival timing of the concurrently transmitted packets are actually not perfectly aligned. Finally, the center carrier frequencies of the packets also differ from each other due to the inevitable variations of the oscillators in the transmitters.

(a) Power offset

Having a larger offset between the concurrently transmitted packets are actually beneficial for the packet reception due to the capture effect [28]. The capture effect originally refers to a phenomenon in the FM system that only the strongest signal of multiple co-channel ones would be demodulated. In CT research, it has been widely adopted to describe the successful reception of a wanted signals when its signal power is significantly larger than the interferences'. The required power offsets to enable the capture effect depends on the required signal-to-interference-plus-noise ratio (SINR) of the demodulation.

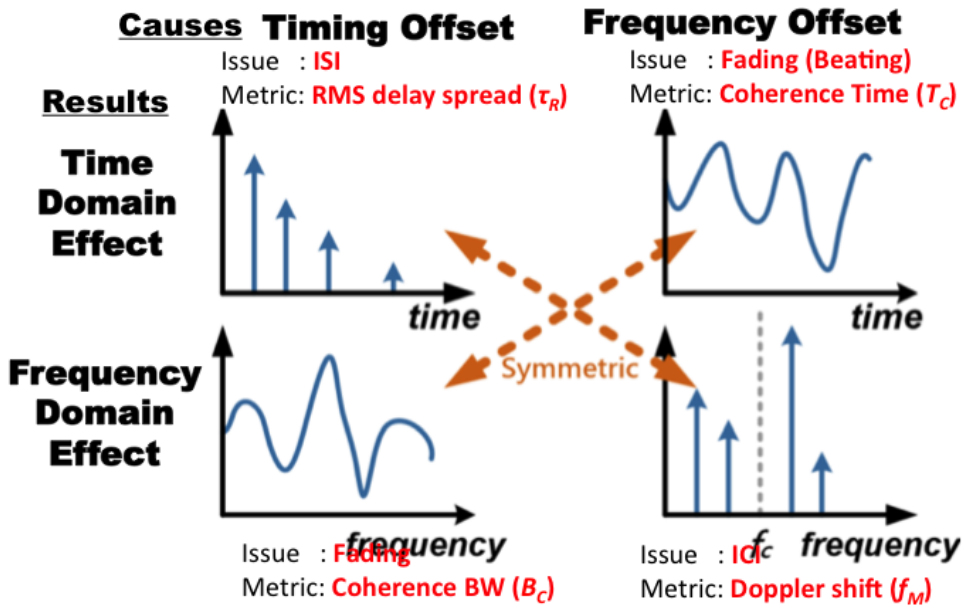

Fig. 2.3 The effect of timing and frequency offset.

In the contexts of IEEE 802.15.4 system, many experimental results [22, 29, 30] have verified that a 3 dB power difference is sufficient for the packets to be captured. However, the capture effect cannot depict the whole picture of the concurrent transmission since there is still a significant probability that the packet is not dominated by one packet.

(b) Phase offset

A static phase offset between the packets results in constant destructive combination. The effect of static phase offset in IEEE 802.15.4 system has been well investigated in [31]. However, in the presence of CFO, the phase is seldom static but constantly shifting. Therefore, the effect of static phase offset is only relevant to the performance only when the CFO is sufficiently small.

(c) Timing Offset

The arriving timing offsets between the concurrent transmission packets result in an effect similar to the multi-path channel, which leads to harmful inter-symbol interference

(ISI) and frequency-selective fading as illustrated in Fig. 2.3. In the IEEE 802.15.4 system, the effect of timing offset has been studied. As a short conclusion, the timing offset needs to be kept as small as possible. Ferrari et al. [14] experimentally show that the required timing accuracy should be within 0.5 μs. A more careful investigation in [31], on the other hand, shows that 0.25 μs would be a more accurate requirement. There are two factors that contribute to the timing offset - the processing time variation when performing the retransmission and the propagation delay difference, where the former is considered to be the main contributor. Therefore, there are many works striving to reduce the timing variation of the retransmission. Specifically, Ferrari et al. [14] presented a sophisticated interrupt and transmitter/receiver buffer handling method that allows fast and stable retransmission on the TelosB platform. Recently, a much more accurate timing is achieved in [32], where the resulted timing offset is only 10 to 20 ns.

(d) Carrier frequency offset

While the phase and timing offset have been well investigated in the previous works, the effect of carrier frequency offset (CFO) is often overlooked due to its inaccessibility and uncontrollability. The CFO would keep shifting the phase offset between the packets and result in alternations between constructive and destructive interference. The consequence of such alternations is a dramatic change of the signal envelope, which is commonly referred to as the *beating effect*. In the frequency domain, CFO also introduces the inter-carrier interference (ICI). The effect of CFO is also illustrated in Fig. 2.3. Note that, there is a symmetry between ISI and ICI, and between the fading and beating as well.

2.2.1 CT in conventional wireless communication system

There are several close relatives of CT in the area of wireless communications. CT is the most simple way to utilize the spatial diversity of multiple antennas to increase the coverage or reliability because it requires no cooperations between the transmitters except for the synchronization. Therefore, it can be viewed as a simple case of the simulcast systems [33] or a naive MIMO system [34].

Due to its simplicity, CT used to be adopted in old wireless communication systems, such as famous POCSAG and FLEX high rate data paging system, to provide large area

coverage. However, because of the phase offset resulted from the propagation path difference and the channel effects, CT in many situations results in destructive combination and hence performance degradation. To avoid dead zones of reception resulted from destructive combinations, careful power/delay managements of the transmitters are required [35]. Moreover, in practical systems where the synchronizations are not perfect, the beating effect occurs in both time and frequency domain [35]. The valley of beating generally leads to significant SNR degradation and demodulation error floor [36, 37]. In addition, timing and frequency offsets also result in inter-symbol interference (ISI) and inter-carrier interference (ICI). To guarantee the performance in simulcasting systems, ITU-R imposes strict regulations on the timing and frequency synchronization [38].

In view of the risk of performance degradation, later systems usually avoid transmitting duplicated waveforms when performing simulcasting. Instead, more sophisticated cooperations between transmitters are adopted to guarantee coherent (or at least nondestructive) combination in the receivers, such as beam forming [39], space-time block coding (STBC) [40], and opportunistic transmitter selection [41]. Adding optimized timing or frequency offsets is also a simple but effective countermeasure of destructive interference, such as time-domain cyclic delay diversity (CDD) [42] adopted in 802.11, or frequency offset adopted in the wide area ubiquitous network (WAUN) [43].

The cooperation between transmitters could be sub-divided into four main categories. First, in the case that CSI is available, the beam-forming techniques can be adopted to form coherent combination [39]. Second, if only limited feedback (e.g., SNR or link quality) is allowed, opportunistic algorithm the selects the best transmitter can be applied [41]. Third, while the CSI is not available, diversity coding, such as the space-time block coding (STBC) [40], is usually adopted [44]. Finally, adding optimized timing or frequency offsets is also a simple but effective countermeasure for destructive interference. For multi-carrier system such as orthogonal frequency division multiplexing (OFDM), time-domain cyclic delay diversity (CDD) [42] is usually adopted; on the other hand, carrier frequency offsets are more often introduced in the single carrier system [45]. As a practical example, IEEE 802.11n utilizes the CDD, while the wide area ubiquitous network (WAUN) proposed by NTT [43] adopts CFO.

2.3 Physical-layer investigations on CT

In this section, we review the previous physical-layer investigations on CT. First of all, many researches attributed the success of receptions to the low SINR requirement of IEEE 802.15.4, which allows capture effect to happen easily. Specifically, many experimental results [22, 29, 30] verified that only a 3 dB power difference is sufficient for the strongest signal to survive.

Next, Ferrari et al. [14] highlighted the timing offset issue and concluded that the receiver survives as long as the synchronization error is within 0.5 ¯s. A further study of the distribution of the synchronization error was presented in [24], and the error accumulation issue was tackled in [15]. However, these works obviously overlooked one important factor, i.e., the effect of aforementioned CFO and phase offset.

After many reports of experiment results, an analytical model of the receiver performance under CT based on a coherent matched-filter architecture was provided in [31]. Besides the capture effect and timing offset, Wilhelm et al. [31] further took the static phase offset into consideration. Although they considered by far the most extensive impairment model, the CFO and beating issue were not tackled. Moreover, since their model is based on the assumption of coherent receivers and perfect phase and frequency synchronization, their mathematical analyses are not valid in real scenarios with CFOs. Finally, there are a few works addressed the beating issue in CT, e.g. [46, 47]. However, only limited experimental observations that address the possible degradation are presented, while the conditions and mechanisms for IEEE 802.15.4 receiver to survive beating were still unclear.

2.4 Summary

In this chapter, we introduced the CT flooding protocols in detail. Specifically, the basic operation principle and the advantages and disadvantages are presented. We also enumerated the recently developed CT-based protocol to the blooming of the CT research. Next, we discuss the physical-layer non-ideal effect of CT, including the cause and consequence. The reason why conventional wireless communication systems did not adopt CT and the countermeasure of CT are also discussed. Finally, we provide a survey on the previous physical-layer investigations on CT.

Chapter 3

Analyses of the CT Characteristics

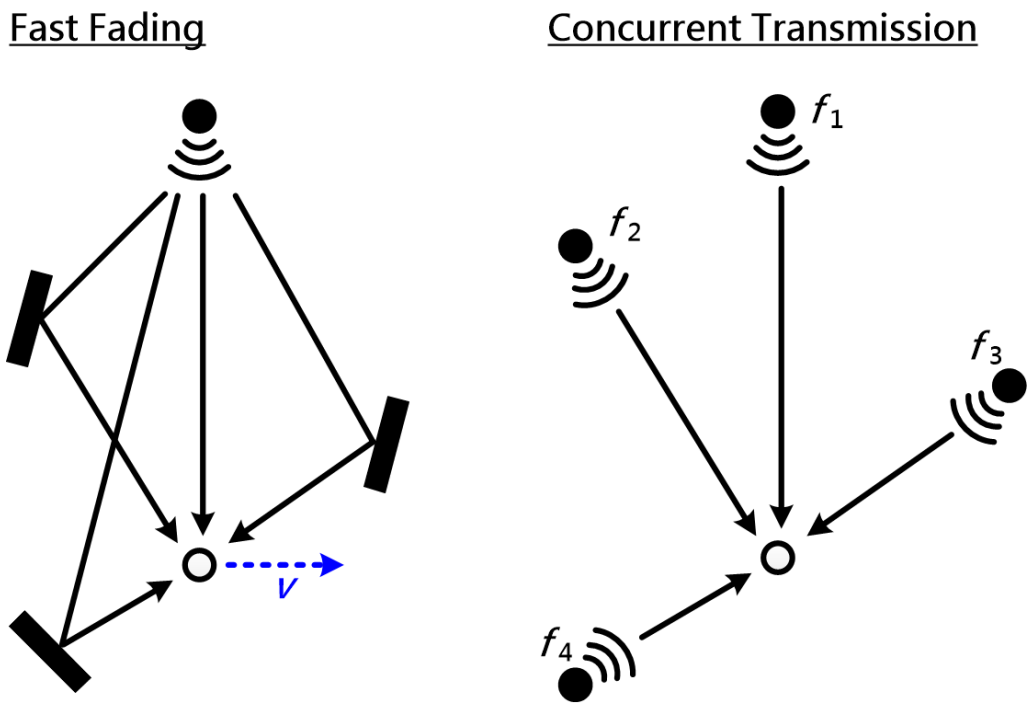

Fig. 3.1 The comparison between multi-path channel and CT.

In this chapter, we introduce our first contribution - modeling the one-hop CT behavior as a wireless multi-path fading channel and analyzing the CT characteristics. Then, we will identify the suitable systems for CT based on the channel characteristics, Next, we present the most important part of this chapter, where we theoretically derive two important second order channel, the level crossing rate (LCR) and average fading duration (AFD), of the beating signal under the CT and verify it by Monte-Carlo method. We theoretically prove that the AFD is affected by two main factors, i.e., the deviations of CFO and the number of transmitters that join the CT. By analyzing the AFD, the performance degradation due to the beating effect can be characterized.

3.1 Analyzing CT as a fading channel

3.1.1 Similarity between CT and multi-path channel

We first point out that the behavior of the multiple nodes performing concurrent transmission is very similar to the wireless multi-path channel. Fig. 3.1 illustrate a comparison

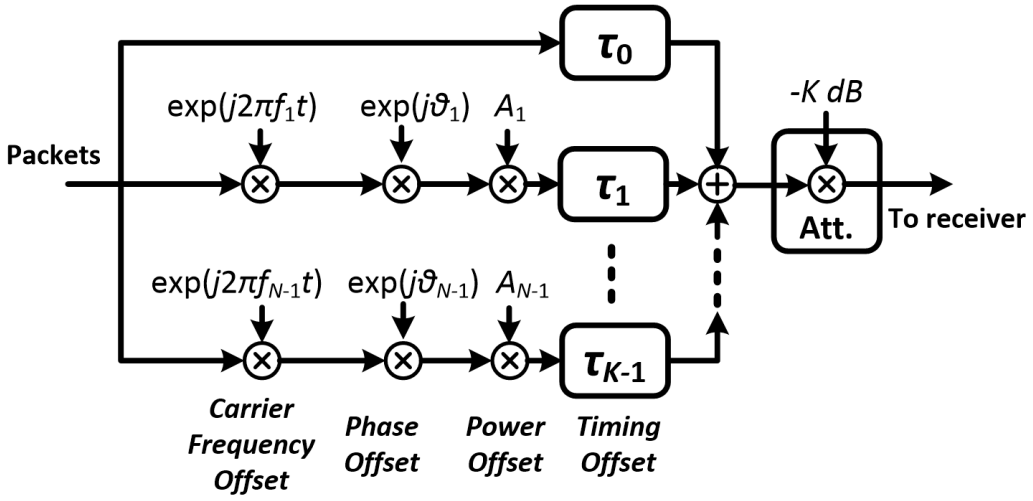

Fig. 3.2 The equivalent one-hop channel model of CT.

between multi-path channel and CT. We can see that in both cases, the receiver receives multiple copies from a common packet, and those packets are passing through different paths. Therefore, the received packets in both cases are with inevitable power, phase, and timing offset. Besides, in the CT scenario, a significant portion of the timing offset are contributed from the variation of the hardware and software processing time when performing retransmission. Moreover, in the scenario that the transmitter or the receiver is moving, the carrier frequency of the packet would be shifted due to the Doppler effect, and the among of the frequency shifts is determined by the angle of arrival and hence varies from path to path. On the other hand, even the CT scenario is static, the carrier frequency of the CT packets are still different due to the fabrication variation of the oscillator. Therefore, we conclude that the both receivers under CT and multi-path channel are affected by the power, phase, timing offset, and CFO.

3.1.2 One-hop Channel Model of CT

The one-hop behavior of such packet collisions can be modeled as an additive composite channel shown in Fig. 3.2, where the received packets from multiple transmitters are modeled as one common packet passing through different paths with independent power, phase, timing offset, and CFO. In typical WSN scenarios, where the sensor nodes are usually static and communicate within a short range, it is reasonable to assume the channel

between each transmitter and the receiver to be slow- and flat-fading, and each channel can be thus modeled as an independent power and phase offsets. Moreover, due to the variation of the processing time for re-transmission, the propagation delay, and the oscillator frequency between the transmitters, the arrived packets are with inevitable timing offset and CFO.

3.1.3 Numerical comparisons

Although the dominating effects are the same, the numerical scales of individual effects are quite different. This is particular the case when we are talking about the CFO since the root cause of the CFO in CT and multi-path channel are fundamentally different. Besides, the different in timing offset is also noticeable and worthwhile to have a detailed discuss. In the following, we will address these two offsets respectively.

(a) Numerical comparison of CFO

The Doppler shift caused by mobility can bring only mild CFO. To give specific examples, let us use the channel model defined in IMT-2000 [48]. Assuming the wireless communication system works at 2 GHz, the maximum Doppler shift resulting from a pedestrian in an outdoor environment is less than 10 Hz. In the vehicular cases, the resulted maximum Doppler shift is only around 100 Hz. Even in the extreme case, such as the high-speed train case, the maximum Doppler shift seldom goes beyond 400 Hz.

On the other hand, the CFO resulting from the oscillator fabrication variation is remarkably larger than the aforementioned Doppler shifts. Specifically, the allowed maximum frequency variation of the oscillators is in the order of several ten ppm. For example, the IEEE 802.15.4 allows a maximum ± 40 ppm variation. Considering the frequency offset in the worst scenario $(40 - (-40)$ ppm), the maximum frequency offset between the IEEE 802.15.4 packet in the 2.4 GHz band is as large as 192 KHz. According to our actual measurement on the many real sensor nodes, the typical CFO resulting from the oscillator variation is around 10 to 20 KHz.

(b) Numerical comparison of timing offset

in contrast to the CFO, the timing offset in the wireless multi-path channel is relatively larger, since many wireless communication systems are designed to provide wide coverage. Taking again the IMT-2000 channel model as an example, the maximum delay spread of the outdoor vehicular model is about 350 ns.

In CT, there are two factors that contribute to the timing offset - the processing time variation when performing the retransmission and the propagation delay difference. However, in the CT scenario, the propagation delay difference is usually considered a minor factor. Particularly in the short-range systems such as IEEE 802.15.4 system, the effective communication range is only a few tens of meters, which already limits the maximum propagation delay to be smaller than 0.3 us. Moreover, since it is the difference that matters and it only matters when the packets are received with similar power, the difference of propagation delay is typically much smaller than the total propagation delay.

The processing time variation during retransmission is considered to be the main contributor of the timing offset in CT. Particularly, in some WSN platforms whose RF module is discrete from the microprocessor and controlled by a slow interface, the retransmission time could vary significantly. For example, the famous IEEE802.15.4 platform, TelosB, uses an 8-MHz SPI to control the RF module, and a drift of only a few clocks already violates the timing requirement. Toward this, Ferrari et al. [14] presented a sophisticated interrupt and transmitter/receiver buffer handling method that allows fast and stable retransmission on the TelosB platform, and Yuan et al. [24] experimentally verified that the achieved standard deviation is 0.14 μs. Moreover, this variation can be further improved by adopting more advanced platforms that provide good integration of the RF module. For example, a timing synchronization system is realized based on the CT flooding in [32], where a platform capable of doing nanosecond-order retransmission is adopted. The resulted timing offset is only 10 to 20 ns.

3.2 Suitable systems for CT

From the analysis in the previous sections, we can know that the CFO issue is actually a more severe problem in the CT. However, none of the current wireless communication systems take such severe CFO into consideration in their design stage. Therefore, when

people are developing a multi-hop system using CT, it is very important to consider the impact the CFO could bring.

As we discuss in the previous chapter, the CFO not only introduce the ICI in the frequency domain but also results in the fading-like beating effect in the time domain. We next discsss these two effects in the following subsections.

3.2.1 Systems considerations for beating effect

If the system performs the timing domain modulation (such as the IEEE 802.15.4), the beating effect results from the CT needs to be taken into consideration. The beating effect in CT is similar to the fast fading in the mobile multi-path wireless channel. The main difference is that the frequency shift in CT mainly results from CFO between the transmitters, while that in fast fading channel is caused by the Doppler effect from movement. The beating results in dramatic phase and magnitude variations. We will discuss the communication systems design considerations under the effects of these two variations as follows.

(a) Coding for deep fading

When the beating occurs, the magnitude of the signal varies dramatically along with the time. Although it is possible for the magnitude to be enhanced, it is also likely that the magnitude becomes very small so that burst demodulation errors occur due to the insufficient of signal-to-noise ratio (SNR). This situation is commonly referred to as *deep fading*, and the burst error occurs in the deep fading region would dominate the overall error rate performance.

The *fading duration*, the duration where the magnitude of the signal remains below a specified fading threshold as illustrated in Fig. 3.3, is a very important factor to quantify the effect of the deep fading. In wireless communication systems, an effective counter measurement to combat fading is to apply error correcting code (ECC) to recover the deeply faded symbols. For the ECC to be effective, an interleaver whose length is longer than the fading duration is needed to scatter the burst error caused by fading [49]. As a result, the receiver performance in CT system would be significantly affected by the ratio between the fading duration of the beating and the length of the ECC and interleaver. However, due to the requirement of RDS, there is a strict limitation on the post-proceeding

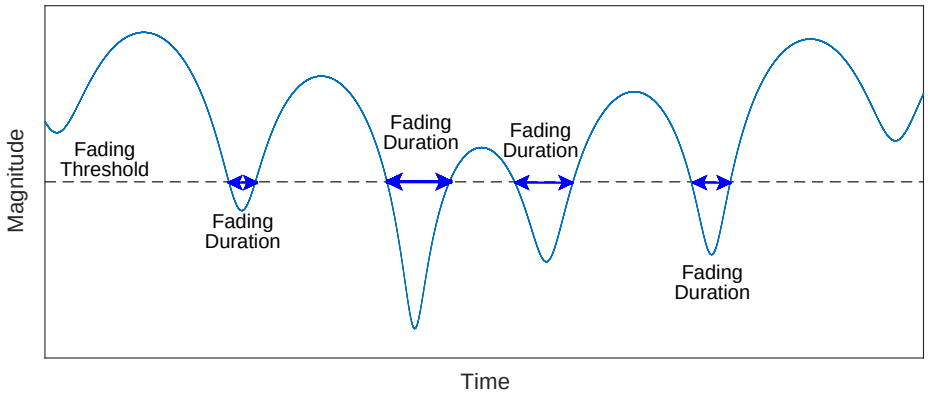

Fig. 3.3 The illustrations of beating and the fading duration.

time in CT system, which greatly restricts the applicable ECC and interleaver length in CT systems.

(b) Non-coherent modulation for phase and magnitude variation

In the wireless communication system, a coherent modulation modulates the data on the phase and magnitude of a signal. Some examples are like the phase shift keying (PSK) or the amplitude shift keying (ASK). In the receiver side, the receiver needs to restore the phase synchronization with the transmitter in order to demodulate the data. Generally, the coherent modulation is considered to be a more spectrally efficient modulation, and also enjoys a better SNR performance [50]

However, the beating effect prohibits the usage of coherent modulation and demodulation, since the phase and magnitude dramatically and continuously vary along with the time which makes the receiver very difficult to restore the phase synchronization. On the other hand, non-coherent modulation methods, such as the frequency shift keying (FSK) modulation where the receiver are not required to get phase synchronized with the sender carrier signal, are more suitable for CT.

3.2.2 Systems considerations for ICI

If the system performs the frequency domain modulation, the ICI results from the CT needs to be taken into consideration. Particularly, in many multi-carrier systems,

such as the famous orthogonal frequency division modulation (OFDM) adopted in IEEE 802.11a/g/n [8], it is by default that the ICI is considered to be ignorable due to the orthogonal modulation for guard band insertion. For such systems, it is expected that the receivers are not able to deliver good performance under CT due to the severe ICI. On the other hand, a single carrier system that does not suffer from the ICI is more appropriate for CT.

3.2.3 Summarizing the suitable systems for CT

In sum, we briefly conclude that the systems which are suitable for CT need to satisfy the following conditions:

（1） Protected by short block code
（2） Adopts non-coherent modulation
（3） Single carrier system

3.3 Fading Duration of beating

In the previous section, we have shown that the CFO is a dominating factor to the receiver performance, and it is the fading duration of the beating that matters. But is there any simple but effective indicator that could help us to judge whether the beating is harmful or not (like the 3 dB threshold in capture effect or the 0.5 μs in timing error)? Unfortunately, the beating pattern is regular only in 2-Tx cases and generally random in most of the cases. Therefore, it is difficult to judge directly from the value of CFO. To tackle this, we present a series of analyses to characterize the fading duration of the beating signal. Specifically, we will present two indicators, the maximum fading duration (MFD) and the average fading duration (AFD).

3.3.1 Maximum fading duration (MFD)

(a) Definition

Given that the strongest concurrent transmitted signal is normalized to unity, we define a fading duration of the beating pattern as a continuous period whose magnitude is lower -3 dB. By searching the fading duration with the maximum width through a beating

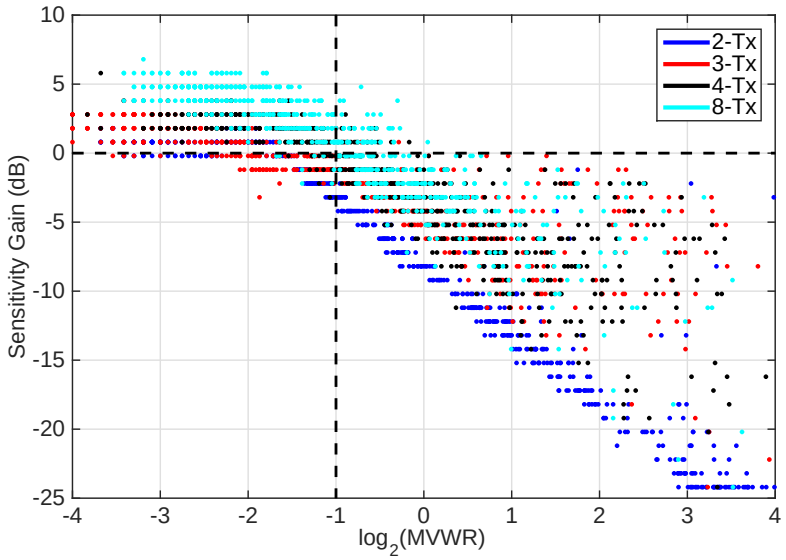

Fig. 3.4 The relationship between the sensitivity gain and MFD.

pattern, we then find the MFD duration of a beating pattern. Fig. 3.3 illustrates an example of the valleys and maximum valley width of a beating pattern.

Note that for regular beating in 2-Tx cases, the MFD can be derived as

$$\frac{1}{\pi \cdot \Delta f} \cos^{-1} \frac{2\alpha^2 + 1}{4\alpha}, \tag{3.1}$$

where Δf and α are the CFO and power ratio between the small and large signal. Note that the magnitude of the signal goes below -3 dB only if $\alpha \geq 1 - 1/\sqrt{2}$.

(b) MFD vs. sensitivity gain

Next, we prove that the MFD is an effective hard indicator to reflect the performance degradation resulted from beating in multiple transmitter cases.

We consider CT scenarios with 2, 3, 4, and 8 transmitters, which are denoted as 2-Tx, 3-Tx, 4-Tx, and 8-Tx, respectively. For each scenarios, more than 100 realizations of CFO combinations are randomly generated. For each combination, the MFD of a packet as well as the PER vs. SNR performance in terms of the sensitivity gain are measured by simulation. (The definition of the sensitivity gain will be elaborate in Chap. 4) To reduce the evaluation space, we set power offset and timing offset to be zero.

Fig. 3.4 shows the relation between MFD and sensitivity gain by simulation. That horizontal axis represents the log value (base 2) of the ratio between the MFD and DSSS symbol length, and the vertical axis indicates the sensitivity gain. Each point on the figure illustrates a realization of a random CFO combination.

We can see that regardless of the transmitter number, the receiver generally enjoys non-negative sensitivity gain as long as the the ratio between the MFD and DSSS symbol length is lower than 0.5. According to (3.1), this corresponds to a 28.8 kHz of CFO in the 2-Tx case with 0 dB power offset, which match the simulation and emulation results in Evaluation 1.

In addition, while in 2-Tx case the sensitivity gain is mostly 0dB, higher sensitivity gains can be observed in the higher transmitter cases. On the other hand, once the MVWR is larger than 0.5, the receiver performance degrades accordingly. Note that, in 2-Tx cases, the beating pattern is regular and the minimum of the beating valley has zero power. Therefore, the degradation in 2-Tx case is particularly worse and highly correlated with the MFD. In the other cases with more transmitters, the degradation can be alleviated, but the performance is still generally worse than the 1-Tx links.

3.3.2 Average fading duration (AFD)

The MFD indeed provide an effective indication of the performance loss, and the threshold for no-loss reception is clear. However, in the cases with more transmitters joining the CT, the MFD can not be analytically evaluated. Toward providing an indicator that can quantify the CFO effect more straightforwardly, we next present a theoretical analysis of the AFD of the beating by modeling the power, phase offset, and the CFO as random variables. Note that, as we discussed in the previous section, the feasibility of small timing offset has been proven. To simplify the derivation, the timing offset is assumed to be zero in the theoretical analysis. In the later evaluation, we will show that the derived AFD has a high correlation to the receiver performance even in the presence of the timing offset. In addition, we present a CFO measurement over a large number of sensor nodes to estimate the AFD in practical systems.

(a) Definition

The AFD has been studied for the fast-fading channel where the distribution of frequency shift follows the U-shape Doppler spectrum [51]. On the other hand, since the CFO in the CT mainly results from the inevitable part-to-part variation of the oscillators, we derive the closed form for the AFD of the beating by assuming the CFO of the transmitter follows the normal distribution.

Consider the one-hop CT scenario with N transmitters simultaneously transmitting packets with identical contents to a receiver. For the n^{th} transmitter, we denote its carrier frequency offset and the path gain to the receiver as f_n and C_n.

Without losing the generality, we assume that the transmitted signal is an unmodulated signal tone at the carrier frequency. The noiseless low-pass equivalent complex envelope of the received signal can thus be written as

$$r(t) = \sum_{n=1}^{N} C_n \cos\left(2\pi(f_c + f_n)t + \theta_n\right) \tag{3.2}$$

where θ_n is a random phase uniformly distributed from 0 to 2π. We can rewrite the equation into

$$r(t) = s_I(t)\cos(2\pi f_c t) - s_Q(t)\sin(2\pi f_c t), \tag{3.3}$$

where

$$s_I(t) = \sum_{n=1}^{N} C_n \cos\left(2\pi f_n t + \theta_n\right), \tag{3.4}$$

$$s_Q(t) = \sum_{n=1}^{N} C_n \sin\left(2\pi f_n t + \theta_n\right), \tag{3.5}$$

and the noiseless received band-pass waveform can then be written as

$$s(t) = s_I(t) + j s_Q(t). \tag{3.6}$$

Assuming the process is wide-sense stationary, the autocorrelation function of $s(t)$ can be written as

$$\begin{aligned} \phi_{ss}(\tau) &= \frac{1}{2} E\left[s^*(t)s(t+\tau)\right] \\ &= \phi_{s_I s_I}(\tau) + j\phi_{s_I s_Q}(\tau). \end{aligned} \tag{3.7}$$

Since the θ_n and θ_m are independent for $n \neq m$, the autocorrelation $\phi_{s_I s_I}(\tau)$ and $\phi_{s_I s_Q}(\tau)$ can be obtained as

$$\begin{aligned}\phi_{s_I s_I}(\tau) &= \phi_{s_Q s_Q}(\tau) \\ &= E\left[\sum_{n=1}^{N} C_n^2 \cos\left(2\pi f_n t + \theta_n\right) \cos\left(2\pi f_n (t+\tau) + \theta_n\right)\right]\end{aligned} \tag{3.8}$$

$$\begin{aligned}\phi_{s_I s_Q}(\tau) &= -\phi_{s_Q s_I}(\tau) \\ &= E\left[\sum_{n=1}^{N} C_n^2 \cos\left(2\pi f_n t + \theta_n\right) \sin\left(2\pi f_n (t+\tau) + \theta_n\right)\right]\end{aligned} \tag{3.9}$$

In the conventional fast fading model, the frequency offset is resulted from the Doppler shift introduced by movement, and can be written as

$$f_n = \frac{v}{\lambda_c} \cos \phi_n, \tag{3.10}$$

where v, λ_c, and ϕ_n are the moving speed, wavelength, and the arriving angle.

In CT, the frequency is due to the inevitable processing variation. In this work, we assume the CFOs of the transmitters follow the normal distribution, and write

$$f_n \sim \mathcal{N}(0, f_m^2), \tag{3.11}$$

where f_m is the standard deviation (STD) of the CFOs. We further assume the path gain C_n is a normalized Rayleigh distribution. For the other models, such as the Rician distribution, the same derivation flow still follows.

With this assumption, the autocorrelation functions in (3.8) and (3.9) then become

$$\begin{aligned}\phi_{s_I s_I}(\tau) &= \frac{N}{2} E\left[\cos(2\pi f_n \tau)\right] \\ &= \frac{N}{2} \int_{-\infty}^{\infty} \cos(2\pi f \tau) \cdot \frac{1}{\sqrt{2\pi} f_m} \exp\left(-\frac{f^2}{2 f_m^2}\right) df \\ &= \frac{N}{2} \exp\left(-2\pi^2 f_m^2 \tau^2\right),\end{aligned} \tag{3.12}$$

and

$$\begin{aligned}\phi_{s_I s_Q}(\tau) &= \frac{N}{2} E\left[\sin(2\pi f_n \tau)\right] \\ &= 0\end{aligned} \tag{3.13}$$

The power spectral density (PSD) can then be obtained by taking the Fourier transform of the autocorrelation function.

$$\begin{aligned} S_{ss}(f) &= \mathcal{F}\{\phi_{ss}(\tau)\} \\ &= \frac{N}{2}\int_{-\infty}^{\infty} \exp\left(-2\pi^2 f_m^2 \tau^2\right) \exp\left(-j2\pi^2 f\tau\right) d\tau \\ &= \frac{N}{2\sqrt{2\pi} f_m} \exp\left(-\frac{f^2}{2f_m^2}\right). \end{aligned} \tag{3.14}$$

The moments are essential information for the calculation of AFD. Particularly, we need the zeroth, first, and second-order moments. Given the PSD $S_{ss}(f)$, the n^{th} order moment b_n is

$$b_n = (2\pi)^n \int_{-\infty}^{\infty} S_{ss}(f) f^n df. \tag{3.15}$$

Using the integration result that $\int_{-\infty}^{\infty} e^{(-x^2)} dx = \sqrt{2\pi}$ and $\int_{-\infty}^{\infty} x^2 e^{(-x^2)} dx = \sqrt{\pi}/2$, we can derive the zeroth and the second order moments as

$$b_0 = \frac{N}{2}, \tag{3.16}$$

$$b_2 = \frac{N}{2}(2\pi f_m)^2. \tag{3.17}$$

The first order moment, on the other hand, can straightforwardly be proven to be 0 due to the symmetric property of $S_{ss}(f)$.

For any random process $r(t)$ whose envelope $\alpha(t) = |r(t)|$, the AFD, defined as the average duration that the envelope level remains below a specified threshold R, can be derived as [51]

$$T(R) = \frac{\int_0^R p(\alpha) d\alpha}{L(R)}, \tag{3.18}$$

where the $p(\alpha)$ is the probability density function (PDF) of α, and $L(R)$ is the level crossing rate (LCR) associated with the level R, defined as the rate (times per second) for the envelope to cross the level R in the positive (or negative) going direction. From [51], the LCR for any random process can be calculated as

$$L(R) = \int_0^{\infty} \dot{\alpha} p(\alpha = R, \dot{\alpha}) d\dot{\alpha}, \tag{3.19}$$

where $\dot{\alpha}$ is the first derivative of α, and $p(\alpha = R, \dot{\alpha})$ is the joint PDF of α and $\dot{\alpha}$ at $\alpha = R$,

$$p(\alpha, \dot{\alpha}) = \frac{\alpha}{b_0} \exp\left(-\frac{\alpha^2}{2b_0}\right) \cdot \frac{1}{\sqrt{2\pi b_2}} \exp\left(-\frac{\dot{\alpha}^2}{2b_2}\right). \tag{3.20}$$

By substituting the moments b_0 and b_2 obtained from (3.16) and (3.17) into (3.20), we than have the closed form of LCR as

$$L(R) = \frac{2\sqrt{\pi} f_m R}{\sqrt{N}} \exp\left(-\frac{R^2}{N}\right). \tag{3.21}$$

Finally, by assuming the envelop α following Rayleigh distribution and substituting (3.21) into (3.18), we can derive the closed form of AFD as

$$T(R) = \frac{\sqrt{N}}{2\sqrt{\pi} f_m R} \left(\exp\left(\frac{R^2}{N}\right) - 1\right). \tag{3.22}$$

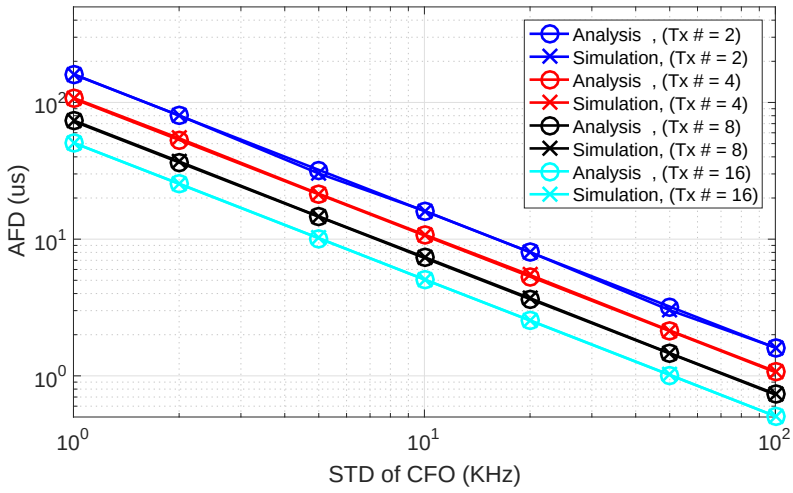

Fig. 3.5 The comparison of analytical AFD results and Monte-Carlo simulation..

(b) Validity of the AFD derivation

We conduct a Monte-Carlo simulation to verify the derivation. Specifically, we generate the beating signal by passing a continuous wave with 0-dB power through the CT channel shown in Fig. 3.2. The CFO and the power offset are set to follow the Gaussian distribution and normalized Rayleigh distribution to fit the AFD model. The phase offsets are again set as a uniformly distributed random variable between 0 to 2π. We consider the CT scenarios with transmitter numbers of 2, 4, 8, and 16. For each scenario, we sweep the STD of CFO to from 1 kHz to 100 kHz, and the threshold R is set to be -3 dB. For each of the combination,10000 realizations are randomly generated under a 10 MHz sample rate.

Fig. 3.5 shows the simulated and calculated AFD results versus different transmitter antenna numbers. The lines with circle markers represented the AFD calculated by (3.22) and those with cross markers are the simulation results. In addition, different colors represent the AFD of different transmitter number.

From the results, two observations can be made. First, we can see that the analytical results closely match the simulation results, which proves the validity of the derivation. Next, the results confirm that, with the increasing of transmitter number and the STD of CFO, the AFD decreases.

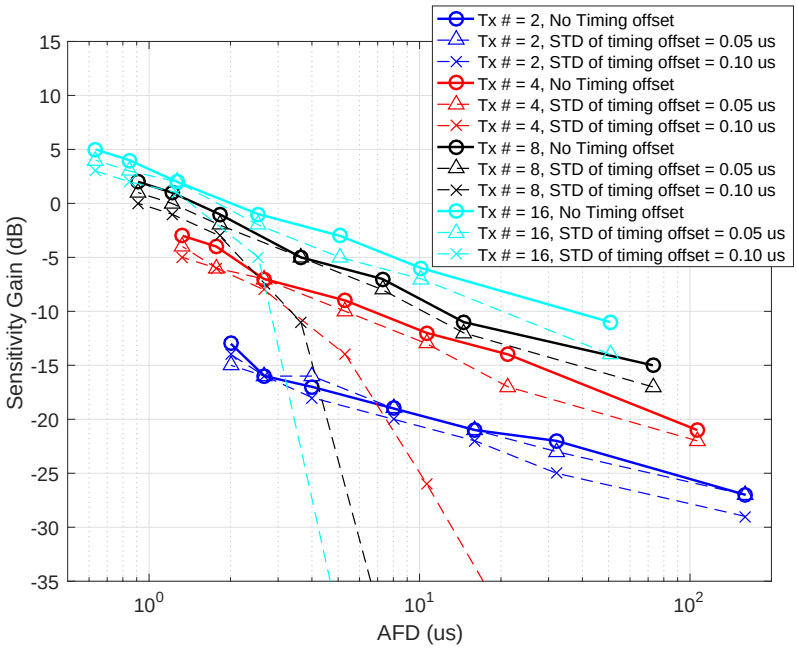

Fig. 3.6 The relationship between AFD and the sensitivity gain under the effect of timing offset.

(c) AFD v.s. sensitivity Gain

Next, we evaluate the receiver performance under different AFD. The reception performance is estimated in terms of the sensitivity gain and based on the simulation platform of the IEEE 802.15.4 system. The model of power offset, CFO, and phase offset are the same as those in the Monte-Carlo simulation. The AFDs are calculated according to the transmitter number and the STD of CFO, and the threshold is set to be -3 dB again. In addition, we also evaluate the effect of timing offset by modeling it as a Gaussian random variable. The timing offsets with different STD (0, 0.05 μs, 0.1 μs, and 0.2 μs) are evaluated. Each sensitivity gain is measured with 10000 randomly generated 20-byte packets.

Fig. 3.6 shows the relationship between the averaged sensitivity gain of each combination and the corresponding AFD. The transmitter number is color-coded, and the different timing offsets are presented by different marks.

First of all, we can see that the AFD has a high correlation with the sensitivity gain, and we prove that a small AFD is a necessary condition for good performance. When the

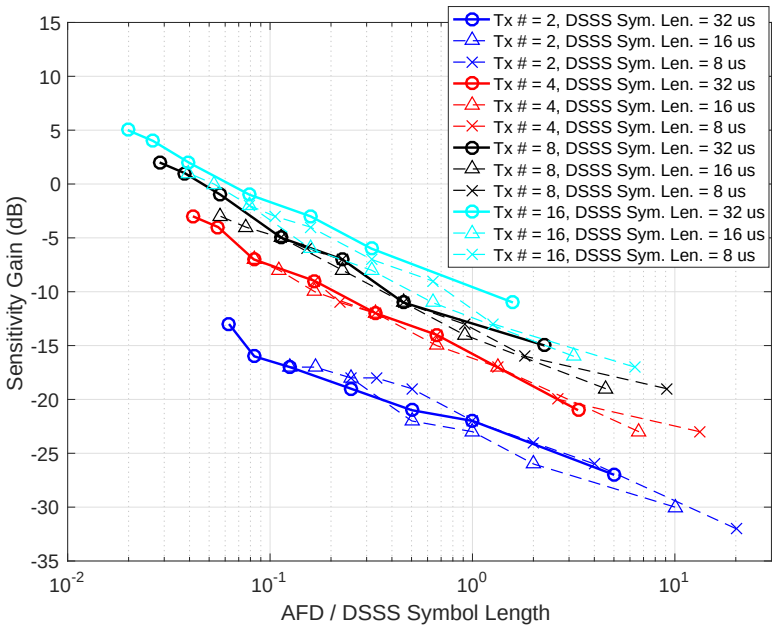

Fig. 3.7 The relationship between AFD and the sensitivity gain by using different DSSS symbol length.

timing offset is zero or small (0.05 μs of STD), the receiver only suffers from the fading-like beating effect, and the sensitivity gain is almost linear to the AFD in the log domain. On the other hand, in the presence of larger timing offsets (0.1 μs of STD), the resulted ISI bounds the maximum achievable signal-to-interference-plus-noise (SINR). In such cases, the correlation still holds, but the relationship is no longer linear. Particularly, in the large AFD region where a high SINR is required for successful receptions, the bounded SINR leads to a PER floor and makes the sensitivity gain diverge. Note that a timing offset with larger than 0.2 μs STD always leads to PER floors regardless of the AFD, so the results are not shown in the figure.

Then, we discuss the effect of multiple transmitters. The effect of having more transmitters is two-sided. It increases the total received power and reduces the AFD. On the other hand, it also reduces the achievable SINR when the timing offset exists. To elaborate, when counting the SINR, all the transmitters contribute to the signal power, but the number of the transmitters contributing to the interference power is always one fewer since there would be one treated as the wanted signal. This difference in the contributor number is especially significant when the transmitter number is small, which makes

the small transmitter number case (particularly the two-transmitter case) more beneficial from the SINR point of view.

From the evaluation results, if the timing offset is negligible (such as the cases with the STD of timing offset being 0 or 0.05 μs), we can see that more transmitters generally lead to better performance. On the other hand, in the presence of large timing offset (the case with the STD of timing offset being 0.1 μs), having more than two transmitters instead leads to PER floors in the large AFD region. In short, whether increasing the transmitter number is beneficial or not strongly depends on the degree of the timing offset.

3.3.3 AFD and the DSSS symbol Length

In order to investigate the relationship between the AFD and DSSS symbol length, we next evaluate the receiver performance under difference DSSS symbol lengths. We fix the up-sampling rate as 8 times and generate two shorter DSS codes, i.e. 1-bit-to-8-chip and 2-bit-to-16-chip, by using parts of the original 4-bit-to-32-chip DSSS code. The resulted DSSS symbol lengths are 8 and 16 us, respectively. The other setup is similar to the previous evaluation, and we focus on the evaluation of zero timing offset only.

Fig. 3.7 shows the evaluation result. In the X-axis, we normalize the AFD by the corresponding DSSS symbol length. We can see that after the normalization, the sensitivity-gain-to-AFD curves for different DSSS symbol lengths are very similar, and the sensitivity loss becomes minor when the AFD is smaller than 0.1 times of the DSSS symbol length.

3.3.4 Real Measurement of the STD of CFO

Finally, to estimate the actual AFD in practical systems, we measure the STD of CFO of 83 TelosB nodes, which are representative sensors that equip with 2.4-GHz IEEE-802.15.4-compliant transceiver chips, TI CC2420. We find that the distribution is close to Gaussian, and the measured STD of CFO is 17.94 kHz. From this result, we calculate the estimations of the AFD for different transmitters by again setting the threshold to be -3 dB. Moreover, by mapping the estimation of the AFD on Fig. 3.6, the sensitivity loss can also be estimated. We list the estimated AFD and the expected sensitivity gain in Table 4.1 ("TO" represents the timing offset).

Table 3.1 Estimated AFD and sensitivity loss for different transmitters

Transmitter Number		2	4	8	16
AFD (us)		8.9	5.9	4.0	2.8
Sensitivity	No TO	19.3	9.2	5.2	1.6
Loss	STD of TO: 0.05 μs	19.3	10.4	5.3	2.4
(dB)	STD of TO: 0.1 μs	20.3	15.8	14.8	9.8

3.4 Summary

We analyzed the channel model and fading characteristics of CT in this chapter. We showed that CT is very similar to the wireless multi-hop fading channel, and the affecting factors are the same - the power, phase, timing offset, and CFO. Moreover, we highlight the difference in the numerical scale between the CT the the multi-path channel. Particularly, the CFO in CT is typically orders larger than that of multi-path channel, which makes the CFO a dominating factor to the receiver performance in CT. Next, we discussed the systems that have more potentiality to be applied in CT, and we also pointed out the the fading duration of the beating signal resulting from the CFO is an important parameter to the receiver performance. In order to character the performance degradation resulted from the beating signal, the LCR and AFD, two important factors that characterizes the fading behavior of the beating, were derived. With the information of AFD, the average width of deep fading resulted from beating can be estimated, and hence the potential performance degradation resulted from CT can be assessed. Simulation results were given to prove the correctness of the derivation and to demonstrate the close correlation between AFD and the sensitivity loss caused by CT. As the final and most important conclusion, we proved that the AFD decreases with the increasing of the transmitter number and the CFO deviations of the transmitters.

Chapter 4

Evaluations of CT on IoT Standards

In this section, we present our comprehensive evaluation of the receiver performance under CT. We first discuss our considerations toward conducting fair and extensive evaluations. A comprehensive and reproducibility evaluation methodology will be presented, which take not only the impairment modeling but also evaluation metrics and platform into full consideration. Specifically, all the significant transmitter impairments, including, the power, timing, phase, and most importantly the CFO between the transmitters are modeled and evaluated jointly. For the evaluation metrics, instead of adopting the degradation-insensitive packet reception rate (PRR), we measure the real packet error rate (PER) over SNR performance of CT. With this metric, apple-to-apple comparisons between the performance of CT links and conventional collision-free can be conducted. Considering the controllability and reproducibility of the evaluation platform, the packets under the CT effect is generated by a baseband simulator and synthesized by a signal generator. The receiver performance is then evaluated by both real on-the-shelf transceiver module as well as the simulator to obtain representative results. Finally, the evaluation results on the IEEE 802.15.4, the IEEE 802.15.4g, and LoRa system will be demonstrated.

4.1 Evaluation methodology

In this section, we discuss our methodology for fair and comprehensive evaluation of the receiver performance under CT. There would be two subsections addressing the evaluation metric and evaluation platform, respectively.

4.1.1 Evaluation platform

The evaluations in previous work are mainly conducted experimentally on local or public wireless sensor network testbeds. However, the reproducibility on local test beds and the controllability of environment on the public test beds are of great concerns. Particular, the test beds usually provide no accessibility to the CFO of each node as well as the link attenuation of each link.

In order to provide fine-grained and reproducible control to the attenuation and the other transmitter offsets, we implement a software packets generator as well as a transmitter offset simulator to model the signal under CT. To obtain convincing results, a joint software-simulation and real-chip-emulation platform is implemented. While the

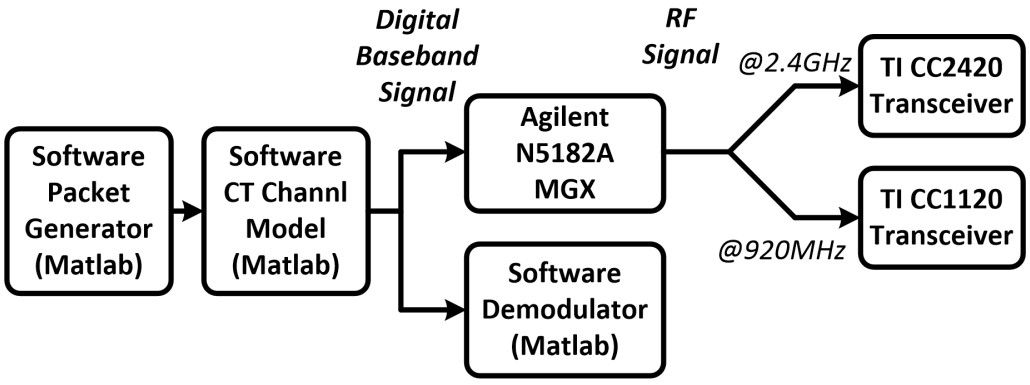

Fig. 4.1 The illustration of the joint simulation-and-emulation platform.

simulation platform allows us to gain more insight of the how CT affects the receiver, the emulation platform enables us to examine the real performance of off-the-shelf RF module.

We implement a software packets generator and a CT channel simulator on Matlab. The generated packets are then fed to a software demodulator and off-the-shelf RF modules for demodulation. For the real-chip emulation, an Agilent N5182A MXG signal generator is used to up-convert the baseband packets to 2.4 GHz and 920 MHz band. Next, we configure the TI CC2420 [52], a 2.4 GHz IEEE 802.15.4 compliant transceiver chip, and TI CC1120 [53], a sub-GHz IEEE 802.15.4g compliant transceiver chip, to perform demodulation for the RF packets. Fig. 4.1 illustrates the evaluation platform.

4.1.2 Evaluation metric

A discriminative metric is crucial for a fair evaluation of CT. However, the packet reception rate (PRR), the metric being adopted in many previous works for reliability evaluation, is often over-optimistic. Instead of indicating how much margin is left for reliable receiving, PRR simply reflects the error rate performance under a particular received power level. In most of the cases where the nodes are deployed to allow reliable receptions in ST links with power margins, the possible degradation resulted from CT might be underestimated.

To honestly reflect the gain and loss of CT, we define a new metric, the *sensitivity gain* between CT and collision-free one-transmitter (1-Tx) link, for our evaluations. Sensitivity, defined as the minimum received power to guarantee a certain error rate performance,

is widely adopted to evaluate the capability of receivers. For example, the sensitivity specification in IEEE 802.15.4 standard is to be able to receive a 20-byte packet whose input power is less than -85 dBm with less than 1 % packet error rate (PER).

However, the conventional sensitivity measurement does not reflect the multiple transmitter effects in CT, since it the power is normalized in receiver input. To tackle this, we measure the *maximum allowable attenuation* to guarantee a PER performance of 1 %. In our evaluation, we assume that transmitter 1 in Fig. 3.2 with the unity transmission power and the others are with a minus power offset against transmitter 1. After the combination, the signal is attenuated by K dB before fed to the receiver. In our evaluation, the attenuation K will be gradually increased until the PER reaches 1 %, and the corresponding K value represents the maximum allowable attenuation.

Since what we really care is the gain and loss between CT and ST links, the absolute K value, which strongly depends on the noise model and the receiver architecture, is irrelevant in this work. As the final outcome of our evaluation, we calculate the relative difference of K value between the CT and ST link. We refer the aforementioned difference to as *sensitivity gain* in this work. To give an intuitive explanation, if CT results in constructive combination, the combined signal should be able to endure greater attenuation while keeping the same error rate performance. In this case, the K value in the CT link would be larger than that in the ST one and results in a positive sensitivity gain. (A positive sensitivity gain indicates that the receiver is more reliable in CT link and vice versa.)

4.1.3 Evaluation scenario

The purpose of this evaluation is to comprehensively evaluate the receiver performance under all effects and give specific numbers about the requirements. We consider two CT scenarios. The first one is the two-transmitter (2-Tx) scenario, where the first one is assumed to have zero offsets and larger power. We sweep the power, timing offset, and CFO of the second transmitter in a three-dimension offset space, and evaluate the corresponding receiver performance in terms of sensitivity gain. Besides, we introduce a random phase offset uniformly distributed between 0 and 2π to the second transmitter for every individual packet, instead of making the phase offset as the fourth dimension since it is less relevant.

The second one is the multiple-transmitter (M-Tx) scenario. In the 2-Tx scenario, the fading duration is fixed and can be easily calculated by a given CFO and power offset. However, the number of the transmitter joining the CT in the practical WSN scenario is not controllable. Therefore, we also evaluate the M-Tx scenario. One thing we need to emphasized is that, in the M-Tx scenario, every transmitter creates a degree of freedom to all the offsets, the dimension of the offset space grows dramatically, which makes it no longer feasible and informative to consider the offset in each transmitter individually. Toward this, our strategy is to model the offsets as different random variables and evaluate the average effects.

4.2 Evaluations on IEEE 802.15.4

4.2.1 Overview of IEEE 802.15.4

IEEE 802 WG15 published IEEE 802.15.4 standard which specifies the lower communication protocol layer, i.e., the physical layer (PHY) and medium access control layer (MAC), for low-rate WPSN [12]. IEEE 802.15.4 has been a widely adopted in WSN applications. Particularly, the ZigBee Alliance releases the ZigBee specifications based on IEEE 802.15.4 standard for short range applications such as the smart home. Moreover, IETF develops the 6LoWPAN to sent IPv6 packets over IEEE 802.15.4 standard-based networks. The Thread platform promoted by many companies including Google also adopts IEEE 802.15.4 as its fundament.

4.2.2 Physical-layer design of IEEE 802.15.4

From the PHY point of view, the IEEE 802.15.4 adopts the direct sequence spread spectrum (DSSS), which spread the signal to a wider band to increase the robustness over interference and jamming. For the physical channel, 802.15.4 specifies the operation in three frequency band 1) 2.4 GHz world-wide ISM band, 2) 868 MHz band for Europe, and 3) 915 MHz band for America. The 2.4 GHz band, ranging from 2400-2483.5 MHz, supports 16 channels with a guard band of 5 MHz, and support a data rate of 250 kb/s. In 2,4GHz, the 32-chip PN sequences are employed for spreading 4 bits, and therefore, the

spreading rate is 8 times. The chips are then modulated using offset quadrature phase-shift keying (O-QPSK) with half-sine pulse shaping. The 868 MHz band supports only 1 channel, but 10 channels are defined in the 915 MHz band. In 868 MHz, the data rate supported is 20 kb/s while the 915 MHz band offers a data rate of 40 kb/s. Furthermore, the 868/915 MHz PHY employs binary phase-shift keying (BPSK) with raised cosine pulse shaping for chip modulation. For spread spectrum; each bit is mapped into a 16-chip PN sequence.

4.2.3 Evaluation parameters

In this evaluation, we focus on the most commonly adopted O-QPSK PHY mode f the IEEE 802.15.4 with O-QPSK modulation, 250-Kbps bit rate, and 8-time up-sampling by DSSS. In the 2-Tx scenario, the power offset of 0, 1, 3, and 5 dB are investigated. We sweep the timing offset and CFO from of 0 μs to 0.75 μs and 0 Hz to 200 kHz, respectively. We choose such a range because 200 kHz is slightly over the maximum allowable CFO, and 0.75 μs is 0.75 times of the chip time in the IEEE 802.15.4 system. Note that, we have confirmed that the effect of the negative value of timing offset is symmetric to the positive one in the interesting region (several chip time). The evaluation in [31] also proves the symmetricity between the positive and negative time-offset. In order to reduce redundancy and improve readability, we present the result of the positive offset only. For each combination of the offsets, the corresponding the sensitivity gain would be evaluated by more than 1000 randomly generated 20-byte packets.

In the M-Tx scenario, we evaluate the scenario with transmitter number being 2, 4, 8, and 16. The offset are modeled as independent random variables for different transmitters. Specifically, the power offset is modeled as Rayleigh distribution, the CFO and timing offset are modeled as Gaussian distribution, and the phase offset is again modeled as uniform distribution. In the simulation, we assume the timing and frequency of the receiver are perfectly synchronized to the strongest packet.

4.2.4 Receiver architecture

We compare two different receiver architectures. We call the first architectures the practical architecture, where the receiver performs O-QPSK demodulation and de-spreading

individually (first demodulation and then de-spreading). This is the actual design that adopted in the IEEE 802.15.4 RF module due to its simplicity. We adopt the non-coherent limiter-discriminator [54] for demodulation. Note that the modulation in IEEE 802.15.4 is O-QPSK [12], which can not only be treated as QPSK and received by coherent demodulator but also can be viewed as MSK and demodulated by non-coherent FSK receiver [55]. Next, the demodulated chips are further de-spread by a hard-input de-spreader.

For a comparison, we also evaluate the conventional DSSS matched filter based design. Specifically, in the receiver, there are 16 matched filters that correspond to the timing-domain O-QPSK-modulated waveform of the 16 possible DSSS code. The receiver correlate the the received signal with 16 matched filter and select the one with maximum correlation value. The matched filter receiver can provide better sensitivity, and is robust to the timing offset due to the pulse-like auto-correlation property. However, since the matched filter receiver correlate the whole DSSS code, the autocorrelation property can be easily corrupted by CFO. Moreover, the matched filter is much expensive than the first one. Therefore, it is not adopted in practical IEEE 802.15.4 solutions.

4.2.5 Results and observations

Fig. 4.2 and Fig. 4.3 show the simulation and emulation results for the IEEE 802.15.4 systems under 2-Tx scenario. Specifically, in each figure, subplot (a) to (d) show the results for 0, 1, 3 and 5 dB power offset, respectively. For each subplot, the X- and Y-axis indicate the CFO and timing offset, respectively. We use the colored-coded 2D contour maps to illustrate the sensitivity gain, where the blue color indicates positive sensitivity gain, and the red color indicates minus one, or more intuitively, sensitivity loss. The deeper the color is, the larger the gain or loss is, and white color indicates that CT performance evenly with the collision-free 1-Tx links.

Fig. 4.4 and Fig. 4.5 show the simulation results for the IEEE 802.15.4 systems. Specifically, in each figure, subplot (a) to (d) show the results for the case of 2, 4, 8, and 16 transmitters, respectively. For each subplot, the X- and Y-axis indicate the STD of CFO and timing offset, respectively.

Let us first examine the most critical case - the case with zero power offset shown in the subplot (a) of Fig. 4.2 and Fig. 4.3. In this case, the timing offset and CFO become critical to the receiver performance. For the IEEE 802.15.4 system, both the simulation

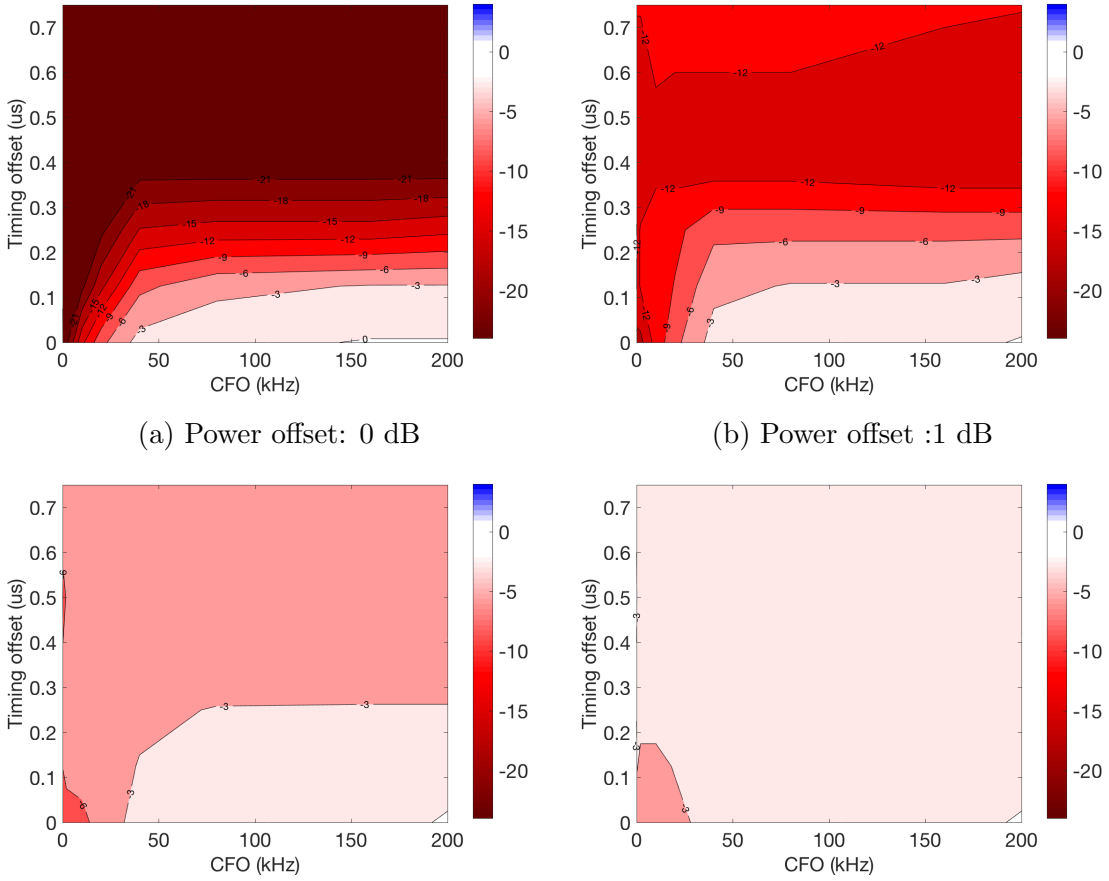

(a) Power offset: 0 dB

(b) Power offset :1 dB

(c) Power offset: 3 dB

(d) Power offset: 5 dB

Fig. 4.2 Simulation results for IEEE 802.15.4 system over different power, timing offset, and CFO using practical receiver architecture under 2-Tx scenario.

and emulation show a surviving zone for almost no-loss reception in the area where the frequency offset is larger than 30 kHz and the timing offset is smaller than 0.2 μs. This surviving zone, which allows the receiver to survive CT even in the scenarios without the capture effect, is of great importance for the success in CT.

As has been reported in the previous work [14], the timing offset needs to be kept as small as possible. However, the 0.5 μs requirement reported in the previous work is obviously too loose. For our evaluation, 0.2 μs is a more accurate criterion for the timing offset in order to ensure no-loss receptions for the IEEE 802.15.4 receivers.

Next, we examine our main effect - the CFO. Both the simulation and emulation show a surviving zone in the higher CFO region. As we discuss later, the higher CFO results in

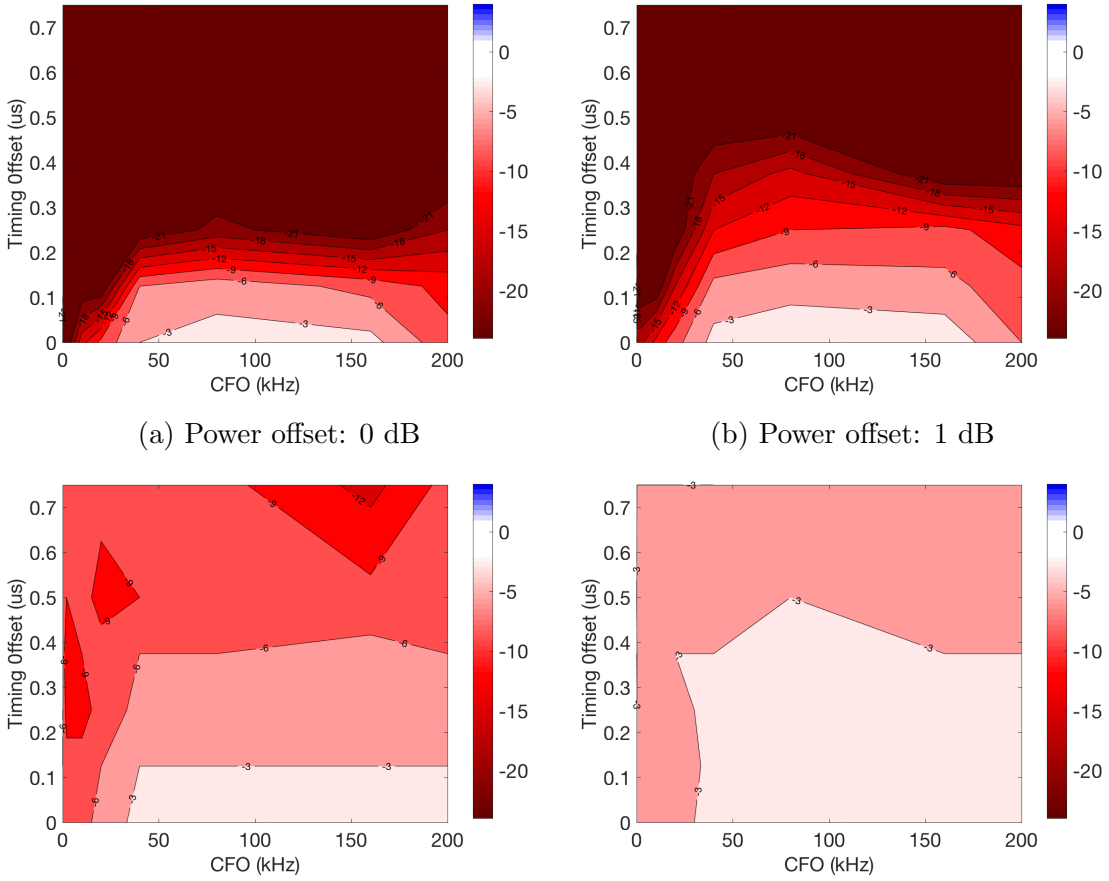

(a) Power offset: 0 dB

(b) Power offset: 1 dB

(c) Power offset: 3 dB

(d) Power offset: 5 dB

Fig. 4.3 Emulation results for IEEE 802.15.4 system over power, timing offset, and CFO under 2-Tx scenario.

shorter fading duration. We can see that the packets affected by the beating with short fading duration enjoy comparable reliability as collision-free 1-Tx links. On the other hand, when the CFO is small, the fading duration of the beating is too long, the symbol and hence the whole packet could fail even with zero timing offset.

We see a mismatch between the simulation and emulation when the CFO is larger than 180 kHz. While the loss becomes significant in the emulation, but the receiver in the simulation is not affected. This is because our simulation assumes the receiver is perfectly synchronized with the first transmitter, while in the real chip, the large CFO could affect the accuracy of the preamble detection, timing acquisition, and frequency recovery. Lastly, we can see that the light-color area increases when the power offset increases, and a 3-dB power offset is generally enough to allow the capture effect.

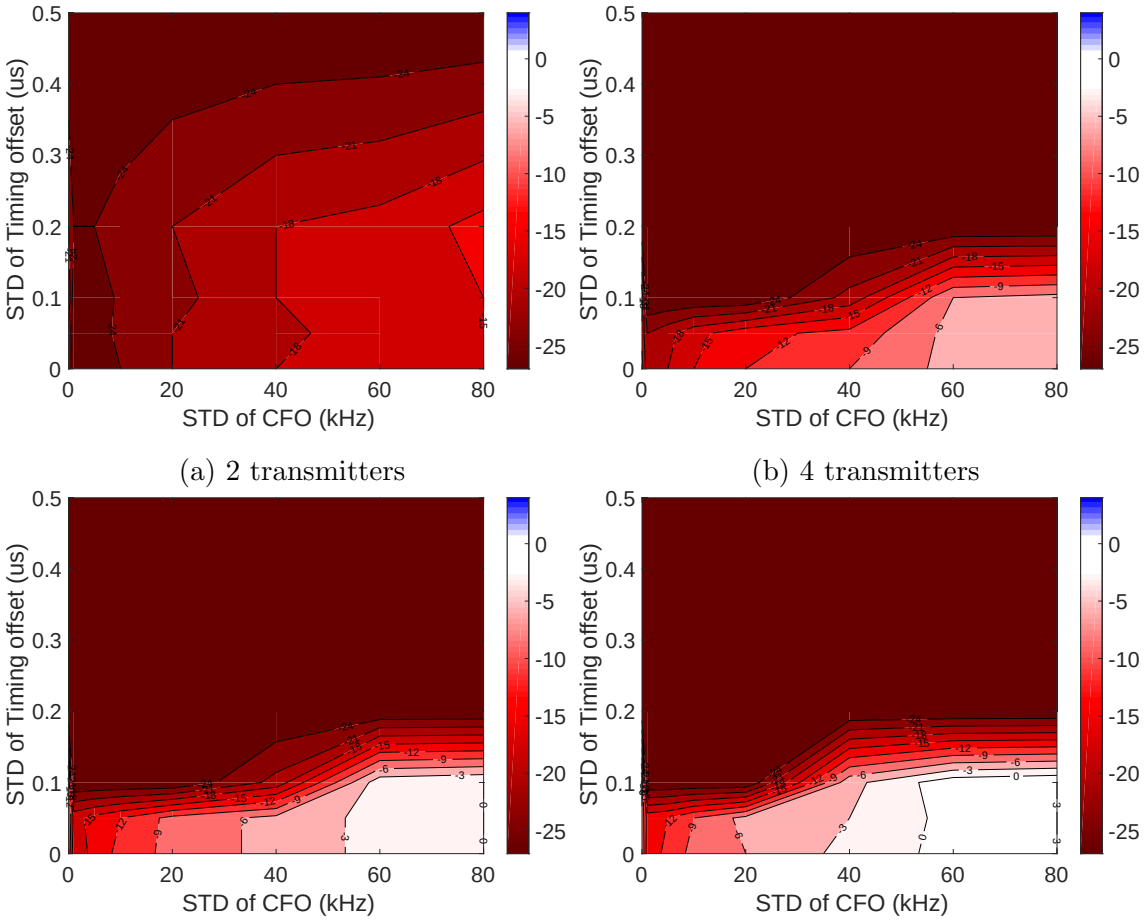

(a) 2 transmitters (b) 4 transmitters

(c) 8 transmitters (d) 16 transmitters

Fig. 4.4 Simulation results for IEEE 802.15.4 system over different transmitter number using the practical receiver under M-Tx scenario.

In the M-Tx scenario with random offset, the conclusion is the sam as that of 2-Tx case. In Fig. 4.4, we can see that the surviving zone is locates at low timing offset and high CFO area. Moreover, we also observe the trend that more transmitters, the better the performance in the surviving zone.

Finally, we can see that the matched-filter architecture is valuable to CT. As shown in in Fig. 4.5, the matched filter can tolerate high timing offset due to the good auto-correlation property of the DSSS code. However, in the presence of the CFO, the auto-correlation property is ruined, and hence the immunity to interference degrades significantly. Moreover, we can see that, if the matched filter is adopted, the performance degrades dramatically when the transmitter number is larger than four. The reason is, in the presence

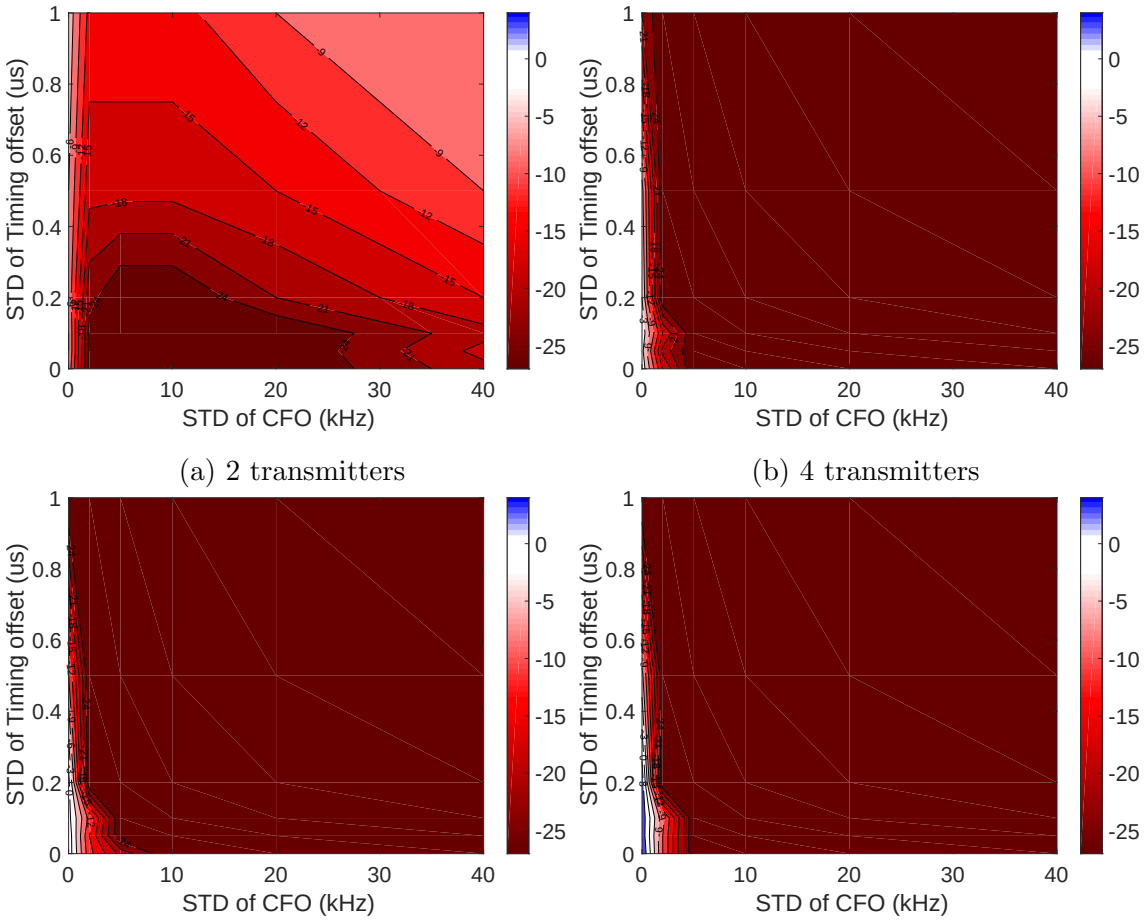

(a) 2 transmitters (b) 4 transmitters

(c) 8 transmitters (d) 16 transmitters

Fig. 4.5 Simulation results for IEEE 802.15.4 system over different transmitter number using the matched-filter receiver under M-Tx scenario.

of either timing offset or CFO, the concurrent transmitted packet becomes independent interference instead. Therefore, increasing the transmitter number only enhance the interference power.

4.2.6 Discussion of IEEE 802.15.4 under CT

Next, we investigate the phenomena that the high CFO and results into better performance. As we have discussed in the Chapter 3, the ECC is a key factor to determine whether a system can survive the CT or not. In the IEEE 802.15.4system, the direct sequence spread spectrum (DSSS) technique adopted, which encodes 4 contiguous bits into

a longer symbol that consists of 32 cross-correlated chips, can be treated as an ECC with a rate of 1/8. However, since the encoding is performed on contiguous bits, DSSS could fail to recover the symbols if the fading duration is longer than the DSSS symbol.

To illustrate, we conduct simulations to examine the chip error of demodulation and bit error of de-spreading under different fading durations. Fig. 4.6 (a) and (b) show the simulation result of packet reception under a two-transmitter (2-Tx) CT scenario with 32 kHz and 4 kHz CFO and zero power and timing offset. The two CFO values correspond to the long and short fading duration cases, respectively, where the higher CFO results in shorter AFD. We can see that the bursty chip errors occur in the deeply faded part of beating in both cases. However, bit errors can be found only in the long fading duration scenario (subplot (b)), while in short fading duration scenario, the demodulation errors are fully recovered by DSSS.

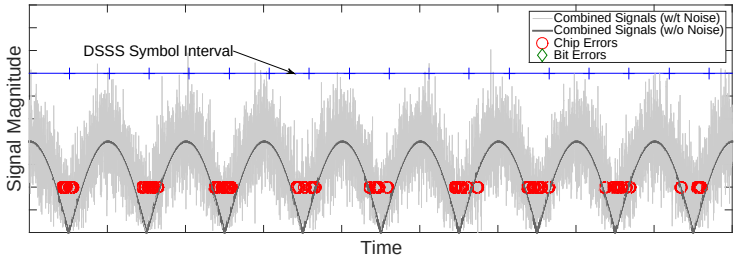

(a) Beating with short fading duration

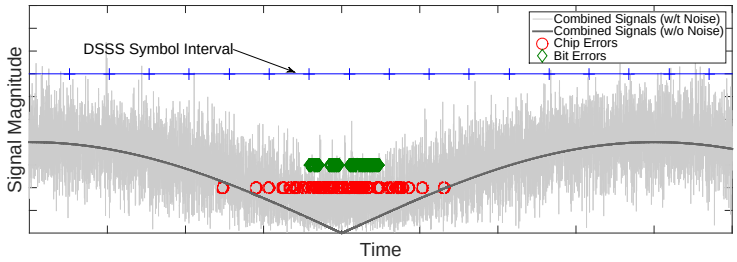

(b) Beating with long fading duration

Fig. 4.6 The illustrations of beatings with short and long fading duration and the resulted decoding errors.

We also confirm that degradation results from long fading duration actually occurs in real over-the-air scenarios. Specifically, we demonstrate that the variation of RSSI values increases significantly due to the beating effect. Moreover, we show that the short beating

Table 4.1 CFO of the nodes used in the experiment

	1-Tx	2-Tx narrow	2-Tx wide	2-Tx very wide
Node	A	A+B	A+C	A+D
CFO	N/A	37.8 kHz	3.8 kHz	0.2 kHz

results in no worse performance than the 1-Tx links, but wide and very wide beating hurt the performance significantly.

Based on the Glossy protocol implementation [14] and TelosB sensors, we build up the experiment environment with one initiator, one or two relays, and five receivers nodes. The initiator sends an packet, which triggers the CT of the relay nodes in the next Glossy slots. The PRR and RSSI of the CT packets will then be recored, while the trigger packet will be ignored.

The five receivers, located 3, 6, 9, 12, and 15 m away from the relay nodes, are programmed to record the PRR and RSSI. In order to test the small power offset scenarios, the relay nodes are placed close to each other. Like the previous simulation and emulation, random generated 20-byte packets are adopted, and the experiment is carried out on channel 26 whose center frequency is 2.48GHz. In addition, the output power of all the relay nodes is adjusted to -15 dBm.

We benchmark the 2-Tx CT links of narrow, wide, and very wide beating with the 1-Tx link. Specifically, four nodes are particularly selected as the relay nodes, whose carrier frequencies offset when operating at channel 26 are listed in Table 4.1. We use Node A as the main reference node, and the CFO between Node A and Node B, C, and D correspond to narrow, wide, and very wide beating, respectively. Finally, the experiment is carried out over 16 independent places, including long corridors, large seminar halls, and open space.

Fig. 4.7 (a) to (c) show the results for the mean of the RSSI, the standard deviation of the RSSI, and the PRR, respectively. The horizontal axes are the distance between the relay and receiver nodes, and all of the three subplots are the averaged results over 16 places. We can see clearly that 2-Tx CT links indeed enhance the mean value of RSSI about 3 dB, but the standard deviation also increases significantly due to the beating effect. From the PRR point of view, we can see that the 2-Tx link with narrow beating performs evenly with the 1-Tx one, but the PRRs of the 2-Tx links with wide and very wide beating degrade significantly.

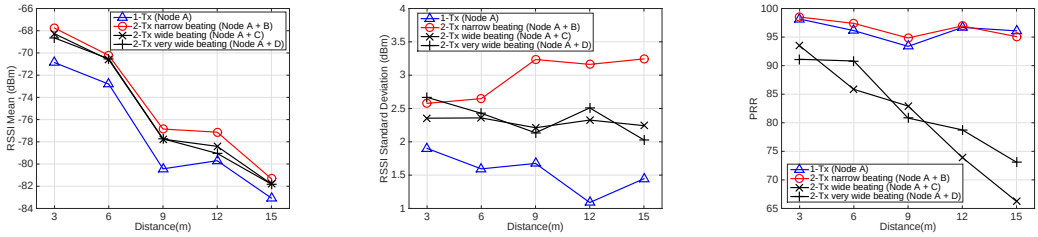

(a) Mean of RSSI (b) Standard deviation of RSSI (c) Average PRR

Fig. 4.7 The measurement result of RSSI and PRR in the IEEE 802.15.4 over-the-air experiments.

4.3 Evaluations on IEEE 802.15.4g

4.3.1 Overview of IEEE 802.15.4g

The IEEE 802.15.4g is a new IoT-oriented physical-layer standard particular for smart grids [56]. In the early stage of IEEE 802.15.4 standardization, amendment of 802.15.4 to meet the requirement of the smart grid is considered. However, the communication range, robustness, and coexistence characteristics required for smart gird application have not been met with existing 802 standards including IEEE 802.15.4. Therefore, IEEE standardizes a new PHY for SUN application as IEEE 802.15.4g. IEEE 802.15.4g addresses principally outdoor low-rate network requirements for wireless smart metering utility. It defines an alternate PHY and only those MAC modifications needed to support its implementation.

4.3.2 Physical-layer design of IEEE 802.15.4g

Three alternative physical layer design are provided for SUN devices. The MR-FSK PHY was selected to provide good transmit power efficiency due to the constant envelope of the transmit signal. The MR-O-QPSK(DSSS) PHY shares the characteristics of the current IEEE 802.15.4 O-QPSK PHY, making multi-mode systems more cost-effective and easier to design. Finally, the MR-OFDM PHY was designed to provide higher data rates in channels that have significant delay spread. In this work, we mainly focus on the MR-FSK PHY since it is the most common adopted one.

The feature of 802.15.4g is as follows. IEEE 802.15.4g supports the operation in any of the regionally available license-exempt frequency bands. The main operation band is 920MHz. The date rate is from 4.8 kbps to 1000 kbps. The link margin of 802.15.4g is optimized for the environmental conditions encountered in smart grid deployments, which is principally outdoor and with a maximum range of 1 km. The PHY frame sizes up to 1500 bytes. IEEE 802.15.4g is designed for the connectivity to at least one thousand direct neighbors characteristic of dense urban deployment

4.3.3 Evaluation parameters

For the IEEE 802.15.4g system [56] on the sub-GHz band, we evaluate the MR-FSK mode on the 920 MHz band, with bare 2-FSK modulation, 100-Kbps bit rate, and without any error correcting mechanism. Similar to the IEEE 802.15.4 evaluation, the power offset of 0, 1, 3, and 5 dB are investigated. We sweep the timing offset and CFO from of 0 μs to 10 μs and 0 Hz to 40 kHz, respectively. Similarly, we choose the parameter to cover the maximum allowable CFO and the symbol time in the IEEE 802.15.4g system. For each combination of the offsets, the corresponding the sensitivity gain would be evaluated by more than 1000 randomly generated 20-byte packets.

4.3.4 Results and discussions

Fig. 4.8 and Fig. 4.9 show the evaluation results for the IEEE 802.15.4g systems. Comparing with the results of the IEEE 802.15.4 system, it is obviously that there is no similar surviving zone for reliable receiving in the IEEE 802.15.4g system. This meets our expectation that the deep fading of the beating effect causes unrecoverable demodulation errors and prohibits the PER from being lower than 1%. Second, the threshold for capture effect of the IEEE 802.15.4g system is higher than that of the IEEE 802.15.4 system. We can see that the sensitivity loss is still large even with 3 dB power offset. Moreover, we find that the performance in emulation is significantly worse than that in the simulation. Note that, while the preamble of the IEEE 802.15.4 is also protected by DSSS, that of the IEEE 802.15.4g is only a sequence of FSK-modulated symbols. The emulation results indicate that the preamble detection, timing acquisition, and frequency recovery function are more seriously affected by CT. Therefore, we conclude that the applicability of CT in the IEEE 802.15.4g system is weak.

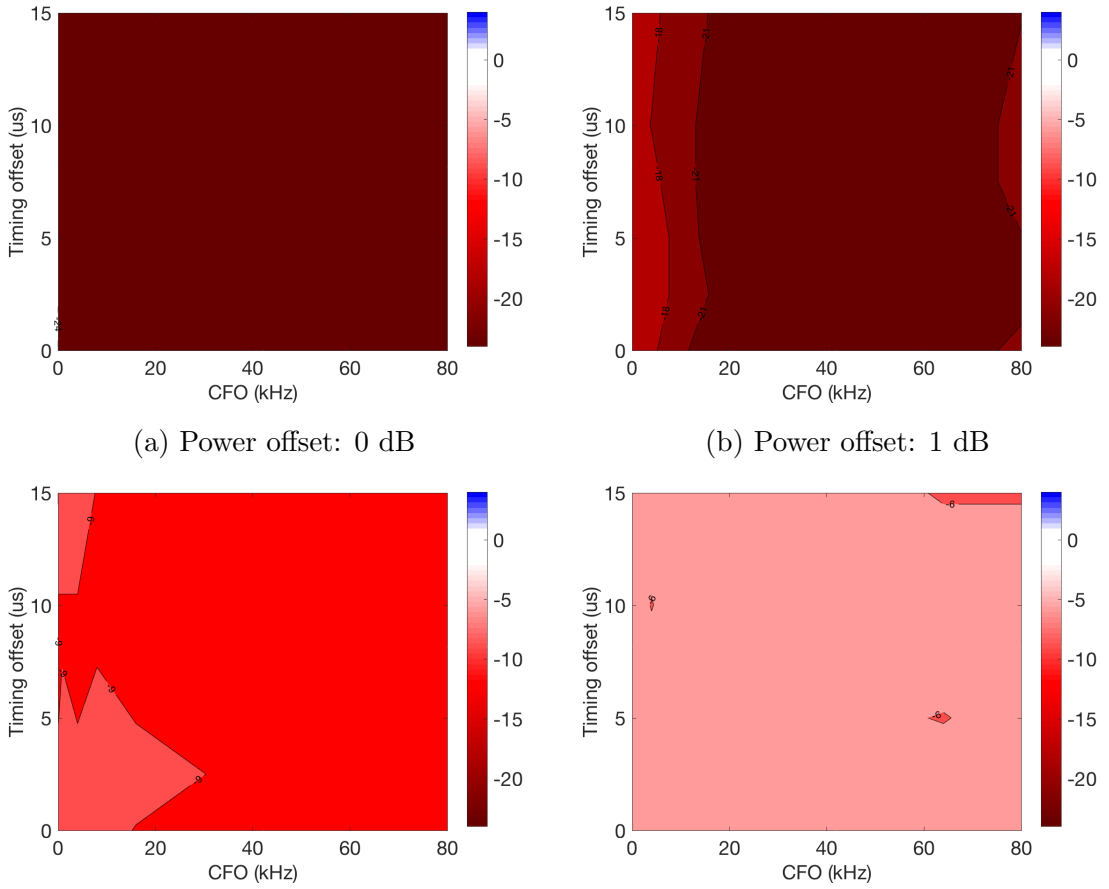

(a) Power offset: 0 dB

(b) Power offset: 1 dB

(c) Power offset: 3 dB

(d) Power offset: 5 dB

Fig. 4.8 Simulation results for IEEE 802.15.4g system over power, timing offset, and CFO.

4.4 Evaluations on LoRa

4.4.1 Overview of LoRa

Lora is one of the Low Power Wide Area Network (LPWAN) specifications that recently attracts much attention. LoRa is a proprietary Sub-GHz physical-layer standard that adopts M-ary FSK modulation and Chirp Spread Spectrum (CSS) technique [57]. Thanks to the CSS, LoRa is robust to interference and its transmission range can be longer than 10 km when configured into the lowest rate-mode (293 bps) [58]. The merits of Lora include not only the wide coverage (the communication range is reported to be 15 km) but also the great flexibility to trade the sensitivity for higher throughput (can speed up 100X by sacrificing 20 dB sensitivity). In both academia and industry, many groups

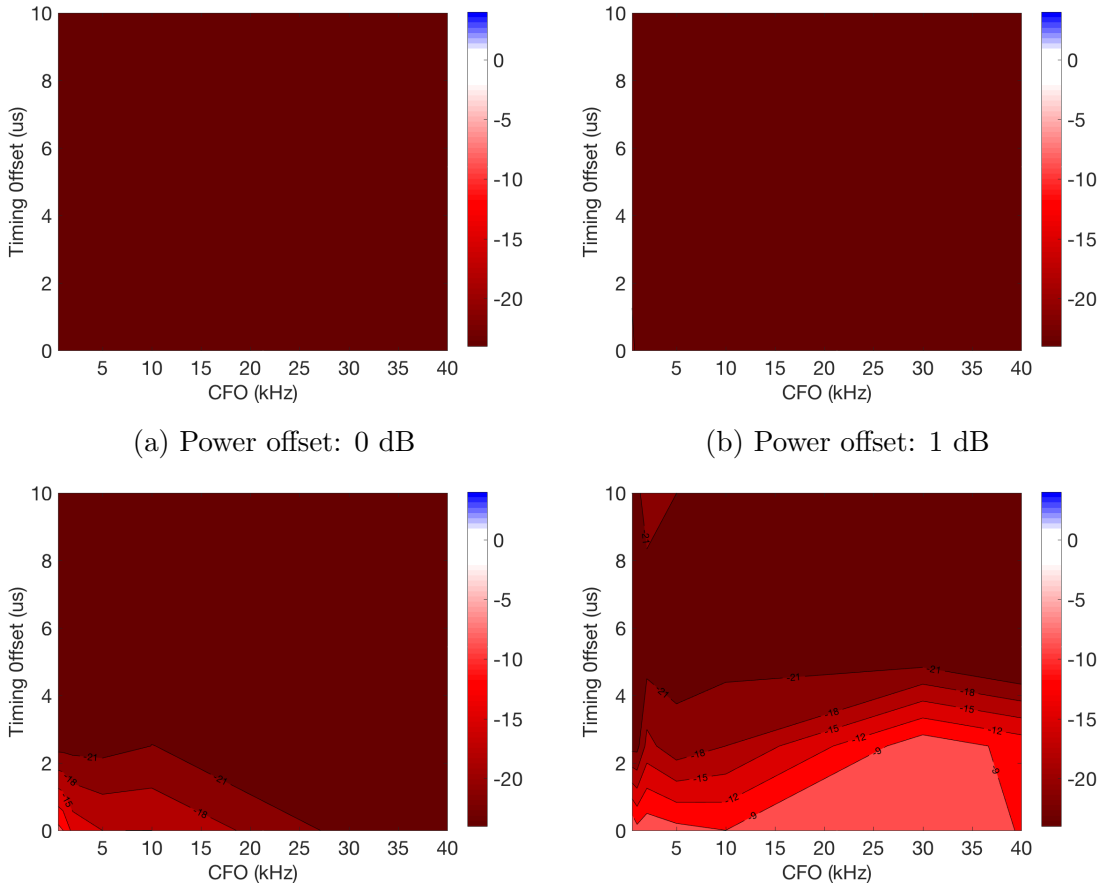

(a) Power offset: 0 dB

(b) Power offset: 1 dB

(c) Power offset: 3 dB

(d) Power offset: 5 dB

Fig. 4.9 Emulation results for IEEE 802.15.4g system over power, timing offset, and CFO.

are dedicatedly developing various LoRa applications, such as remote health and well-being monitoring system or long-range surveillance system [59, 60]. LoRa also has great potentiality on the fields like smart grid or smart agriculture. Until 2017, LoRa network has been widely deployed in more than 120 cities over 17 countries. Particularly, there are some countries, including Korean, Holland, and Switzerland, even planning to build a nationwide LoRa network.

4.4.2 Physical-layer design of LoRa

Although LoRa is a proprietary standard, from the waveform analysis [61–63] and the public information [57], it can still be inferred that LoRa is a chirp-modulated high-order M-ary FSK system.

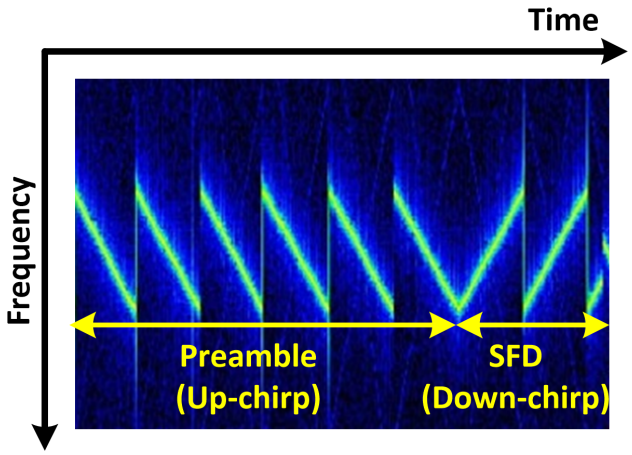

(a) Preamble part

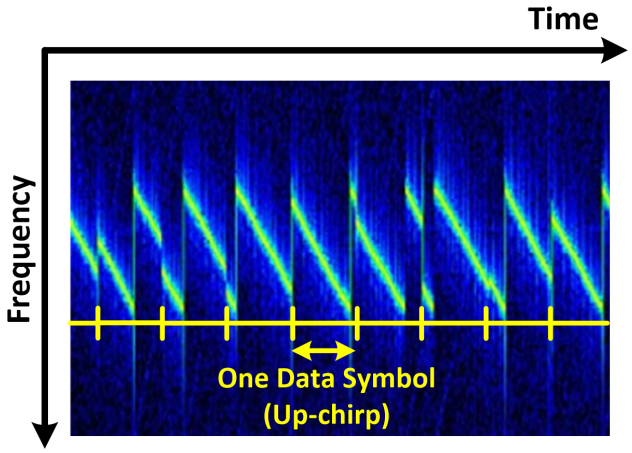

(b) Date part

Fig. 4.10 The spectrogram excerpt of the LoRa signal modified from [61].

First, from the time-frequency spectrogram shown in Fig. 4.10 (modified from the figures in [61]), it can be seen that the LoRa packet consists of a series discontinuous chirp symbols. Subplot (a) shows the preamble part with several up-chirps for packet detection, gain control, and frequency recovery and down-chirps for the start of frame delimiter (SFD). Subplot (b) shows the data part consisting of several discontinuous up-chirps, where the data is modulated by the initial position of each chirp. Despite the 2 down-chirps in the end of preamble part (the start of frame delimiter (SFD)), the other chirps are linear up-chirp that always shifts toward the positive direction with the same slope until reaching the edge of the frequency band. This indicates that the chirp is used only for spectrum

spreading and not for data modulation. Moreover, we can see that the initial positions of the chirp in the data part vary from symbol to symbol, which suggests that it is the initial point of each chirp that is used for data modulation. In other words, if removing the frequency shift caused by the chirps, the LoRa is basically an FSK modulation system.

Second, from the document of LoRa modulation spec [57], one LoRa symbol consists of 2^{SF} samples and carries SF coded bits, where SF is the spreading factor. For low-power standard like LoRa, it is very reasonable to assume that FSK and only FSK is adopted for data modulation in order to spare the burden of coherent demodulation. Therefore, it is very likely that LoRa adopts a 2^{SF}-ary FSK modulation. This suggest that LoRa is a 2^{SF}-ary FSK system, where the frequency band is divided into 2^{SF} discrete subcarriers, and only one subcarrier per symbol would be selected for data transmission. To be more specific, it is the position of the selected subcarrier not the signal loaded on that subcarrier that represents the data. The 2^{SF}-ary FSK system is very similar to the multi-carrier OFDM system, where a time-domain symbol consists of 2^{SF} symbol and meanwhile the frequency band is divided into 2^{SF} discrete subcarriers.

Fig. 4.11 shows a possible realization of the LoRa transceiver structure. The bit stream is first interleaved and encoded. Then, every SF bits from the coded stream are then mapped to a 2^{SF} bits to the IFFT engine for the 2^{SF}-ary FSK modulation. Finally, the time-domain signal is further modulated by the chirp signal. In the receiver, the received signal is first de-chirped and passed to an FFT engine. The demodulation is done by simply selecting the subcarrier with maximum power at the FFT output.

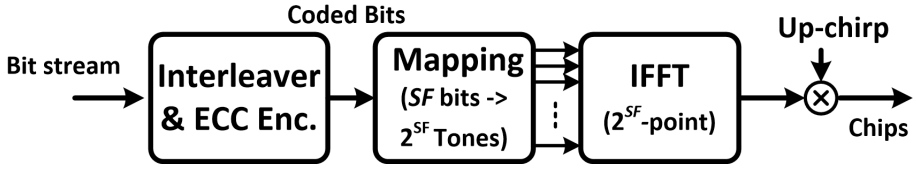

(a) Transmitter

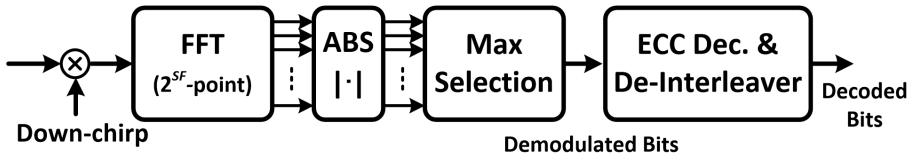

(b) Receiver

Fig. 4.11 One possible realization of the LoRa transceiver.

4.4.3 Discussion of LoRa under CT

The LoRa has two unique characteristics that make it behave very differently than other low-power wireless standards under CT. (Our discussion mainly focuses on the low-rate LoRa mode with high SF and narrowest bandwidth that provides wide coverage.)

The first feature is its long symbol time which is aiming to trade for good sensitivity performance. Specifically, when the LoRa is configured at the lowest rate mode (with SF and the bandwidth being 12 and 125 KHz, respectively), one data symbol consist of 4096 samples, which is as long as 32.7 ms. In CT scenario, the long symbol makes LoRa immune to the beating effect caused by CFO. As we mentioned in the previous section, beating is fading-like effect, which results in bursty demodulation error when deep fading occurs. We have shown that the effect of beating is negligible if the fading duration of the beating is narrower than the symbol time. Moreover, we showed that the beating caused by CFO typically has a fading duration of the order of several μs. Since the LoRa has a ms-order symbol time, it is very unlikely for the beating to deeply fade a whole LoRa symbol.

The second feature of LoRa, which is also empowered by the long symbol length, is that LoRa adopts a very high-order M-ary FSK modulation in order to increase the spectral efficiency. As a result, the frequency deviation of M-ary FSK modulation is extremely small compared to CFO. Specifically, when LoRa is configured as the lowest-rate mode, the FSK is in 4096-ary, and the frequency deviation is only 30.5 Hz, while the CFO between the transmitters typical has a standard deviation of several KHz. In the CT scenario, even though that the concurrently transmitted packets all carry the same payload, the CFO could easily bias the FSK modulation and distort the packet as if they are carrying independent payloads. To illustrate, Fig. 4.12 shows an example of LoRa demodulation under a CT scenario of two transmitters. The stronger packet (blue arrow) is treated as the wanted signal by the receiver, while the weaker one (red arrow) becomes the interference. Since the CFO biases the interference to another subcarrier, the wanted packet could only be successfully decoded when the power offset is large enough. Subplot (a) illustrates a case without energy spreading effect, where the CFO and the timing offset are the integer times of f_{dev} and T_S, respectively. When the CFO is not the integer of f_{dev} (Subplot (b)), or the timing offset is not the integer times of T_S (Subplot (c)), the energy of the interference is spread on multiple subcarriers and results in larger power offset.

Under such independent packet collisions, the capture effect (the presence of a significantly strong packet) is obviously the only reason that the packet reception could succeed, and this seems to make LoRa incompatible with CT. However, also thanks to the high-order M-ary FSK modulation property, there are two effects that allow an extra margin for the capture effect, and hence significantly increase the probability of surviving. We refer to these two effects as the *frequency-domain* and *time-domain energy spreading* effect.

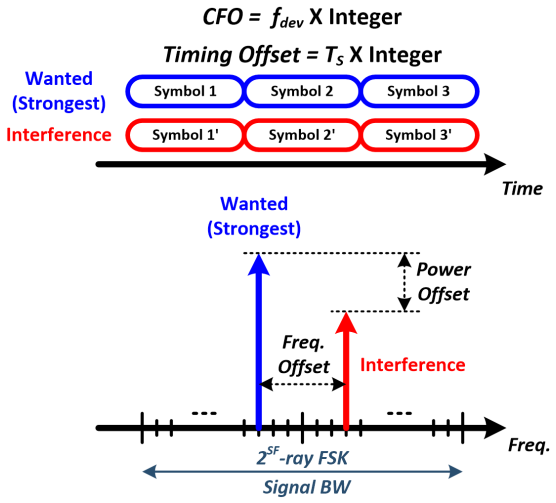

(a) No energy spreading effect

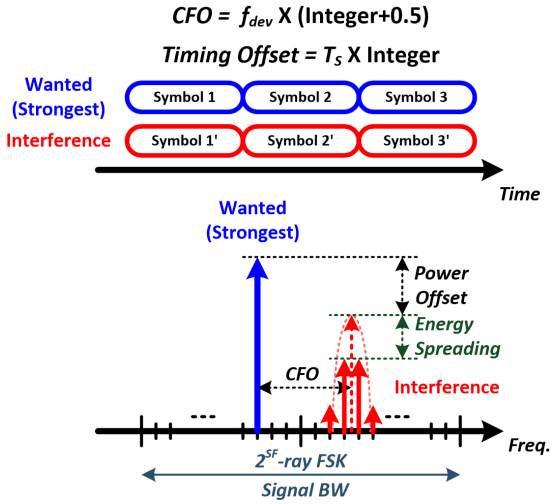

(b) Frequency-domain energy spreading effect

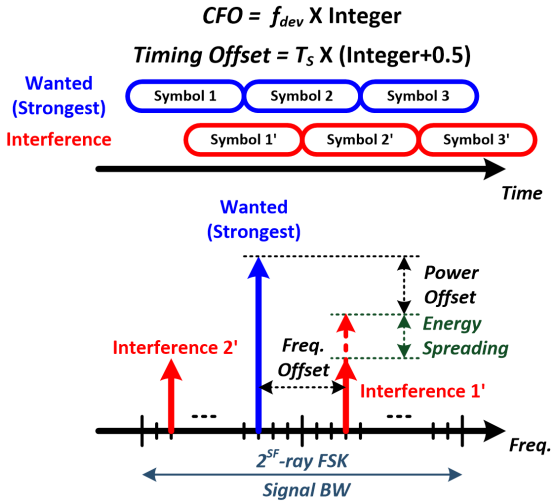

(c) Time-domain energy spreading effect

Fig. 4.12 An example of the LoRa demodulation under a two-transmitter CT scenario.

- ***Frequency-domain energy spreading effect***: Since the CFO is a continuous random value that is typically larger than the frequency deviation, it is very likely that the interference tone locates between two subcarriers. In such cases, the energy of the interference tone would spread among the adjacent subcarriers as shown in Fig. 4.12 (b), and hence results in an extra power offset between the strongest tone and interference tone. We refer to this effect as the frequency-domain energy spreading effect. The maximum frequency-domain energy spreading happens when the interference locates exactly in the middle of two subcarriers so that the energy spread out on that two adjacent are equal. In such cases, there would be at least an extra 3 dB power margin, which is large enough to allow LoRa receiver to survive the non-capture scenario.
- ***Time-domain energy spreading effect***: The other energy spreading effect happens when there is timing offset between the received packets. We use the example in Fig. 4.12 (c) to illustrate. When there is timing offset, each symbol of the wanted packet would be affected by two adjacent symbols of the interference packet, and each interfering symbol contributes only part of its power. Since each LoRa symbol carries independent SF bits, the probability for the adjacent symbols to be different is $(2^{SF}-1)/2^{SF}$, which is very close to 1 since SF is large in LoRa. Therefore, the partial power of interference would be very likely to locate on independent tone, which also results in more power margin for demodulation. Moreover, we expect that the optimum timing offset would be half of the symbol time, and the resulted power margin is also larger than 3 dB.

As we will prove shortly in the next subsection, due to these two energy spreading effects, LoRa receiver can still have a high probability of surviving the CT scenario even without the capture effect. Therefore, LoRa is a candidate for constructing the CT-based multi-hop network.

Next, we analyze the power margin obtained by the two energy spreading effects. Before the chirp modulation, the baseband signal of an M-ary FSK LoRa symbol using the k^{th} subcarrier can be represented as

$$s_k(t) = e^{j2\pi k f_d t}, (t \in [0, T_s]) \tag{4.1}$$

where T_s and f_d are the symbol time and frequency deviation, respectively Therefore, a de-chirped LoRa symbol using the k^{th} subcarrier ($k \in [-\frac{M}{2}, \frac{M}{2}-1]$) and being affected

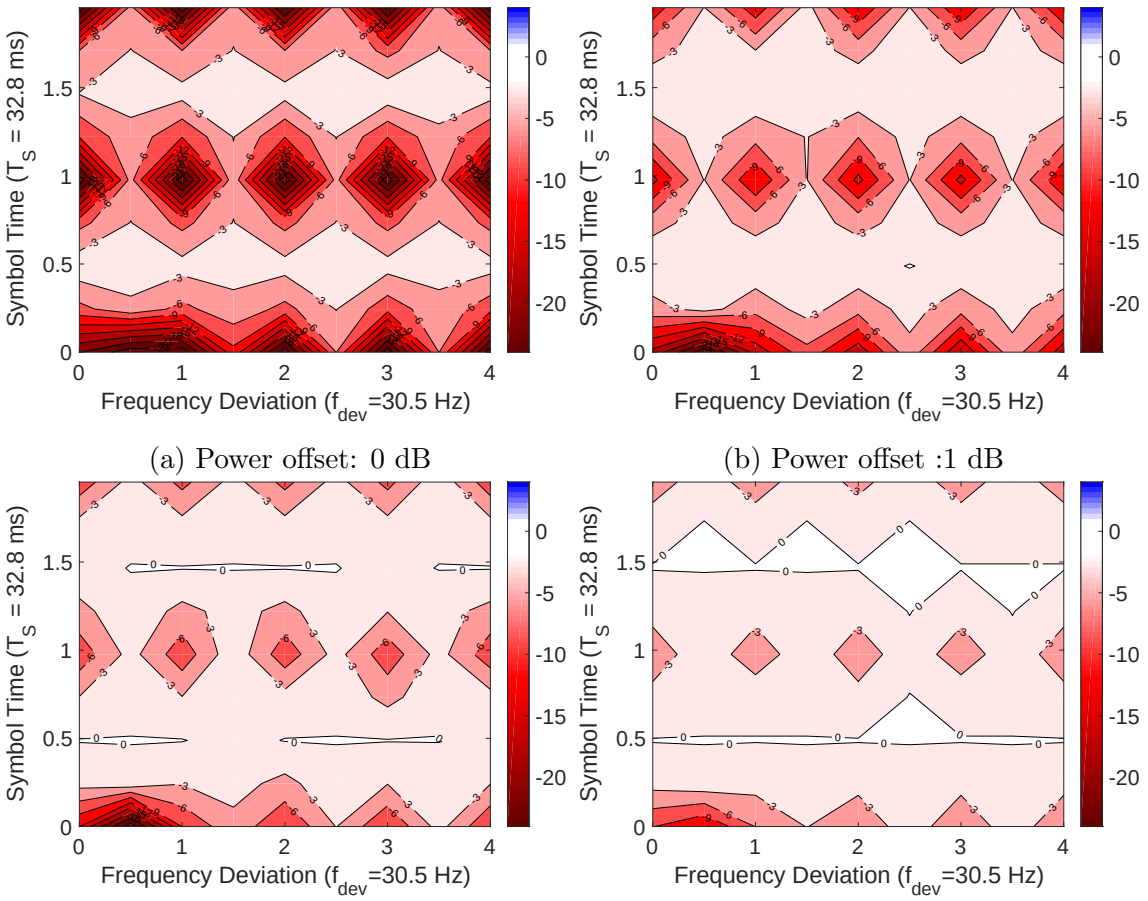

(a) Power offset: 0 dB

(b) Power offset :1 dB

(c) Power offset: 2 dB

(d) Power offset: 3 dB

Fig. 4.13 The sensitivity gain simulation results for *LoRa* receiver performance under a 2-Tx CT scenario over different power, timing offset, and CFO.

by a CFO αf_d and a timing offset βT_s can be represented as

$$s'_k(t) = e^{j2\pi(k+\alpha)f_d(t-\beta T_s)}, (t \in [\beta T_s, \beta T_s + T_s]), \tag{4.2}$$

where α and β are factors for normalizing the CFO and timing offset, respectively. Without losing of generality, we assume both α and β are in the range of $(0, \frac{1}{2}]$.

As shown in the Fig. 4.11 (b), after the de-chirp operation, the non-coherent matched filter receiver estimates the transmitted FSK symbol by selecting the subcarrier with maximum magnitude from the outputs of the M matched filters as

$$\hat{m} = \underset{m\in[-\frac{M}{2}, \frac{M}{2}-1]}{\arg\max} |\sum_{n=0}^{M-1} (r(nT_c)e^{-j2\pi m f_d n T_c})|, \tag{4.3}$$

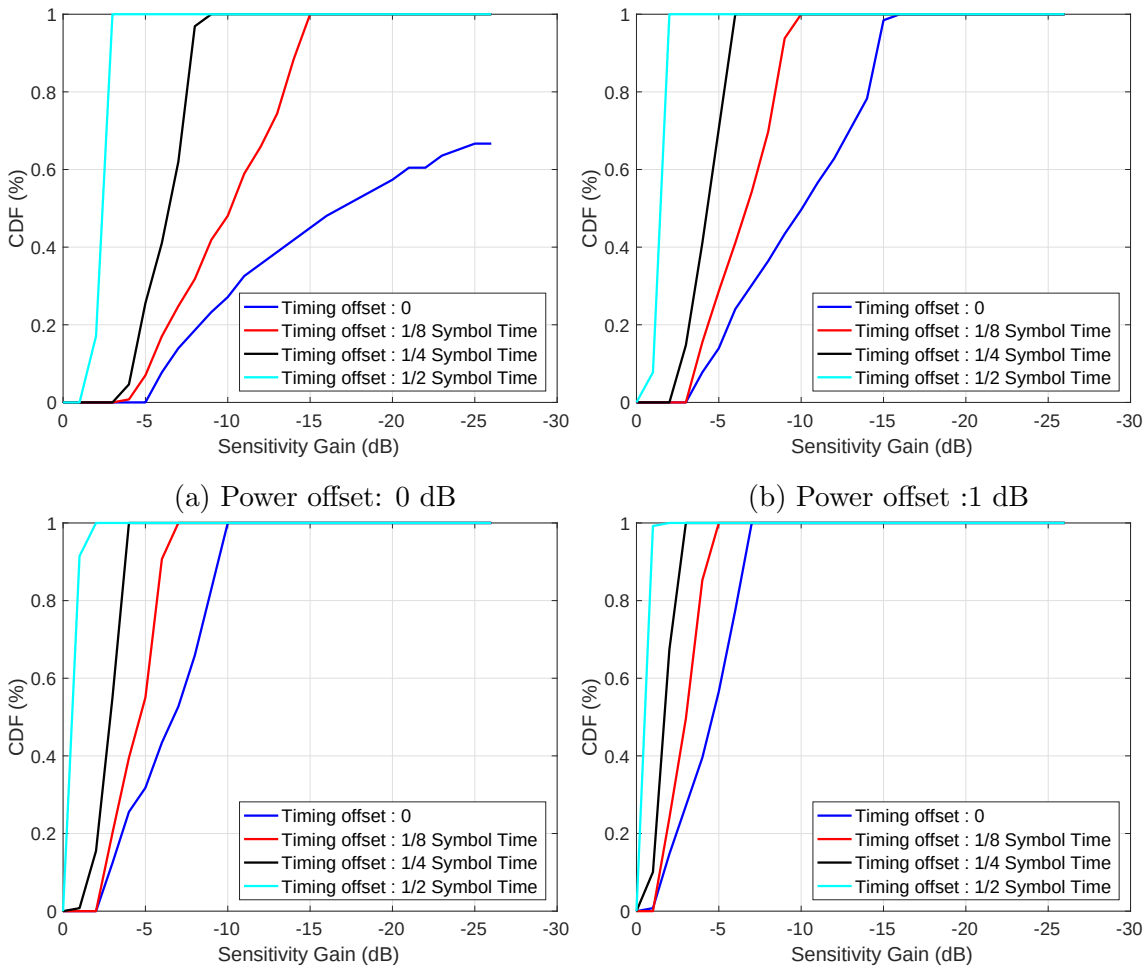

(a) Power offset: 0 dB

(b) Power offset :1 dB

(c) Power offset: 2 dB

(d) Power offset: 3 dB

Fig. 4.14 The CDF function of the sensitivity gain for the two-transmitter case.

where $\hat{m}$ is the estimated subcarrier number, T_c is the chip time, and $r(t)$ is the received signal. Note that, in the LoRa system, the symbol time T_s, chip time T_c, frequency deviation f_d, and system bandwidth W satisfy the following equations.

$$T_s = MT_c = \frac{1}{f_d} = \frac{M}{W}. \tag{4.4}$$

Assuming that the $s_k(t)$ is transmitted and there is no CFO and timing offset, it is straightforward to show that only the k^{th} matched filter would have the maximal value, and the other matched filter would output zero due to the orthogonality between the subcarriers. By substituting $s_k(t)$ for $r(t)$ in (4.3), the maximal value can be simply calculated as M.

On the other hand, with the presence of CFO and timing offset, the orthogonality is corrupted and the energy would be spread around multiple subcarriers. Since most of the energy would still concentrate on the subcarriers near to the k^{th} one, we substituting the offset LoRa symbol $s'_k(t)$ for $r(t)$ in (4.3) and calculate the corresponding output magnitude of the $(k+\Delta)^{\text{th}}$ matched filter output as

$$\begin{aligned} A(\Delta,\alpha,\beta) &= |\sum_{n=0}^{M-1}(s'_k(nT_c)\times e^{-j2\pi(k+\Delta)f_d nT_c})| \\ &= |\sum_{n=\lceil\beta M\rceil}^{M-1}(e^{j2\pi\frac{(\alpha-\Delta)n}{M}})| \\ &= |\frac{1-e^{j2\pi\frac{(\alpha-\Delta)(M-\lceil\beta M\rceil)}{M}}}{1-e^{j2\pi\frac{(\alpha-\Delta)}{M}}}|, \end{aligned} \tag{4.5}$$

where $\lceil\cdot\rceil$ is the ceiling function.

Finally, the power margin can be evaluated by calculating the ratio between the magnitude $A(\Delta,\alpha,\beta)$ with the maximal value M of the non-offset case, or specifically

$$\rho(\Delta,\alpha,\beta) = 20\times\log_{10}(A(\Delta,\alpha,\beta)/M). \tag{4.6}$$

Fig. 4.15 illustrates the numerical results of the ρ value for different Δ, α, and β. Specifically, Subplot (a) to (d) correspond to the case with Δ equal to -1, 0, 1, and 2, respectively. These are the three nearest subcarriers to the k^{th} one. The X- and Y-axis in each subplot correspond to the value of α and β, respectively.

From the numerical results, the following observations can be made

- Most of the energy concentrates on the nearest two subcarriers, and the maximal value appears on the nearest subcarrier with $\Delta = 0$. Therefore the receiver performance would be dominated by the case with $\Delta = 0$.
- The results show that the timing offset and CFO help to increase the power margin. In the the case where $\Delta = 0$ in Fig. 4.15 (b), a more than 6 dB power margin can be obtained by the two energy spreading effects if both α and β are both 0.5.
- The power margin resulting from the time-domain energy spreading effect is more significant than that from the frequency-domain one.

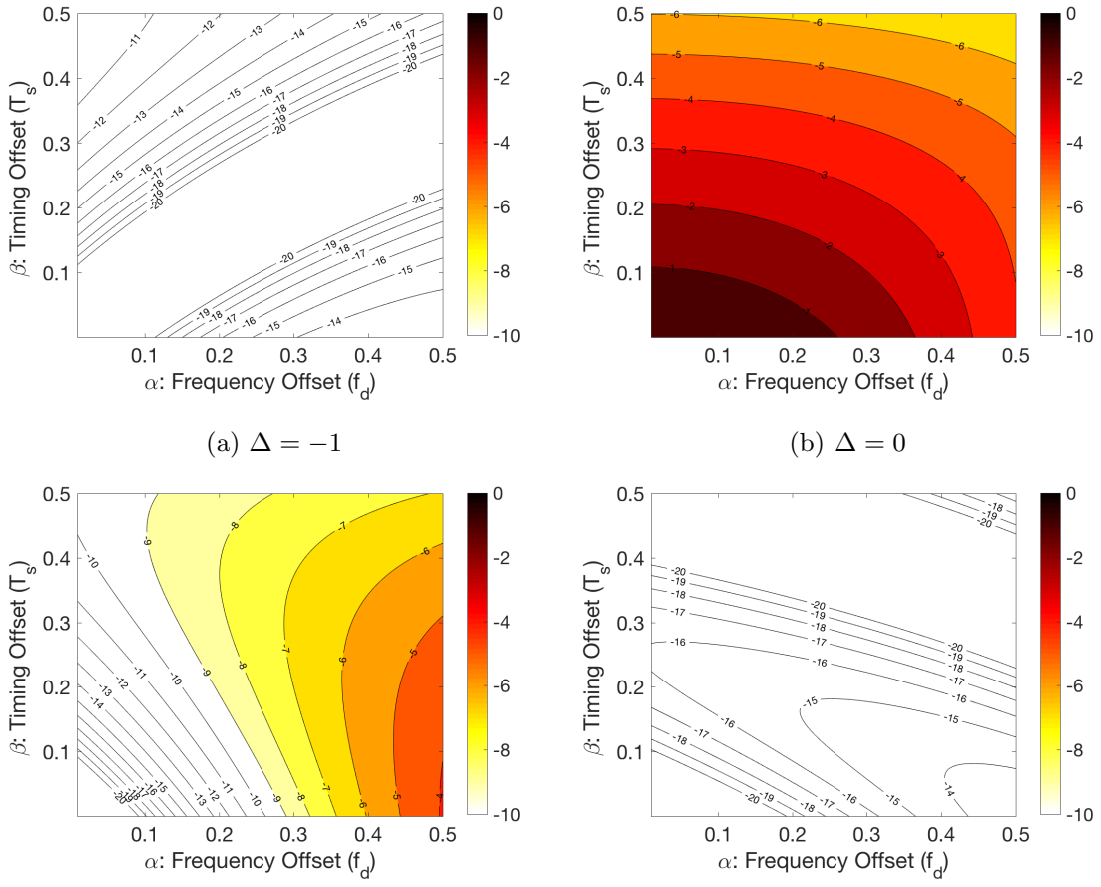

(a) $\Delta = -1$ (b) $\Delta = 0$

(c) $\Delta = 1$ (d) $\Delta = 2$

Fig. 4.15 The power margin obtained by the two energy spreading effects.

4.4.4 Evaluation parameters

We evaluate the receiver performance by the typical one-hop transmitter-channel-receiver model. Specifically, LoRa packets are first generated according to the transmitter block diagram shown in Fig. 4.11 (a), passed through a CT equivalent channel model, and demodulated by the receiver shown in Fig. 4.11 (b).

In our simulation, randomly generated 15-byte packets with SF-12 and BW-125KHz mode are used. To simplify the evaluation dimension, we first evaluate the CT scenario of two transmitters. We evaluate the sensitivity gain under a three-dimensional parameter space consisting of the power offset, the timing offset, and the CFO. Specifically, the power offset, the timing offset, and the CFO between the two transmitters are swept from 0 to

3dB, from 0 to 2 symbol time (32.7 ms), and from 0 to 4 frequency deviation (30.7 Hz), respectively. The phase offset is set to be a random variable uniform distributed from 0 to 2π for every packet.

4.4.5 Results and discussions

Fig. 4.13 (a) to (d) show the results of the sensitivity gain for power offset 0 dB, 1 dB, 2 dB, and 3dB, respectively. In these figures, we use the colored-coded 2D contour maps to illustrate the sensitivity gain, where the darkness of the red color indicates minus sensitivity gain, or more intuitively the sensitivity loss. The X- and Y-axis indicate the CFO and timing offset, respectively.

Several observations can be made from the simulation.

- ***Capture effect***: First, we can find the required power offset that ensure the capture effect for LoRa. From Fig. 4.13 (d), we can see that, similar to the IEEE 802.15.4 system, if there is a 3 dB power offset between that two packets 3 dB, the receiver can enjoy a comparable performance as the collision-free links regardless of the value of the timing offset and the CFO .
- ***Frequency-domain energy spreading effect***: For the non-capture effect show in Fig. 4.13 (a) and (b), we can see that the CFO value affects the receiver performance significantly. Particularly, there is a clear periodicity of the receiver performance that varies according to the CFO value (the horizontal direction). When the CFO value is the integration times of the f_{dev}, the sensitivity suffers significantly. On the other hand, the sensitivity performance improves greatly while the CFO is not integer times of f_{dev}. This verifies our previous analysis about the frequency-domain energy spreading effect.
- ***Time-domain energy spreading effect***: Similar periodicity can also be observed in the time-domain (the vertical direction). The sensitivity suffers the most when the timing offset is the integration times of the symbol time, while the sensitivity performance is comparable to the collision free case when the timing offset is 0.5 times offset from the integer symbol time. This verifies our analysis on the time-domain energy spreading effect.

- ***The slow beating area***: Finally, we observe an exceptional bad-performance area between when the CFO is between 0 and 1 f_{dev} in Fig. 4.13 (a). This is the slow beating region where the fading duration of beating is wider than the symbol. In this region, some symbols could be totally deeply faded and failed to be demodulated. However, the probability for the CFO to full in this region is negligible due the very small f_{dev} of LoRa modulation.

Note that, if the CFO is larger than f_{dev}, the relation between the sensitivity performance and the CFO can be estimated by calculating the remainder after dividing the CFO by f_{dev}. Moreover, since the standard deviation of CFO in practical systems is a random variable whose standard deviation is typically much larger than the f_{dev}, the remainder can be regarded as a random variable uniformly distributed between 0 and f_{dev}. Therefore, the CDF of the sensitivity performance can be calculated as shown in Fig. 4.14, where Subplot (a) to (d) show the CDF versus sensitivity gain for power offset 0 dB, 1 dB, 2 dB, and 3 dB, respectively. The results of different timing offset are also shown in Fig. 4.14. From the results, we can find that in the worse case with 0 dB power offset and zero timing offset, there would be at least 5 dB of sensitivity loss and more than 50 % of change that the sensitivity loss is larger than 15 dB. On the other hand, if the power offset is increased to 1 dB or if there is a 1/8 symbol time of timing offset, the sensitivity loss can be guaranteed to be smaller than 15 dB, and there is 50 % of chance that the loss is less than 10 dB.

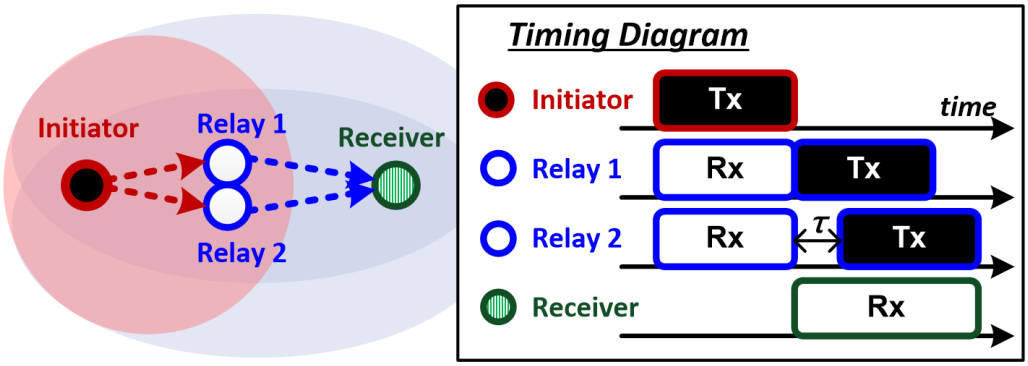

Fig. 4.16 The setup for a two-transmitter CT experiment consisting of one initiator, two relays, and one receiver.

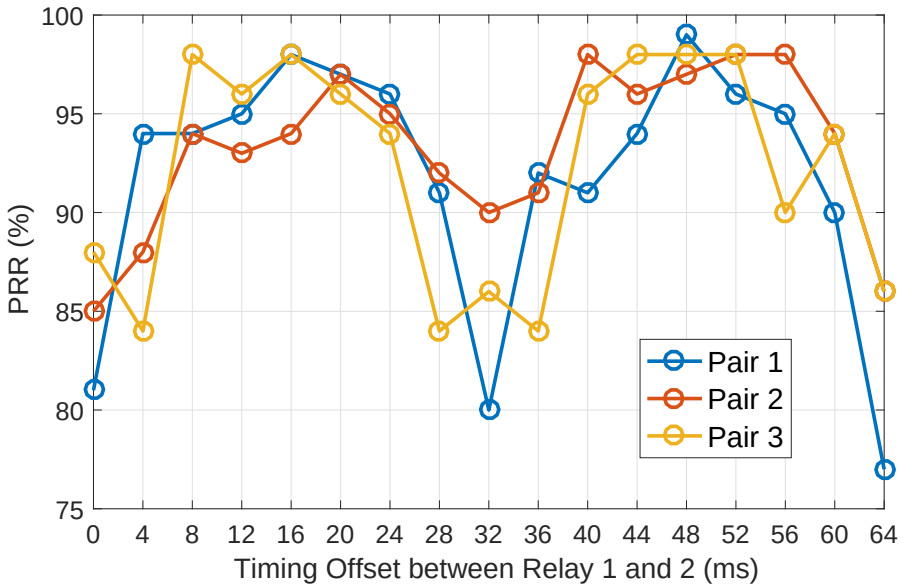

Fig. 4.17 The experimental result of the two-transmitter CT experiment by using three pairs of RF modules as the relays.

4.4.6 Real-chip experiments

Besides the simulation, we further conduct real-chip experiments to double confirm our analysis about the LoRa receiver's performance under CT. In the experiment, we focus more on verifying the effect of timing offset on the receiver performance.

We adopt an RF module consisting of a Semtech SX1272 LoRa RF transceiver [64] and an STM32L151 micro-processor [65]. We build up the experiment environment with one initiator, two relays, and one receiver, as illustrated in Fig. 4.16. The initiator periodically sends out a packet to trig the CT of the two relays, and the receiver is programmed to only listen to the second-hop packets from the relays and record the PRR. For the first relay, we let it perform retransmission right after the reception is finished, while for the second one, we intentionally insert a timing delay before the retransmission.

In order to test the critical scenario, the two relays are put close to each other to reduce the power offset, and the receiver is put in a shielded location such that the received packet is slightly higher than the sensitivity level. Before conducting the real CT experiment, we verified that the receiver can receive the packet from each individual relay with an over 99% PRR to make sure that the packet loss is caused by CT instead of insufficient SNR.

The experiment is conducted several times by using three different pairs of RF modules as the relay nodes. Random generated 15-byte packets are used for evaluation, and the correctness of packet reception is determined by the CRC check. Finally, the experiment is conducted on the 920.6 MHz band, with SF, bandwidth, and code rate being 12, 125 KHz, and 4/5, respectively.

Fig. 4.17 shows the experimental results, or more specifically, the relationship between the PRR and the timing offset. We can see that the experimental results match the simulation. While the PPR is worst when the timing offset is close to the integer of T_S (32.7ms), when the timing offset is away from the integer of T_S, the receiver can still enjoy a high PRR.

4.5 Summary

In this chapter, the comprehensive evaluations of the receiver performance of many representative IoT-oriented standard under CT were presented. Specifically, we evaluate the IEEE 802.15.4, IEEE 802.15.4g, and LoRa system.

For the IEEE 802.15.4 system, we clarified that the beating effect resulting from the CFO significantly affects to the reception, and the DSSS is the key for the receiver to survive the beating. Moreover, we showed that even with DSSS, the performance of the IEEE 802.15.4 receiver could still be significantly degraded if the fading duration of the beating is relatively longer than the DSSS symbol length. On the other hand, the IEEE 802.15.4g system, which is not protected by any error correcting mechanism, performs poorly in CT links.

For the LoRa system, we showed that LoRa can survive under CT with a high chance. The 3dB requirement to allow capture effect is no greater than the other CT-compatible standard, such as the IEEE 802.15.4 system. Next, in the non-capture scenario, there is a great probability of surviving due to the frequency-domain energy spreading effect. Finally, we show the potential of introducing timing offset to further increase the surviving probability, while in IEEE 802.15.4 system, timing synchronization error needs to be kept as small as possible to guarantee the receiver performance.

Chapter 5

Novel CT-enabled Applications

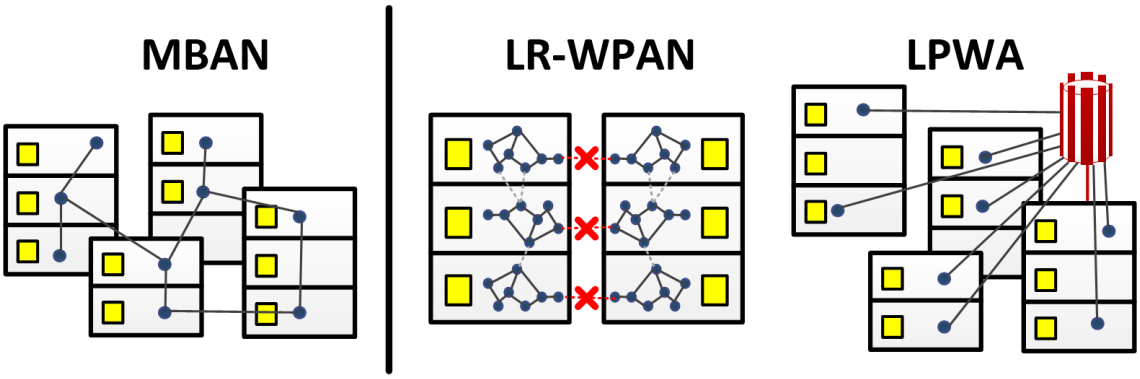

Fig. 5.1 The concept of MBAN, a long-life, easy-to-deploy, and autonomous wireless networks that connect indoor devices deployed over several adjacent buildings.

From the analysis and evaluation in the previous chapters, we have presented a comprehensive investigation on the physical-layer receiver behavior under CT, and many insights have been obtained from the investigations. In this chapter, we will show that these insights not only help people to understand the CT better, but more importantly allow people to better utilize the advantage of CT to create better systems. Specifically, we will present two novel CT-enabled applications:

（1） Multi-building area network (MBAN) by CT-enabled multi-hop LoRa (CT-LoRa)

（2） Real-time and reliable communication (RRC) system by CT-enabled distributed antenna system (CT-DAS)

5.1 CT-LoRa

5.1.1 Overview of MBAN

In the upcoming Internet of Things (IoT) era, buildings are going to become smart. Many smart systems, such as energy management, surveillance and access control, and environmental monitoring systems, are expected to be widely deployed in future buildings [66]. Moreover, in many cases such as school campuses, office building groups, or house complexes, it is essential for the smart systems to cover several buildings

Toward this, we present the design and the implementation of the multiple-building area network (MBAN) in this work. In short, MBAN is a wireless ad-hoc network that

connects indoor devices deployed over several adjacent buildings. We envision MBAN to be a long-life, easy-to-deploy, and autonomous network that fits the requirements of future smart buildings. Specifically, MBAN has the following features.

- *Extensive indoor coverage over several buildings:* The devices deployed over several buildings should be able to communication with each other reliably.
- *Low power:* All devices should transmit with small power and listen for only a short period of time to ensure a long lifetime.
- *Service-centric (not communication-centric) deployment:* The user should focus on deploying the devices for the service (e.g. sensing, monitoring, or control) instead of the communication. The relay nodes that only serve the communication function should be kept as few as possible.
- *Infrastructure-free:* MBAN should be pure wireless and not rely on any infrastructures, such as powerful base stations.

To meet all the requirements, the physical-layer of MBAN needs to be very robust so that it can endure the large attenuation resulting from the walls or floors while keeping the transmission power small. The conventional 2.4-GHz standard, such as IEEE 802.15.4 [12], are obviously not a good solution because of their weak penetration capability and the heavy interference in that band. We consider the recently proposed Sub-GHz low-power-wide-area (LPWA) technologies, such as Wi-SUN [56] and LoRa [57]), whose transmission range are designed to achieve an order of kilometers in the outdoor environment, as a promising solution to MBAN. On the other hand, even with such long-range technologies, the extensive indoor coverage is still difficult to be achieved by a single-hop star topology, unless a powerful outdoor base station is installed in a proper location [59]. In the infrastructure-free MBAN, a multi-hop relay network is essential to ensure reliable any-to-any communications. However, the current Sub-GHz technologies are either designed for the star-topology (e.g. LoRa) or adopt inefficient collision-avoidance-based multi-hop protocol (e.g. IEEE 802.15.4e).

In order to construct a robust and efficient multi-hop network for the Sub-GHz technology that meets the requirements of MBAN, we focus on the combination of CT and the *LoRa*. (We particularly refer to the CT-based multi-hop LoRa network as *CT-LoRa*.) LoRa is robust to interference and its transmission range can be longer than 10 km when

configured into the lowest rate-mode (293 bps) [58], which make LoRa a promising candidate for the physical-layer standard of MBAN. On the other hand, CT enables very fast back-to-back packet relaying which greatly improve the efficiency of the network. Therefore, we consider CT a better solution for constructing MBAN.

Although CT facilitates the construction of highly efficient multi-hop networks, it is not generally applicable to any wireless standards. Specifically, as we have shown, due to the inevitable timing offset and carrier frequency offset (CFO) between the transmitters, even though the colliding packets carry identical contents, there are still several non-ideal effects that degrade the reliability of the receivers. We further showed that the receiver performance under such packet collisions is vastly different from standard to standard, and a careful physical-layer investigation on the conditions that enable reliable receptions under the packet collisions is an essential step for constructing a reliable CT-based network.

In this chapter, we show the feasibility of CT-LoRa by

（1） proposing a method to increase the reliability of CT-LoRa, and
（2） carrying out practical MBAN experiments using CT-LoRa.

To be more specifically, the main contributions of the CT-LoRa research is as follows.

The proposal of the offset-CT method: In the previous chapter, we have shown the potential of introducing timing offset to further increase the surviving probability. In order to enhance the time-domain energy spreading effect, we further propose the offset-CT method, which is a simple but effective method to increase the timing offset between the packets while maintaining a virtual timing alignment of each hop. The novelty of this proposal is twofold. First, for the practical CT-LoRa usage where the transmitter number cannot be determined, we propose to introduce a random timing delay uniformly distributed between 0 and one-symbol time before every retransmission of the relay packet. Second, in order to prevent the timing offset from diverging, we propose to carry the delay information in each packet, so that the relay who successfully demodulate the packet could insert the complementary delay to align the timing. (Note that, this method is only feasible for the technology like LoRa who survive the CT purely by capture effect.)

Proof-of-concept experiments: Furthermore, we conduct a series of experiments to show the feasibility of CT-LoRa and the validity of the proposed offset-CT method. Specifically, we test two typical MBAN scenarios - the low-density scenario that covers more than many buildings with 1 or 2 nodes per building, and the high-density case that covers

only a few buildings but with each floor of the building equipping 1 or 2 nodes. The typical scenario results show that CT-LoRa is very reliable even without offset-CT. Next, we test the critical scenario for CT, where multiple nodes are put closely to each other to make the power offset between the packet very small. In the critical scenario, we show that offset-CT significantly improves the packet reception rate (PRR).

5.1.2 Offset Concurrent Transmission

As we have shown in the previous chapter, inserting a timing offset between the concurrently transmitted packets helps to increase the time-domain energy spreading effect and hence improves the receiver performance. In this section, we present our proposal of timing offset insertion method, the offset concurrent transmission (offset-CT) method for increasing the reliability of CT-LoRa. We will discuss the design considerations, the implementation, and the simulation results that validate the proposal.

(a) Design considerations

The timing offset insertion method must be compatible with the original CT protocol and bring no degradation the network performance. Specifically, the following two constraints need to be satisfied.

Small overhead: Introducing timing delay makes the packet transmission time longer and degrades the network utilization. Therefore, we need to ensure that the inserted timing offset is small enough compared to the packet length so that the effect on the network utilization is negligible.

Simple and distributed calculations: One of the most important advantages of CT is its simplicity and the distributed nature. That is, the only mechanism that each node needs to follow is to do the retransmission after the reception. There is no need to gather and maintain the global topology information, and there are also no needs to distribute controlling information. Therefore, in order to be compatible to the CT flooding, the calculation and the insertion of the timing offset needs to be done in a simple and distributed way that does not require global information.

Convergency of the timing offset: Introducing the timing offset in multi-hop networks could result in the timing offset accumulation problem. That is, the timing offset between the packet increases as the hop count increases. The diverging timing offset could cause

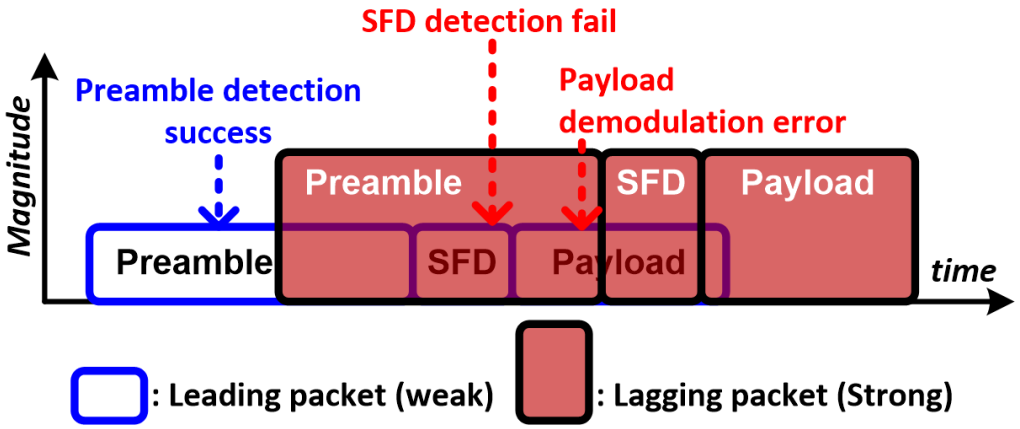

Fig. 5.2 The illustration of the preamble locking problem caused by large timing offset.

problems, such as the *preamble locking problem*. Fig. 5.2 depicts an example of this problem, where two packets are transmitted with large timing offsets and the weak one is received first. In this example, the receiver has already successfully detected the preamble of the weaker one and enter the timing acquisition or even data demodulation state before the strong packet comes. If the receiver does not have the capability of aborting the current packet where there is a later-coming strong signal, the later-coming one would then become a severe interference which may result in the SFD detection failure or the payload modulation error.

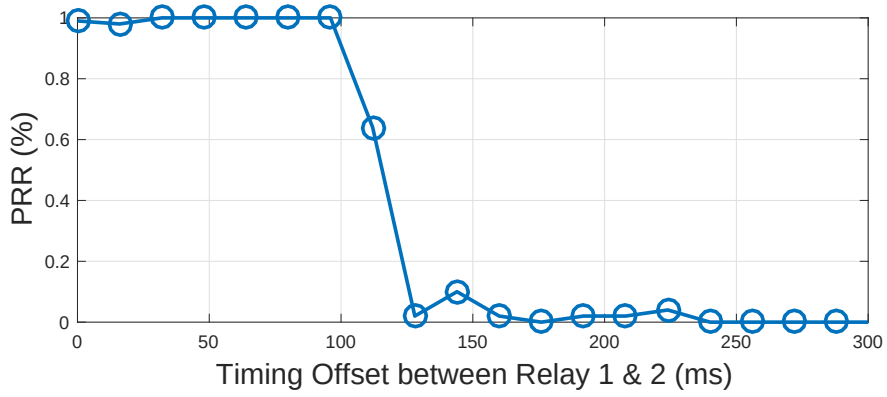

Fig. 5.3 The experiment result that confirms the preamble locking problem.

To demonstrate the preamble locking problem, we conduct an experiment with one initiator, two relays, and one receiver. We adjust the position of the two relays so that the

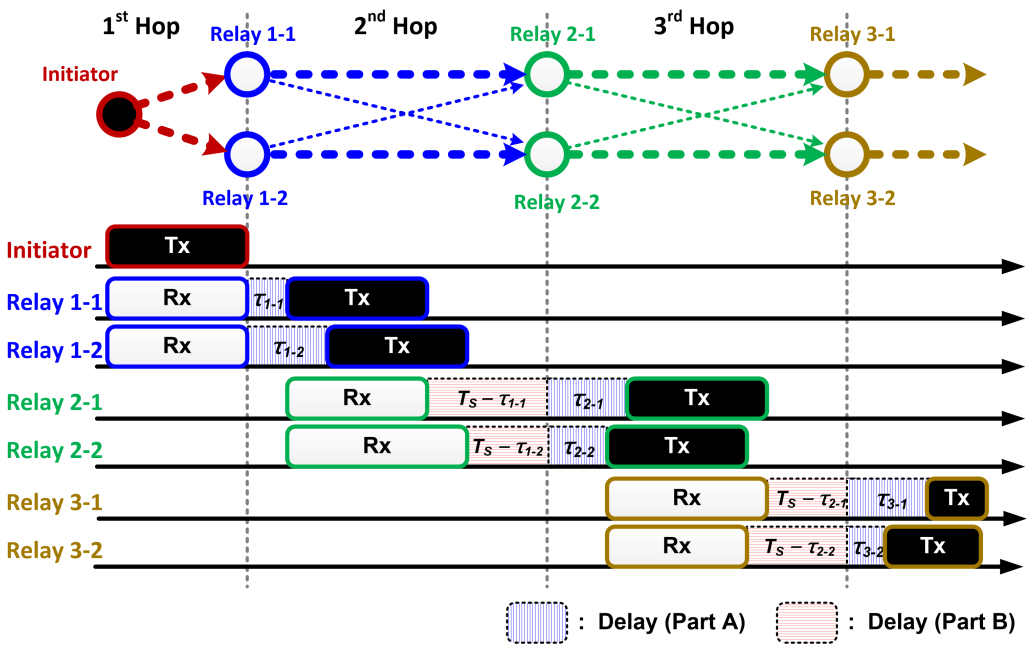

Fig. 5.4 The illustration for the offset-CT method.

packet from Relay 2 is 6 dB larger than that from Relay 1. Similarly, we introduce different timing delay before the retransmission of the Relay 2 and record the corresponding receiver PRR performance as shown in Fig. 5.3. We can see that when the timing offset is larger than 100 ms (about $3T_S$), the receiver could fail to decode the packet. The maximum allowable timing offset without letting the receiver to be locked by the first coming packet depends on the RF modulation design.

(b) The implementation of offset-CT

In our offset-CT method, we propose to insert a delay before each retransmission of the relay packet. The delay consists of two parts (A and B), which will be further elaborated as follows. Fig. 5.4 illustrates an example of the timing diagram of the offset-CT.

Part A: A uniformly distributed random delay: The Part-A delay is simply a uniformly distributed random delay for creating the timing offset between the packets. Specifically, we set the range of this random delay to be one symbol time (T_S). While in the 2-Tx CT cases, the optimum timing offset has been proven to be half of the symbol time, the optimum value for the multiple-transmitter scenario is difficult to find. Moreover, in practical CT scenarios, the number of the transmitters joining the CT is not controllable

and measurable. Therefore, instead of trying optimizing the timing offsets according to the topology, we introduce a random delay to generate timing offset between the packets. As we will show in the later simulation, a uniformly distributed random delay is not only easily to generate, but also provide a significant performance improvement in the multiple-transmitter scenario.

Part B: Delay for timing alignment: In order to prevent the timing offset from diverging, we insert another delay to restore the timing alignment of each hop. To achieve this, in each packet, we add an extra field in the payload to indicate the duration of the aforementioned random delay that the packet has undergone. (For the initial packet, the value is set to zero.) When a relay successfully receives a packet and decodes the delayed duration τ, the relay would first insert a Part-B delay of $T_S - \tau$ and then a newly generated Part-A delay τ' before the retransmission. With these two parts of the delay, we can ensure that the duration of each hop is fixed as one packet length plus T_S while allowing the packets to be randomly shifted in each hop.

To be more specific, let us consider a situation that Relay i receives a packet from Relay j which has been relayed by $(n-1)^{th}$ times (so that Relay i is about to relay the packet for the n^{th} time). We denote the Part-A and Part-B delay inserted by Node i before relaying as $\tau^A_{n,i}$ and $\tau^B_{n,i}$, respectively. Then,

$$\tau^A_{n,i} = \mathcal{U}(0, T_s), n \geq 1 \tag{5.1}$$

$$\tau^B_{n,i} = \begin{cases} T_s - \tau^A_{n-1,j}, & n \geq 2 \\ 0, & \text{otherwise} \end{cases} \tag{5.2}$$

Then, the transmission time of a packet which is about to be relayed for the N^{th} time can then be calculated as

$$\begin{aligned} T_n &= T_P + \tau^A_1 + \sum_{n=2}^{N} (T_P + \tau^B_n + \tau^A_n) + \\ &= T_P + \tau^A_1 + \sum_{n=2}^{N} (T_P + T_s - \tau^A_{n-1} + \tau^A_n) \\ &= T_P + (N-1)(T_P + T_S) + \tau^A_N, \end{aligned} \tag{5.3}$$

where T_P is the packet length. We can see that the duration of each relay is fixed as $T_p + T_s$. With the remaining term τ^A_N, the packets are allowed to be randomly shifted in a range of T_s in each hop.

Note that, the design of carrying individual delay information in each packet is feasible because of the special property of LoRa modulation. As we mentioned in the Sec. 4.4.3, due to the narrow frequency deviation, the CFO would significantly bias the packet contents and the LoRa receivers survive the CT mainly by the capture effect. What makes CT-LoRa feasible is the property that LoRa requires only a very small power offset to allow the capture effect. In other words, no matter whether the concurrently transmitted packets carry the same payload or not, the LoRa receiver has a high probability of decoding the strongest packet. On the other hand, the conventional CT protocols require the packets to always carry the same payload.

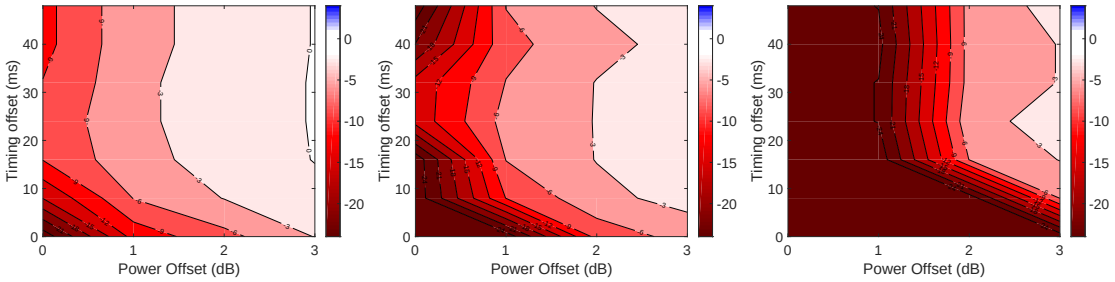

(a) 4 Transmitters (b) 8 Transmitters (c) 16 Transmitters

Fig. 5.5 The simulation results for the *LoRa* receiver performance under multiple-transmitter CT scenarios over different power and timing offset.

5.1.3 Evaluation of the offset-CT method

Next, we present a series of simulations and experiments to show that the proposed offset-CT method can 1) significantly improve the receiver performance in the multi-transmitter scenario, and 2) restore the timing alignment of each hop.

(a) Receiver performance evaluation

We conduct similar simulations and experiments to evaluate the receiver performance under the multiple-transmitter scenarios. The setups are similar to the previous two-transmitter evaluations.

Simulations: The purpose of the simulation is to not only verified the effect of the random timing offset, but also to find a proper range for the uniformly distributed random variable. We again evaluate the uncoded sensitivity gain under the power, timing offset, and CFO.

We set the CFO to be a Gaussian random variable with 1 KHz of standard deviation. (As long as the value is large enough, it is irrelevant to the final results.) Meanwhile, we model the timing offset as a uniformly distributed random variable with different ranges. For the power offset, we set the power of the strongest packet to be unitary and make the other packets have the same power offset against the strongest one. Specifically, we evaluate the cases with 0 to 3 dB power offset. The other parameters are the same as the two-transmitter ones.

Fig. 5.5 (a) to (c) show the results of the sensitivity gain for the cases with 4, 8, and 16 transmitters, respectively. The X-axis is the value of power offset, and the Y-axis is the range of the uniformly distributed random timing offset. The CFO is modeled as a Gaussian random variable whose standard deviation is sufficiently large. From these figures, the following observations can be made.

- The more transmitters, the worse performance. Since the CT packets biased by CFO act as independent packets, having more transmitter would only degrade the performance. We can also see that, in high-transmitter number case, a higher power offset is required for the receiver to survive the packet collisions.
- Introducing the timing offset helps to improve the receiver performance significantly. However, we can see that a larger timing offset does not always result in a better performance.
- From the simulation results, we select the range of uniformly distributed random timing offset to be one symbol time (32.7 ms) in our system.

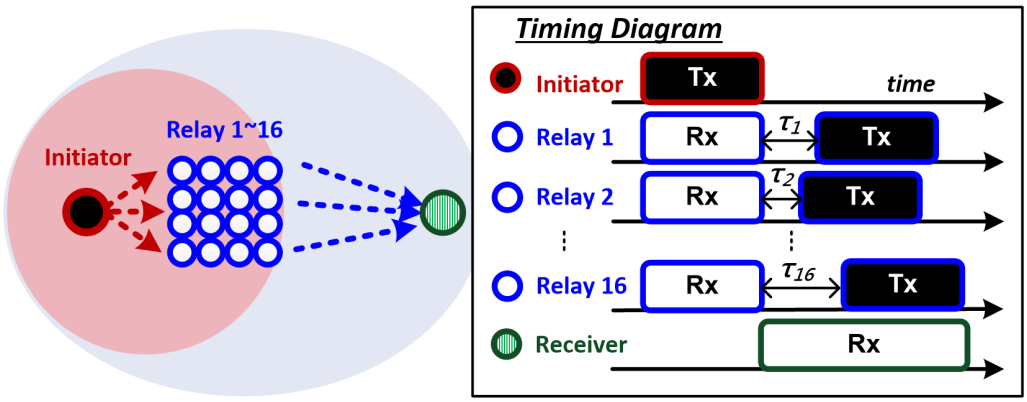

Fig. 5.6 The setup for the multiple-transmitter CT experiment with one initiator, variable numbers (2∼16) of relays, and one receiver.

Experiments: In the experiment, we test the receiver performance with different numbers of relays to verify the performance improvement resulting from the offset-CT method. The experiment setup is with one initiator, 2∼16 relays, and one receiver as shown in Fig. 5.6. Each relay inserts a uniformly distributed random delay from 0 to T_S before the retransmission using the offset-CT method. Since this is the first-hop relay, the Part-B delay is always zero. For reference, we also evaluate the PRR performance of conventional CT without inserting the random delay. Again, those relay nodes are put close to each other to make the power offset small, and we make sure that the receiver has a reliable connection to each relay in the collision-free scenario. The other setups are the same as the two-transmitter ones.

Fig. 5.7 shows the PRR under different relay nodes, where the red bars show the results without inserting timing offset, while the blue ones show those with timing offset. We can see that the results match the conclusion we draw from the simulation. Specifically, the PRR degrades when there are more relays join the CT. Moreover, we can see that the random timing delay significantly improves the PRR by 10% to 30%.

(b) Timing accuracy evaluation

Next, we present the experiment to confirm that the offset-CT method can restore the timing alignment. The experiment setup is shown in Fig. 5.8. Specifically, there is one initiator and four groups of relays, where each group contains four nodes. We configure the relays in each group to receive only the packets from the previous group and the relay in Group 1 receive only the packets from the initiator. By this setting, we force the relays to form a linear four-hop network.

Three kinds of timing offset insertion methods are evaluated: *1)* the conventional CT where both Part-A and Part-B delays are zero, *2)* the offset-CT with both Part-A and Part-B delay, and *3)* the naive timing offset method with only Part-A delay and Part-B delay is zero. We let the initiator periodically transmit packets, and the time stamps of the end of each Part-B delay (the timing of the dashed gray line in Fig. 5.4) are recorded in each relay. By calculating the difference between the adjacent timing stamps, we gather the statistics of the inter-packet interval (IPI) and calculate its variation.

Fig. 5.9 shows the experiment results, we can see that the standard deviation of the IPI of the naive random timing offset method increase significantly with the hop count, while that of the offset-CT is almost the same as that of the conventional CT. (Note that,

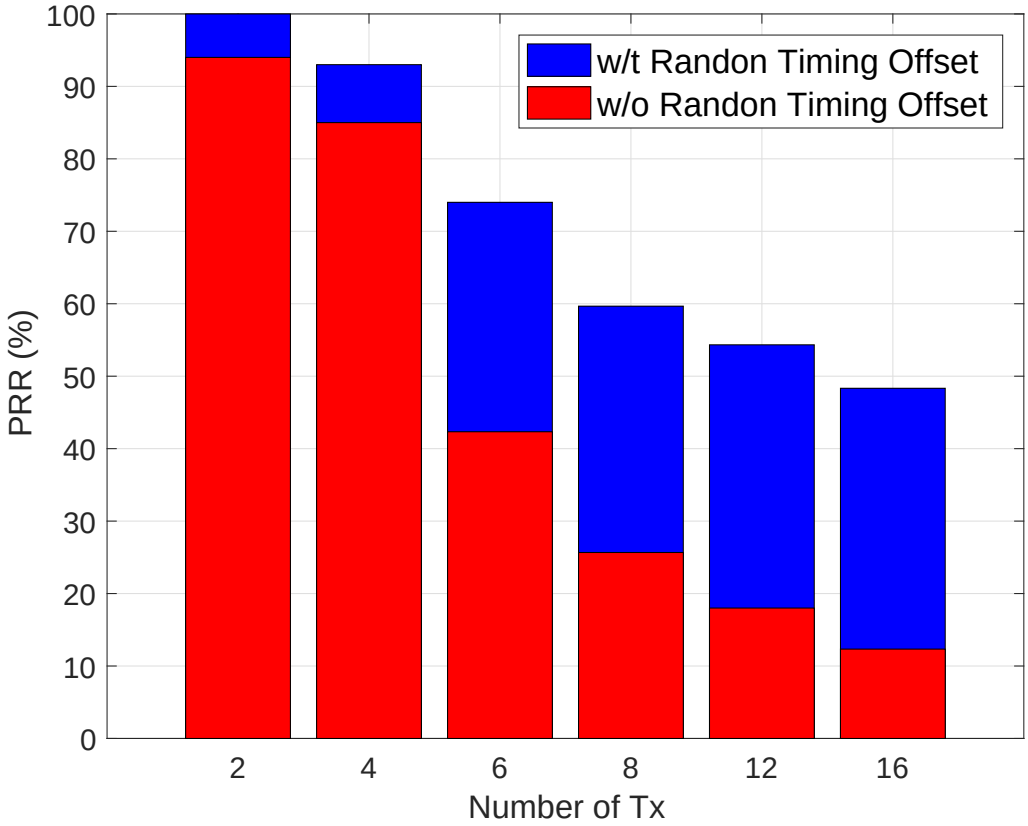

Fig. 5.7 The experimental result of the multiple-transmitter CT experiment with different numbers of relays.

the variation of IPI of the conventional CT is not zero because there are some inevitable variations in the hardware and software processing time.)

(c) Overhead estimation

The offset-CT method is compatible with the original CT flooding protocol. The only overhead is a slight increase in the transmission time of each packet. Specifically, the two-part delay increases the equivalent transmission timing of each packet by one symbol time T_s. In addition, an extra field is needed to indicate the Part-A delay. In this work, we use a 5-bit number to represent the delay.

Comparing to the total packet length, such overhead is very small. To give a specific number on the utilization degradation, let us consider a typical LoRa packet with a payload of 15 bytes. We assume the SF and code rate to be 12 and 4/5, respectively, and the

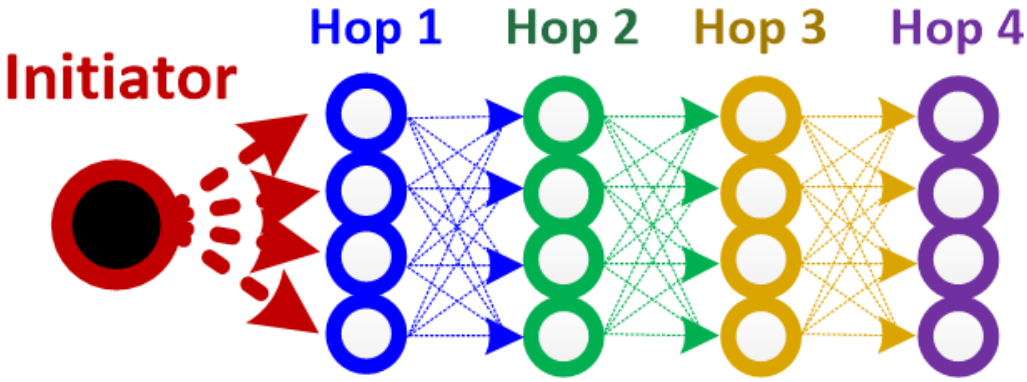

Fig. 5.8 The setup for the timing alignment verification with one initiator, four groups of relays, and each group has four node..

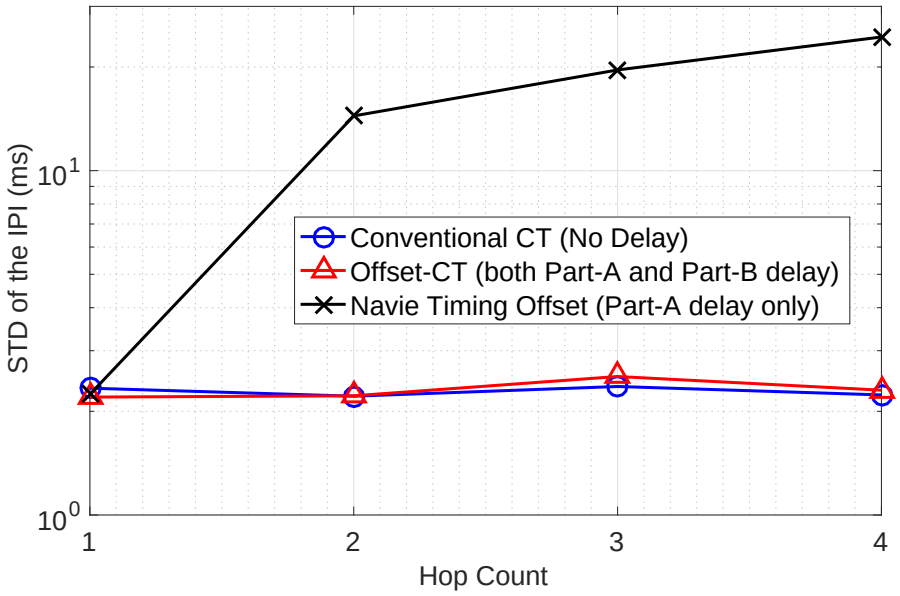

Fig. 5.9 The experimental result of the variation of the IPI versus the hop count.

other parameters (e.g. the preamble and header length) to be the default setup. The transmission time of a packet can be evaluated by the following equation given in [64].

$$T_P = (22.25 + \left\lceil \frac{8PL - 4SF + 42}{4SF} \right\rceil \times \frac{4}{CR})T_s, \tag{5.4}$$

where PL is the payload length in byte and CR is the code rate. Thus, the transmission time of the aforementioned packet can be calculated as 35.25 Ts. With the same equation,

we can evaluate the transmission time after applying the offset-CT method to be 36.25 Ts, and the utilization degradation is only 2.84 %.

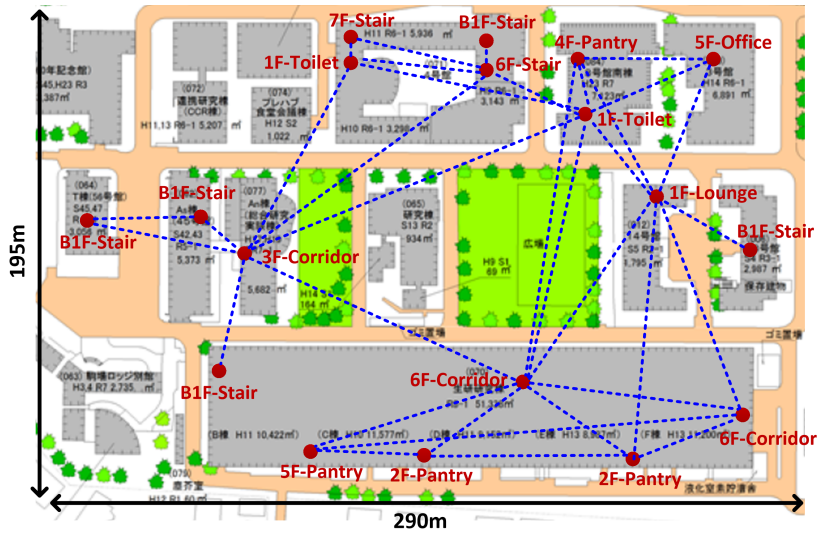

(a) Low-density topology

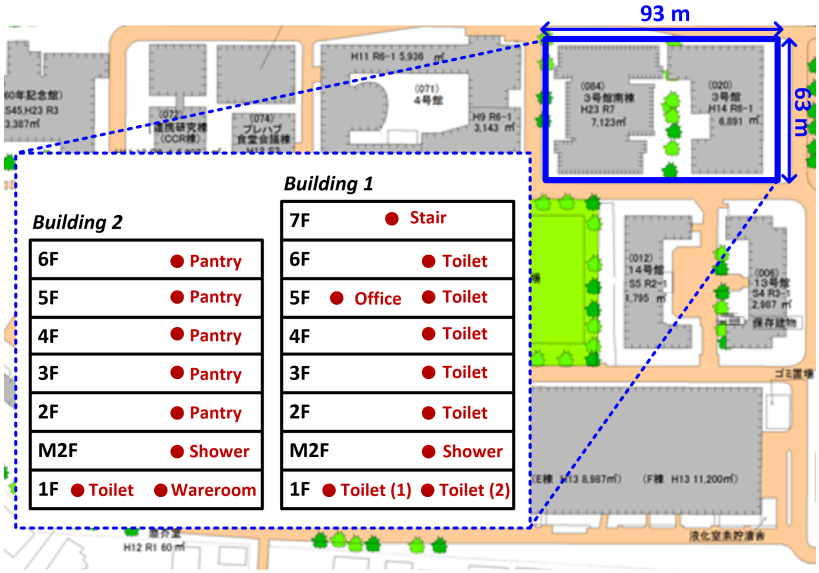

(b) High-density topology

Fig. 5.10 The deployment map of the typical scenario experiment.

5.1.4 Proof-of-concept Experiments for MBAN

In this section, we present a series of prove-of-concept experiments to show the feasibility of realizing MBAN by CT-LoRa. Two sets of experiments, the typical MBAN scenario, and the critical CT scenario, are conducted.

(a) Typical MBAN scenario

In the first set of experiment, we try to emulate the node deployment of a typical MBAN,

Experiment procedure: We use 18 nodes equipped with the RF module described in the previous section for the experiments. Each of them would serve as the initiator in a round-robin manner. The initiator would trigger 100 times of CT flooding by transmitting 100 packets. While one node serves as the initiator, the other nodes would then serve as the relays. If a relay node successfully receives a packet, it would forward the packet, and record the initiator ID and the hop counter of the packet for the performance evaluation. The same packet can be forwarded only once by the same relay. We evaluate the performance of both the conventional CT (i.e. without random timing delay) and the offset-CT method. The parameters of LoRa modulation are the same as the previous section.

Topology: One important factor that affects the reliability of CT-LoRa is the density of the node. In the conventional collision-avoidance-based multi-hop network, a denser deployment could be preferable from the reliability point of view, since it is more likely for a node to have reliable links to the other nodes. However, from the CT point of view, a dense deployment could in the same time increase the possibility of harmful packet collisions, since there would be more nodes joining the CT and the power offset between the CT packets could also be smaller. In view of this dilemma, we conduct experiments under both low-density and high-density deployments.

- ***Low-density deployment***: In the low-density deployment, we deploy the 18 nodes over 14 buildings such that there are at most two nodes in the same building. In addition, we deploy the node in different floors to make the topology more sparse. The detail deployment map of the low-density deployment is shown in Fig. 5.10 (a). We mark every reliable one-hop link (with higher than 90 % of PRR) on the map with blue dashed lines. As the map shows, we try to deploy the nodes in various places, such as corridors, stair rooms, pantries, and office rooms. Moreover, some

of the nodes are deployed in highly shielded locations, such as toilets without a window or basements.

- ***High-density deployment***: In the high-density deployment, we deploy the 18 nodes over 2 adjacent buildings with 8 and 7 floors, respectively. We uniformly deploy the nodes in every floor so that there are at most two nodes in the same floor. The detail deployment map of the high-density topology is shown in Fig. 5.10 (b). Note that, in the high-density case, there are too many reliable links (75 links out of 153 pairs). Therefore, marking all the reliable one-hop links to would make the map unreadable.

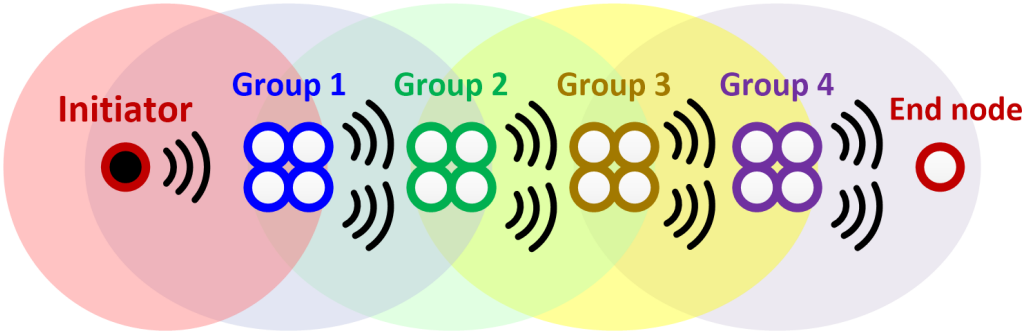

Fig. 5.11 The setup of the critical scenario experiment.

Results and discussions: Table 5.1 shows the statics of the two experiments, including the worst/average PRR and maximum/average hop count between any two nodes. We also provide estimations to the degree of packet collisions by calculating the average and the maximum number of relays that concurrently transmitting packets to one receiver. Specifically, we gather the reliable one-hop link information (as plotted in Fig. 5.10 (a)), construct the flooding diagrams starting from each initiator, and count the numbers of the relays that concurrently transmitting to each receiver. Note that, since the packet collisions happen only after the second-hop relay, the first-hop collision-free transmissions are ignored in the calculation of the relay numbers. From the results, the following observations can be made.

- ***The necessity of a multi-hop relay network***: The results support our argument that, if the nodes are all deployed indoor and transmitted with low power, a multi-hop relay network is needed to ensure the coverage even with a wide-area standard such as LoRa. We can see that even with the longest spreading factor and narrowest

Table 5.1 The experiment result of the typical scenario

	Low-density		High-density	
	CT	Offset-CT	CT	Offset-CT
AVG. Hop Count	2.07	2.04	1.57	1.57
MAX. Hop Count	3.71	3.57	3.06	3.05
AVG. Relay # joining a CT	1.33	1.34	2.98	3.09
MAX. Relay # joining a CT	3	3	7	7
AVG. PRR (%)	98.2	99.1	99.9	99.9
Worst PRR (%)	45	63	88	95

bandwidth, it would still require a maximum of 5-hop relay to link every node deployed in an 180m × 290m campus. Even in the high-density topology that covers only two buildings, there are still some highly shielded nodes that need to be covered by three-hop relays.

- ***The robustness of CT-LoRa***: The experiments show an exciting result - CT-LoRa achieves almost 100% PRR in both high-density and low-density topologies. Particularly, in the high-density topology, severe packet collisions do happen. There would be, on the average, three nodes transmitting packets to a receiver in each relay, and the worst case number is seven. The results show that, by deploying in different floors or rooms, the resulted power offset is already large enough for the nodes to survive such packet collisions even without offset-CT.
- ***The effect of offset-CT***: Since the power offset in the typical scenario already ensures most of the packet receptions to be reliable, the offset-CT method can barely improve the average performance. However, we can still observe significant improvements in the cases that with the worst PRR for both high-density and low-density deployment.

(b) Critical CT scenarios

In the previous experiment, we show that CT-LoRa can deliver a high reliability in the typical MBAN usages. Next, we would like to create a critical scenario for CT-LoRa and evaluate the performance.

Topology: As we have shown in the previous evaluation, the most critical case for a CT-based multi-hop network happens when there are many colliding packets received with the

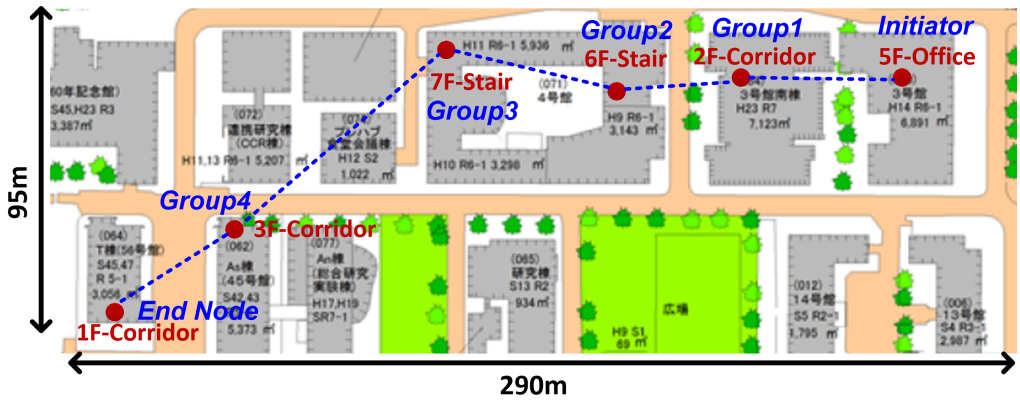

Fig. 5.12 The deployment map of the critical scenario experiment.

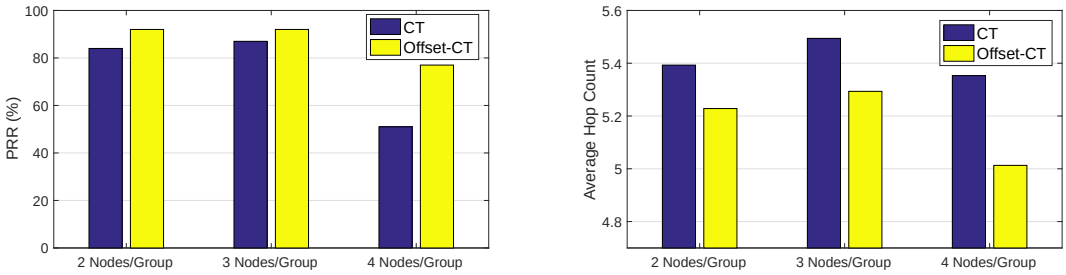

(a) PRR of the end node (b) Average hop count of the end node

Fig. 5.13 The experimental result of the critical scenario experiment.

same power level. In order to create this scenario, we intentionally put the nodes close to each other to reduce the power offset. Moreover, we also expect that the reliability would degrade when the hop-count increases. Therefore, we deploy the nodes in a linear topology that showing in Fig. 5.11 to increase the hop count. Specifically, we select two nodes as the initiator and the end node, and deploy four groups of relays to connect them. In each group, the nodes are put as close as possible to each other. We properly choose the location of each group so that the nodes in each group has reliable connections to those in the previous and next groups only. Besides, the initiator and the end node only have reliable links to the nodes in Group 1 and 4, respectively.

Note that, although this experiment may look very similar to the experiment shown in Sec. (b), there is a fundamental difference. In the experiment in Sec. (b), the relays in different groups are *programmed* to receive only the packet from previous group, while in this experiment, the relays in each group sever exactly the same function (the general

CT relay function without special limitations), and the linear topology is achieved by the careful location selections. Therefore, this critical scenario could happen in the real world, if the user chooses to deploy the nodes in such a manner.

Experiment procedure: The setup of the experiment is similar to the experiment under the typical scenario. The difference is just that the initiator is fixed to one node. We conduct three independent experiments by changing the number of the node in each group from 2 to 4 nodes. Again, the performance for both conventional CT (i.e. without random timing delay) and the offset-CT method are evaluated.

Results and discussions: We plot the PRR and average hop count of the end node in Fig. 5.13 (a) and (b), respectively. The three sets of bars correspond to different node number in a group. In each set, the yellow and the blue bars show the results of the conventional CT method and the offset-CT method, respectively. As we emphasized before, we simply deploy the nodes in a linear topology, while the nodes still follow the basic CT or offset-CT principle to relay the packet. Therefore, it is possible for a packet being relayed back and forth between the groups, so it might take more than 5 hops for a packet to reach the end.

From the results, we can see that, with more nodes in one group, the PRR becomes worse. Moreover, we show that the offset-CT significantly improves the PRR as well as reduces the average hop count in the critical scenario. Particularly, in the case of 4 nodes in a group, the offset-CT improves the PRR from 51% to 77%.

5.2 CT-DAS

5.2.1 Overview of RRC

It has been a long time that the factory automation systems adopts wired solutions instead of wireless ones. Conventionally, wireless communication systems have been only used for non-critical factory applications such as sensing, diagnostics, or open loop control. During the last decades, wireless communication for factory automation have recently gained more and more attention due to the advantages of low installation and maintenance cost, higher flexibility and extensibility options over the wired communication systems [67].

In the next generation of the industry systems (Industry 4.0), the wireless communication is expected to play a key role for factory automation [68]. However, unlike the H2H communication which can tolerate higher level of packet error and latency, factory automation poses very strict latency and reliability requirements to the wireless communication system.

In the wireless communication system, the distributed antenna system (DAS) that ubiquitously deploys many transmit antennas to provide spatial diversity is a very effective method to increase the reliability. Fig. 5.14 show the image when the DAS being applied to factory automation. However, in order to guarantee the spatial diversity, sophisticated transmitter cooperation schemes, such as the antenna selection [69–74] or precoding scheme [40, 75, 76] need to be adopted to prevent the possible performance degradation caused by fading or destructive combinations. Such transmitter cooperation schemes either require the channel state information (CSI) feedback or are not scalable when the antenna number is larger, which makes them infeasible to be adopted in the RRC for factory automation.

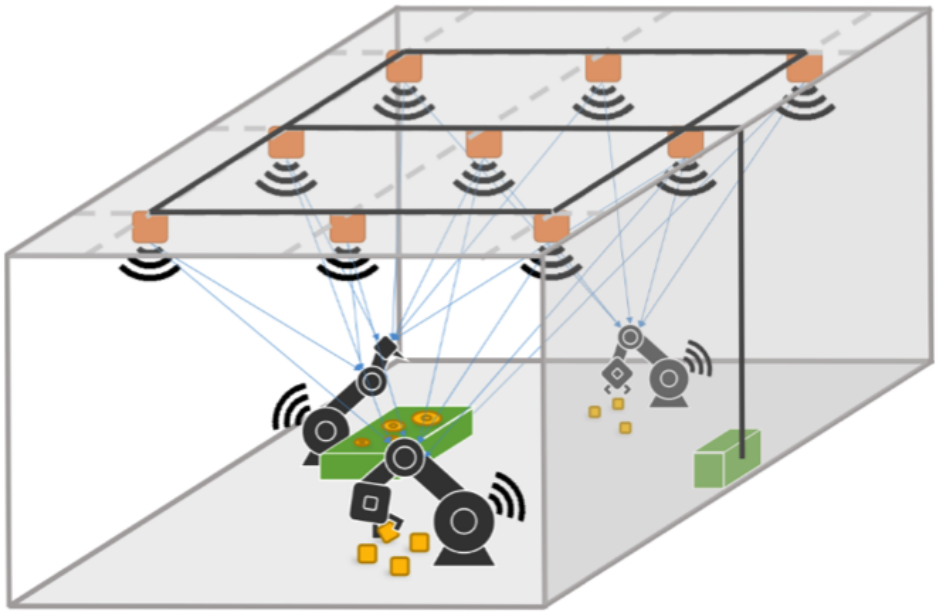

Fig. 5.14 The illustration of a DAS system used for factory automation.

5.2.2 Proposal of CT-DAS

As we discussed in Chpater 2, CT is the most naive way to utilize the spatial diversity. As long as the transmitters are synchronized in timing, every transmitter in CT simple performs the same transmission at the same time. Therefore, it is not necessary to gather or feedback any information, and there is also no scalability problem, which makes CT very suitable for timing-critical applications. On the other hand, the drawback of CT is, of course, the fading or beating problem.

From the analyses in the Chpater 3, we have learned that the fading duration can be reduced by having more antennas and higher CFO deviation. Moreover, we also show the feasibility to apply simple error correcting codes to restore the demodulation error caused by fading as long as the fading duration is shorter than the code length.

In this chapter, we propose the idea of CT-DAS. There are three main essential conditions for CT-DAS to work.

（1） ***Massive and ubiquitous antennas***: Comparing to high deployment and maintenance cost of the wired system, it is still feasible and cost-effective to deploy massive antennas all over the factory. With such antennas, we can not only increase the total reception power and the possibility of having light-of-sight connections, but more importantly ,we can reduce the fading duration as well as the change to have deep fading.

（2） ***Random CFO between the transmitter***: From our previous analyses, increasing the CFO also helps to reduce the fading duration. However, we consider the effect of antenna number is more significant than the randomness of the CFO. As long as the antenna number is sufficiently large, a small randomness would be enough for high reliable receptions.

（3） ***Accurate timing synchronization***: On the other hand, the ISI resulting from the timing offset is purely harmful. Moreover, the degradation resulted from ISI increases along with the transmitter number. Therefore, in CT-DAS where the antenna number is large, the timing synchronization between the antennas need to be accurate.

5.2.3 Simulation

In this subsection, we show the feasibility of the CT-DAS by simulation. Specifically, we assume that there are massive antennas and several receivers deployed over a factory environment with a large area. The positions of transmitter antennas and the receivers are all uniformly distributed in the area. We calculate the path loss between each transmitting antenna and the receiver according to the air propagation model shown as follows [77].

$$P_r(d) = P_r(d_0) + 10n \log_{10} \frac{d}{d_0} + X, \tag{5.5}$$

where $P_r(d_0)$ is the receiving power of at a pre-determined distance d_0 from the transmitter, n is the path-loss exponent, and $X \sim N(0, \sigma)$ is a normally distributed random variable modeling the shadowing effect. Finally, the packets from all the antennas would be multiplied by the corresponding path gain and a random phase rotation uniformly distributed between from 0 to 2π, and combined additively before being fed to each receiver. The receiver would performance packet demodulation and the PER would be recorded.

For the specific parameters, we simulate a factory whose area is 250×250 m^2, and the height difference between the transmit antennas on the ceiling and the receivers on the ground is 4 m. The transmitted power is equally set to be 0 dBm for all the antennas, with the noise floor of -85 dBm to match the sensitivity of the real devices. Using the industrial indoor model provided by [78], we set the air propagation parameters as follows: $P_r(d_0) = 71.84$, $d_0 = 15$ m, $n = 2.16$, and $\sigma = 8.13$. We select the IEEE 802.15.4 standard as a communication standard since we have shown that it is suitable for the application of CT. Over 10,000 packets are transmitted to evaluate the performance of CT-DAS. A location will be defined as a high-reliability area if the PER is smaller than 1 %. In the simulation, we sweep the transmitting antenna number from 1 to more than 100, and the standard deviation of the CFO from $\frac{1}{5} f_D$ to $\frac{1}{2} f_D$, where f_D is the maximum allowable frequency shift in the IEEE 802.15.4 standard, 96 KHz. The timing offset is assumed to be zero.

Finally, we use the averaged PER and the percentage of the high-reliability area (PHRA) as the metrics to evaluate the performance of CT-DAS. The high-reliability area is defined as a location where its PER is less than a given threshold, and PHRA is the percentage of such area over the whole area.

Fig. 5.15 and Fig. 5.16 show the simulation results for the PER and PHRA, respectively. The horizontal axis shows the transmitting antenna number and the different colored lines represent the results for different CFO standard deviation.

From the results, we can make the following observation.

（1） ***Transmitting antenna number***: Increasing the number of transmit antennas improves the PER and increase the PHRA. Specifically, for the given 250×250 m^2, area, we can see that as long as the antenna number is larger than 30, the averaged PER is close to 0, and the PHRA approaches 100%

（2） ***Randomness of CFO***: On the other hand, increasing the standard deviation of CFO helps to reduce the required transmitting antenna number. For example, more than 30 antennas are required to ensure high reliability in the $\frac{1}{5}f_D$ (19.2 kHz) case, while only less than 20 antenna is required in the $\frac{1}{2}f_D$(48 kHz) case.

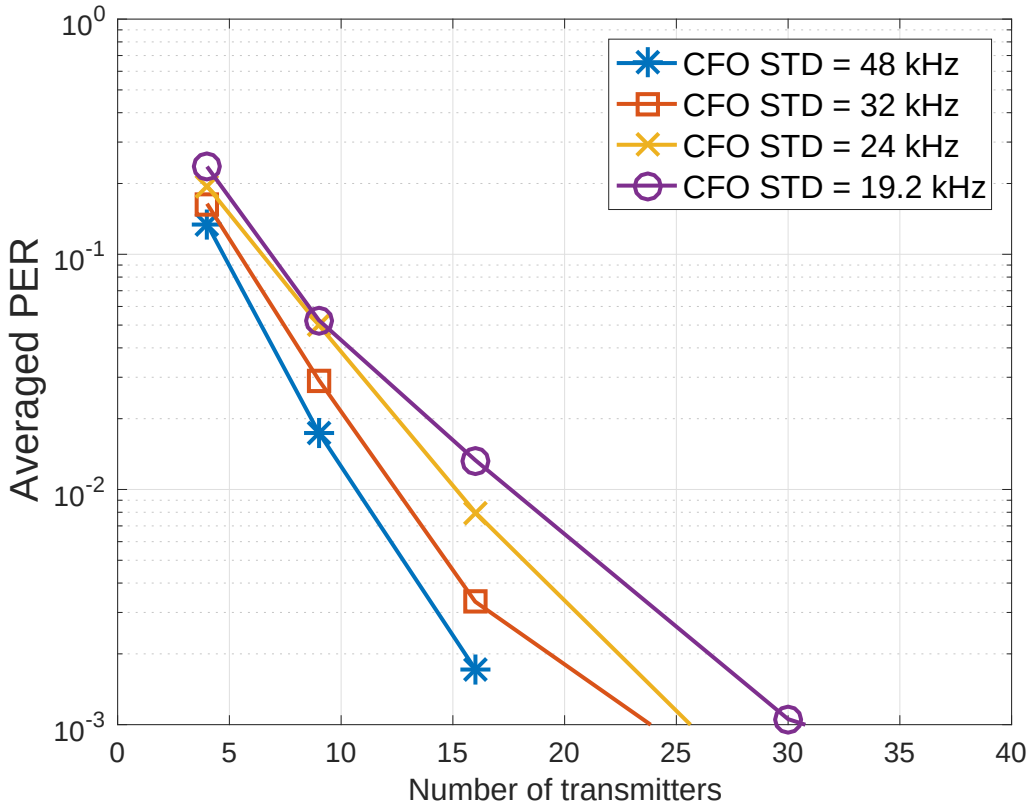

Fig. 5.15 The averaged PER simulation results for CT-DAS.

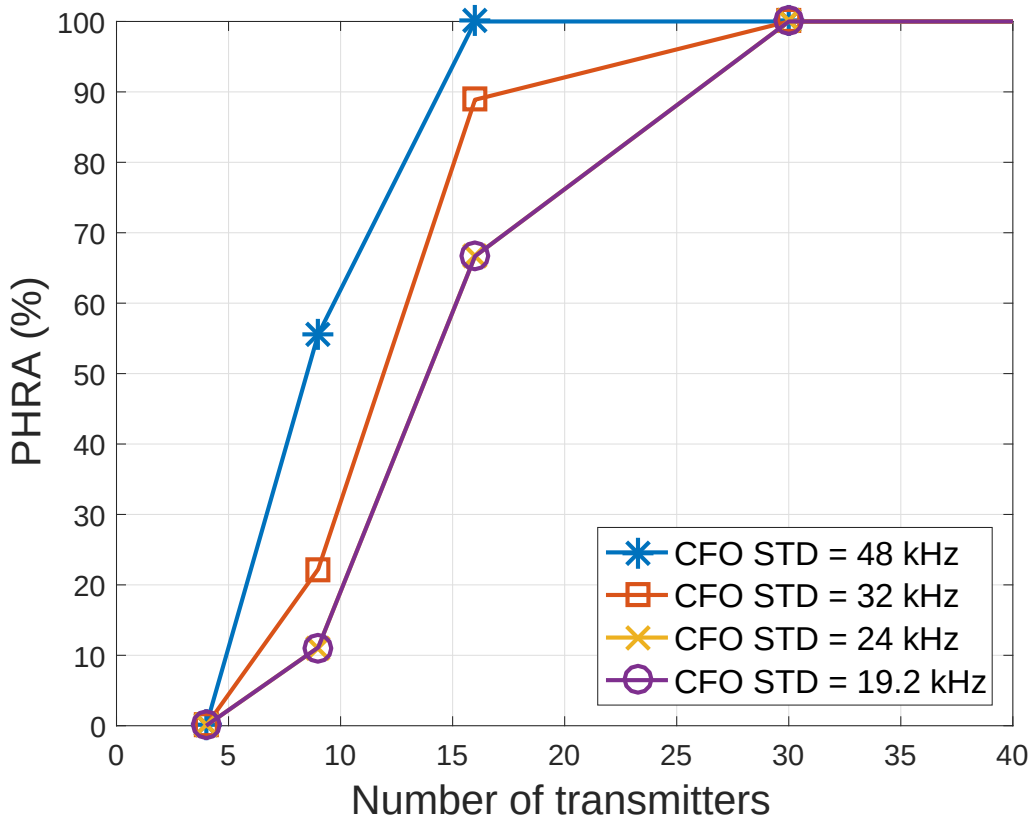

Fig. 5.16 The PHRA simulation results for CT-DAS.

5.3 Summary

In this chapter, we presented two novel CT-enabled applications using the insight obtained from the theoretical analysis and comprehensive evaluations in previous chapters.

First, we proposed to use the CT-based LoRa multi-hop network to realize the MBAN, which is a wireless network widely covering several buildings while consists of only low-power devices deployed indoor. As we have presented in the previous chapter, introducing timing offsets can improve the reliability of LoRa receiver under CT. With this insight, we proposed the offset-CT method, which introduces a uniformly distributed timing offset between the relayed packets while keeping the timing of each hop aligned by inserting a two-part delay. Moreover, we also conducted several proof-of-concept experiments. The experiment results showed that CT-LoRa already enjoys a very high PRR performance under the typical MBAN scenario. On the other hand, in the critical scenario where the nodes are put closely to each other, the offset-CT method significantly improves the PRR.

Second, we present an RRC system using the CT-based DAS system. As we have analyzed in previous sections, the CT is the most naive way to utilize the spatial diversity which requires barely any cooperation between the transmitters and therefore suitable for real-time application. To alleviate the degradation resulting from the beating effect, we proposed to deploy massive antennas and increase the randomness of CFO. To show the feasibility of the CT-DAS system, we conducted the extensive simulations which take the air propagation model measured in real factory environment into consideration, and the simulation results support our proposal.

Chapter 6

Conclusions and Future Works

6.1 Conclusions

In this work, we provided an extensive physical-layer investigation on the concurrent transmission for wireless networks by providing theoretical analyses on the channel characteristics of the CT signal and comprehensive evaluations of the physical-layer receiver performance under CT for various IoT-oriented standards. With the insights obtained from the analyses and evaluations, we further propose novel applications that are enabled by CT.

To under help people to better understand the CT effects, we first drew the analogy between the one-hop CT behavior and the wireless multi-path fading channel. With this analogy, the analysis technique developed in the wireless multi-path fading channel research can be applied to analyze the characteristics of CT. Specifically, we learned that the CFO and the resulted beating effect affect the receiver performance significantly. As a result, we concluded that a single carrier system with non-coherent modulation and error-correcting codes are the suitable systems for CT. Moreover, since it is the fading duration of the beating that really matters, we theoretically derive the AFD the beating under the assumption of Gaussian distributed CFO. Simulation results were given to prove the correctness of the derivation and to demonstrate the close correlation between AFD and the sensitivity loss caused by the beating. CFO measurement results were also given to estimate the actual AFD the sensitivity loss caused by CT. Finally, we showed the receiver performance becomes better with higher CFO deviations for the smaller AFD. On the other hand, we also showed that whether having more transmitters is beneficial or not is closely related to the degree of the timing offset.

Next, we evaluated the receiver performance under CT for three IoT-oriented standards. From our evaluations, we clarified that in the IEEE 802.15.4 system, the DSSS is the key for the receiver to survive the beating. On the other hand, the IEEE 802.15.4g system, which is not protected by any error correcting mechanism, performs poorly in CT links. Moreover, we showed that even with DSSS, the performance of the IEEE 802.15.4 receiver could still be significantly degraded if the fading duration of the beating is relatively longer than the DSSS symbol length. On the other hand, our evaluation for the LoRa system showed that LoRa is robust to CT. Specifically, due to the frequency-domain energy spreading effect enabled by the CFO, LoRa can survive the packet collisions with very high possibility even with small power offset. Moreover, we also demonstrated that,

by intentionally introduce the timing offset between the packets, the surviving probability could be further increased due to the time-domain energy spreading effect.

Finally, we proposed two novel CT-enabled applications. The first one is the MBAN, a network that consists of only low-power nodes while providing extensive indoor coverage over several buildings. Specifically, we proposed to use the sub-GHz LoRa as the physical-layer standard, and construct a multi-hop network based on the CT protocol. To realize a reliable CT-based LoRa multi-hop network, we further proposed the offset-CT method, which introduces a uniformly distributed timing offset between the relayed packets while keeping the timing of each hop aligned by inserting a two-part delay. Finally, we conducted several proof-of-concept experiments. The experiment results showed that CT-LoRa already enjoys a very high PRR performance under the typical MBAN scenario. On the other hand, in the critical scenario where the nodes are put closely to each other, the offset-CT method significantly improves the PRR. Secondly, we also proposed the CT-DAS that utilize CT to achieve real-time data transmission and use massive ubiquitously distributed antennas and large random frequency to reduce the risk of fading. The feasibility of the CT-DAS system shown by the extensive simulations which take the air propagation model measured in real factory environment into consideration.

6.2 Future works

The most important message conveyed in this thesis is simple - although CT is a simple and effective way to construct multi-hop network, CT is not universally applicable to any technology, and the success of CT relies on careful selections of many physical-layer parameters. While the other CT researchers often oversimplified the success of CT, we strive to mutually assess the pros and cons of CT and investigate the essential parts that allow the success of CT.

As an advocator of CT, we are deeply convinced that CT is an efficient technology in the network and MAC layer, and we would also like to carry forward the application of CT. As a future research direction, we are now studying the conditional for the success of CT from a more general viewpoint that takes not only error correction but the whole physical-layer design into consideration. Specifically, it is also interesting to investigate the optimal receiver architectures for CT. Moreover, we are seeking the opportunity to apply CT to more commonly available technologies, such as Bluetooth or WiFi.

Acknowledgments

This dissertation would never have materialized without the warm supports and helps from many individuals. Here, I would like to express my sincere gratitude to them.

First of all, my deepest gratitude goes to my supervisor, Professor Hiroyuki Morikawa. Ever since our first contact, Morikawa-sensei has been generously providing his kindest support for me in every possible way. Without his persistent guidances and support, I would not have been able to finish this degree. Also, I appreciate the committee members who spend time much precious time on examining my dissertation and gave constructive comments.

I sincerely appreciate Dr. Makoto Suzuki and Dr. Yoshiaki Narusue. You have offered invaluable supports and comments that greatly polished my research. I also appreciate Mr. Sotaro Ohara and Ms. Atsuko Kawakita for countless technical and administrative supports. My great thanks to all of my friends in Morikawa Laboratory who have welcomed me, assisted me, and delighted me. Those days that we had lunch or played table tennis together become my precious memory in MLAB. It is my honor to work and fight with you

Finally and most importantly, I would like to say my grateful thanks to my wife, my parents, my parents in law, and my two little kids. It is your unconditional love and sacrifice that support me to come this far. It has been a wonderful wonderful three years for me, and the better is yet to come!

廖 椿豪 *Liao, Chun-Hao*

June 2017

References

[1] B. Gates, N. Myhrvold, and P. Rinearson, *The Road Ahead*. Viking Books, 1995.

[2] "u-Japan 政策," 日本国総務省, 2009. [Online]. Available: http://www.soumu.go.jp/menu_seisaku/ict/u-japan/index.html

[3] "Internet of Things - An action plan for Europe," Commission of the European Communities, 2009.

[4] "White paper - mobile communications systems for 2020 and beyond," Association of Radio Industries and Businesses (ARIB) 2020 and Beyond Ad Hoc Group, Oct. 2014.

[5] A. Osseiran, "The 5G mobile and wireless communications system," in *Proceedings of ETSI Future Mobile Summit*, Nov. 2013.

[6] "Ericsson mobility report - On the pulse of the networked society," Ericsson, Nov. 2016.

[7] "The internet of everything - A $19 trillion opportunity," Cisco Consulting Services, 2014.

[8] "IEEE standard for information technology– local and metropolitan area networks– specific requirements– part 11: Wireless LAN medium access control (MAC)and physical layer (PHY) specifications amendment 5: Enhancements for higher throughput," *IEEE Std 802.11n-2009*, pp. 1–565, Oct. 2009.

[9] "ZigBee specification," ZigBee Alliance, Jan. 2008.

[10] "SmartMesh." [Online]. Available: http://www.linear.com/dust_networks/

[11] "The Thread Group." [Online]. Available: http://threadgroup.org/

[12] "IEEE standard for local and metropolitan area networks–Part 15.4: Low-rate wireless personal area networks (LR-WPANs)," *IEEE Std 802.15.4-2011*, pp. 1–314, Sept. 2011.

[13] P. Dutta, R. Musaloiu-E, I. Stoica, and A. Terzis, "Wireless ACK collisions not considered harmful," in *Proceedings of the 7th Workshop on Hot Topics in Networks (HotNets)*, Oct. 2008.

[14] F. Ferrari, M. Zimmerling, L. Thiele, and O. Saukh, "Efficient network flooding and time synchronization with Glossy," in *Proceedings of the 10th ACM/IEEE International Conference on Information Processing in Sensor Networks (IPSN)*, pp. 73 –84, Apr. 2011.

[15] Y. Wang, Y. He, X. Mao, Y. Liu, and X.-Y. Li, "Exploiting constructive interference for scalable flooding in wireless networks," *IEEE/ACM Transactions on Networking*, vol. 21, no. 6, pp. 1880–1889, Dec. 2013.

[16] V. S. Rao, M. Koppal, R. V. Prasad, T. V. Prabhakar, C. Sarkar, and I. Niemegeers, "Murphy loves CI: Unfolding and improving constructive interference in WSNs," in *Proceedings of IEEE International Conference on Computer Communications 2016 (INFOCOM)*, pp. 1–9, Apr. 2016.

[17] M. Brachmann, O. Landsiedel, and S. Santini, "Concurrent transmissions for communication protocols in the internet of things," in *Proceedings of 2016 IEEE 41st Conference on Local Computer Networks (LCN)*, Nov. 2016.

[18] M. Doddavenkatappa, M. C. Chan, and B. Leong, "Splash: Fast data dissemination with constructive interference in wireless sensor networks," in *Proceedings of 10th USENIX Symposium on Networked Systems Design and Implementation (NSDI)*, pp. 269–282, Apr. 2013.

[19] M. Doddavenkatappa and M. C. Chan, "P^3: A practical packet pipeline using synchronous transmissions for wireless sensor networks," in *Proceedings of the 13th International Symposium on Information Processing in Sensor Networks (IPSN)*, pp. 203–214, Apr. 2014.

[20] F. Ferrari, M. Zimmerling, L. Mottola, and L. Thiele, "Low-power wireless bus," in *Proceedings of the 10th ACM Conference on Embedded Network Sensor Systems (SenSys)*, pp. 1–14, Nov. 2012.

[21] M. Suzuki, S. Ohara, K. Jinno, C. H. Liao, and H. Morikawa, "Wireless-transparent

sensing," in *Proceedings of 2017 International Conference on Embedded Wireless Systems and Networks (EWSN)*, pp. 66–77, Feb. 2017.

[22] P. Dutta, S. Dawson-Haggerty, Y. Chen, C.-J. M. Liang, and A. Terzis, "Design and evaluation of a versatile and efficient receiver-initiated link layer for low-power wireless," in *Proceedings of the 8th ACM Conference on Embedded Networked Sensor Systems (SenSys)*, pp. 1–14, Nov. 2010.

[23] J. Lu and K. Whitehouse, "Flash flooding: Exploiting the capture effect for rapid flooding in wireless sensor networks," in *Proceedings of IEEE International Conference on Computer Communications 2009 (INFOCOM)*, pp. 2491–2499, Apr. 2009.

[24] D. Yuan and M. Hollick, "Let's talk together: Understanding concurrent transmission in wireless sensor networks," in *Proceedings of 38th Annual IEEE Conference on Local Computer Networks (LCN)*, pp. 219–227, Oct. 2013.

[25] D. Yuan, M. Riecker, and M. Hollick, "Making Glossy networks sparkle: Exploiting concurrent transmissions for energy efficient, reliable, ultra-low latency communication in wireless control networks," in *Proceedings of the 11th European Conference on Wireless Sensor Networks (EWSN)*, pp. 133–149, Feb. 2014.

[26] H. Rahul, H. Hassanieh, and D. Katabi, "SourceSync: A distributed wireless architecture for exploiting sender diversity," in *Proceedings of the ACM SIGCOMM 2010 Conference (SIGCOMM)*, pp. 171–182. New York, NY, USA: ACM, Aug. 2010.

[27] D. Carlson, M. Chang, A. Terzis, Y. Chen, and O. Gnawali, "Forwarder selection in multi-transmitter networks," in *Proceedings of 2013 IEEE International Conference on Distributed Computing in Sensor Systems (DCOSS)*, pp. 1–10, May 2013.

[28] K. Leentvaar and J. Flint, "The capture effect in FM receivers," *IEEE Transactions on Communications*, vol. 24, no. 5, pp. 531–539, May 1976.

[29] D. Son, B. Krishnamachari, and J. Heidemann, "Experimental study of concurrent transmission in wireless sensor networks," in *Proceedings of the 4th ACM Conference on Embedded Networked Sensor Systems (SenSys)*, pp. 237–250, Nov. 2006.

[30] C. Gezer, C. Buratti, and R. Verdone, "Capture effect in IEEE 802.15.4 networks: Modeling and experimentation," in *Proceedings of IEEE 5th International Symposium on Wireless Pervasive Computing (ISWPC) 2010*, pp. 204–209, May 2010.

[31] M. Wilhelm, V. Lenders, and J. Schmitt, "On the reception of concurrent transmissions in wireless sensor networks," *IEEE Transactions on Wireless Communications*, vol. 13, no. 12, pp. 6756–6767, Dec. 2014.

[32] B. Kempke, P. Pannuto, B. Campbell, and P. Dutta, "SurePoint: Exploiting ultra wideband flooding and diversity to provide robust, scalable, high-fidelity indoor localization," in *Proceedings of the 14th ACM Conference on Embedded Network Sensor Systems (SenSys)*, pp. 137–149, Nov. 2016.

[33] G. Gray, "The simulcasting technique: An approach to total-area radio coverage," *IEEE Transactions on Vehicular Technology*, vol. 28, no. 2, pp. 117–125, May 1979.

[34] A. Sendonaris, E. Erkip, and B. Aazhang, "User cooperation diversity. part I. system description," *IEEE Transactions on Communications*, vol. 51, no. 11, pp. 1927–1938, Nov. 2003.

[35] T. Sexton, S. Souissi, and C. Hill, "Performance of high data rate paging in simulcast," in *Proceedings of Wireless Communications Conference*, pp. 43–49, Aug. 1997.

[36] R. Petrovic and S. Filipovic, "Error floors of digital FM in simulcast and rayleigh fading," *IEEE Transactions on Vehicular Technology*, vol. 47, no. 3, pp. 954–960, Aug. 1998.

[37] S. Souissi, S. Sek, and H. Xie, "The effect of frequency offsets on the performance of FLEX(R) simulcast systems," in *Proceedings of 1999 IEEE 49th Vehicular Technology Conference (VTC)*, vol. 3, pp. 2348–2352 vol.3, July 1999.

[38] "Multi-transmitter radio systems using quasisynchronous (simulcast) transmission for analogue speech," ITU-R Recommendation M.1077, 1994.

[39] L. Godara, "Application of antenna arrays to mobile communications. II. beamforming and direction-of-arrival considerations," *Proceedings of the IEEE*, vol. 85, no. 8, pp. 1195–1245, Aug. 1997.

[40] S. Alamouti, "A simple transmit diversity technique for wireless communications," *IEEE Journal on Selected Areas in Communications*, vol. 16, no. 8, pp. 1451–1458, Oct. 1998.

[41] A. Bletsas, A. Khisti, D. P. Reed, and A. Lippman, "A simple cooperative diver-

sity method based on network path selection," *IEEE Journal on Selected Areas in Communications*, vol. 24, no. 3, pp. 659–672, Mar. 2006.

[42] M. Bossert, A. Huebner, F. S. H. Haas, and E. Costa, "On cyclic delay diversity in OFDM based transmission schemes," in *Proceedings of the 7th International OFDM-Workshop (InOWo)*, pp. 1–5, Sept. 2002.

[43] Y. Fujino, S. Kuwano, S. Ohmori, T. Fujita, and S. Yoshino, "Cell range extension techniques for wide-area ubiquitous network," in *Proceedings of 2011 10th International Symposium on Autonomous Decentralized Systems (ISADS)*, pp. 35–40, Mar. 2011.

[44] J. N. Laneman and G. W. Wornell, "Distributed space-time coded protocols for exploiting cooperative diversity in wireless networks," in *Proceedings of IEEE 2002 Global Telecommunications Conference (GLOBECOM)*, vol. 1, pp. 77–81 vol.1, Nov. 2002.

[45] T. Hattori and K. Hirade, "Multitransmitter digital signal transmission by using offset frequency strategy in a land-mobile telephone system," *IEEE Transactions on Vehicular Technology*, vol. 27, no. 4, pp. 231–238, Nov. 1978.

[46] Y. Yamashita, Y. Tashiro, M. Suzuki, Y. Hase, and H. Morikawa, "Understanding the effects of carrier frequency difference in concurrent transmission," in *Proceedings of the 11th ACM Conference on Embedded Networked Sensor Systems (SenSys)*, pp. 86:1–86:2, Nov. 2013.

[47] C. Noda, C. M. Perez-Penichet, B. Seeber, M. Zennaro, M. Alves, and A. Moreira, "On the scalability of constructive interference in low-power wireless networks," in *Proceedings of 12th European Conference on Wireless Sensor Networks (EWSN)*, pp. 250–257, Feb. 2015.

[48] "Guidelines for evaluation of radio transmission technologies for IMT-2000," ITU-R Recommendation M.1225, 1997.

[49] G. Caire, G. Taricco, and E. Biglieri, "Bit-interleaved coded modulation," *IEEE Transactions on Information Theory*, vol. 44, no. 3, pp. 927–946, May 1998.

[50] J. G. Proakis, *Digital Communications*. McGraw-Hill, 1995.

[51] S. O. Rice, "Mathematical analysis of random noise," *Bell System Technical Journal*, vol. 23, no. 3, pp. 282–332, 1944.

[52] Texas Instruments, "CC2420 datasheet," 2007.

[53] ——, "CC1120 datasheet," 2015.

[54] M. Simon and C. Wang, "Differential versus limiter–discriminator detection of narrow-band FM," *IEEE Transactions on Communications*, vol. 31, no. 11, pp. 1227–1234, Nov. 1983.

[55] S. Gronemeyer and A. McBride, "MSK and offset QPSK modulation," *IEEE Transactions on Communications*, vol. 24, no. 8, pp. 809–820, Aug. 1976.

[56] "IEEE standard for local and metropolitan area networks–part 15.4: Low-rate wireless personal area networks (LR-WPANs) amendment 3: Physical layer (PHY) specifications for low-data-rate, wireless, smart metering utility networks," *IEEE Std 802.15.4g-2012*, pp. 1–252, Apr. 2012.

[57] SEMTECH, "LoRa$^{\text{tm}}$ modulation basics," May 2015.

[58] J. Petajajarvi, K. Mikhaylov, A. Roivainen, T. Hanninen, and M. Pettissalo, "On the coverage of LPWANs: Range evaluation and channel attenuation model for LoRa technology," in *Proceedings of 2015 14th International Conference on ITS Telecommunications (ITST)*, pp. 55–59, Dec. 2015.

[59] J. Petajajarvi, K. Mikhaylov, M. Hamalainen, and J. Iinatti, "Evaluation of lora lpwan technology for remote health and wellbeing monitoring," in *Proceedings of 2016 10th International Symposium on Medical Information and Communication Technology (ISMICT)*, pp. 1–5, Mar. 2016.

[60] J. Petajajarvi, K. Mikhaylov, R. Yasmin, M. Hamalainen, and J. Iinatti, "Evaluation of LoRa LPWAN technology for indoor remote health and wellbeing monitoring," *International Journal of Wireless Information Networks*, vol. 24, no. 2, pp. 153–165, 2017.

[61] "What is lora." [Online]. Available: https://www.link-labs.com/blog/what-is-lora

[62] "Decodinglora." [Online]. Available: https://revspace.nl/DecodingLora

[63] M. Knight and B. Seeber, "Decoding LoRa: Realizing a modern LPWAN with SDR," in *Proceedings of the GNU Radio Conference*, vol. 1, no. 1, Sept. 2016.

[64] Semtech, "SX1272/73 - 860 mhz to 1020 mhz low power long range transceiver," 2015. [Online]. Available: http://www.semtech.com/images/datasheet/sx1272.pdf

[65] STMicroelectronics, "STM32L151x6/8/B - ultra-low-power 32-bit MCU ARM-based Cortex-M3, 128KB Flash, 16KB SRAM, 4KB EEPROM, LCD, USB, ADC, DAC," 2016.

[66] D. Minoli, K. Sohraby, and B. Occhiogrosso, "IoT considerations, requirements, and architectures for smart buildings - energy optimization and next-generation building management systems," *IEEE Internet of Things Journal*, vol. 4, no. 1, pp. 269–283, Feb. 2017.

[67] B. Holfeld, D. Wieruch, T. Wirth, L. Thiele, S. A. Ashraf, J. Huschke, I. Aktas, and J. Ansari, "Wireless communication for factory automation: an opportunity for LTE and 5G systems," *IEEE Communications Magazine*, vol. 54, no. 6, pp. 36–43, June 2016.

[68] "The tactile Internet," ITU-T Technology Watch Report, Aug. 2014.

[69] A. Gorokhov, "Antenna selection algorithms for MEA transmission systems," in *Proceedings of 2002 IEEE International Conference on Acoustics, Speech, and Signal Processing (ICASSP)*, vol. 3, pp. III–2857–III–2860, May 2002.

[70] M. Gharavi-Alkhansari and A. B. Gershman, "Fast antenna subset selection in wireless MIMO systems," in *Proceedings of 2003 IEEE International Conference on Acoustics, Speech, and Signal Processing (ICASSP)*, vol. 5, pp. V–57–60 vol.5, Apr. 2003.

[71] S. Jin, X. Li, and X. Gao, "Statistical transmit antenna selection for correlated Rayleigh fading MIMO channels," in *Proceedings of IEEE 63rd Vehicular Technology Conference (VTC-Spring)*, vol. 4, pp. 1665–1669, May 2006.

[72] H. Zhang and H. Dai, "Fast transmit antenna selection algorithms for MIMO systems with fading correlation," in *Proceedings of IEEE 60th Vehicular Technology Conference (VTC-Fall)*, vol. 3, pp. 1638–1642 Vol. 3, Sept. 2004.

[73] H.-C. Yang and M. S. Alouini, "Performance analysis of multibranch switched diversity systems," *IEEE Transactions on Communications*, vol. 51, no. 5, pp. 782–794, May 2003.

[74] B. Fang, Z. Qian, W. Shao, and W. Zhong, "RAISE: A new fast transmit antenna

selection algorithm for massive MIMO systems," *Wireless Personal Communications*, vol. 80, no. 3, pp. 1147–1157, 2015.

[75] V. Tarokh, N. Seshadri, and A. R. Calderbank, "Space-time codes for high data rate wireless communication: performance criterion and code construction," *IEEE Transactions on Information Theory*, vol. 44, no. 2, pp. 744–765, Mar. 1998.

[76] V. Tarokh, H. Jafarkhani, and A. R. Calderbank, "Space-time block codes from orthogonal designs," *IEEE Transactions on Information Theory*, vol. 45, no. 5, pp. 1456–1467, July 1999.

[77] T. Rappaport, *Wireless Communications: Principles and Practice*, 2nd ed. Upper Saddle River, NJ, USA: Prentice Hall PTR, 2001.

[78] E. Tanghe, W. Joseph, L. Verloock, L. Martens, H. Capoen, K. V. Herwegen, and W. Vantomme, "The industrial indoor channel: large-scale and temporal fading at 900, 2400, and 5200 mhz," *IEEE Transactions on Wireless Communications*, vol. 7, no. 7, pp. 2740–2751, July 2008.

Publications

学術雑誌等 (査読あり)

[1] C.-H. Liao, M. Suzuki, and H. Morikawa, "Receiver Performance Evaluation and Fading Duration Analysis for Concurrent Transmission," *IEICE Transactions on Communications*, to be published.

[2] C.-H. Liao, G. Zhu, D. Kuwabara, M. Suzuki, and H. Morikawa, "Multi-hop LoRa Networks Enabled by Concurrent Transmission," submitted for publication.

[3] T. Sakdejayont, C.-H. Liao, M. Suzuki, and H. Morikawa, "Subcarrier-Selectable Short Preamble for OFDM Channel Estimation in Real-Time Wireless Control Systems," *IEICE Transactions on Fundamentals of Electronics, Communications and Computer Sciences*, to be published.Sep

国際会議

口頭発表（査読あり）

[4] C.-H. Liao, Y. Katsumata, M. Suzuki, and H. Morikawa, "Revisiting the So-Called Constructive Interference in Concurrent Transmission," in *Proceedings of IEEE 41st Conference on Local Computer Networks (LCN)*, Oct. 2016, pp. 280-288.

[5] K. Chutisemachai, T. Sakdejayont, C.-H. Liao, M. Suzuki and H. Morikawa, "Distributed Antenna System using Concurrent Transmission for Wireless Automation System," in *Proceedings of IEEE 2017 IEEE 86th Vehicular Technology Conference (VTC-Full)*, Sept. 2017.

[6] M. Suzuki, C.-H. Liao, S. Ohara, K. Jinno, and H. Morikawa, "Wireless-Transparent Sensing," in *Proceedings of 2017 International Conference on Embedded Wireless Systems and Networks (EWSN)*, Feb. 2017, pp. 66-77.

[7] T. Sakdejayont, C.-H. Liao, M. Suzuki, and H. Morikawa, "Making preamble shorter in OFDM real-time wireless control systems," in *Proceedings of the 22nd Asia-Pacific Conference on Communications (APCC)*, Aug. 2016, pp. 26-31.

[8] T. Morohashi, C.-H. Liao, A. Koizuka, M. Suzuki, and H. Morikawa, "A high-performance RACH detection scheme for random access overload in LTE-Advanced," in *Proceedings of 2015 IEEE Conference on Standards for Communications and Networking (CSCN)*, Oct. 2015, pp. 1-6.

[9] C.-H. Liao and H. Morikawa, " Latticing the Interference: Non-linear Pre-coding for Non-Orthogonal Multiple Access in Downlink Multi-User MIMO System," in *Proceedings of IEEE 26th Annual International Symposium on Personal, Indoor, and Mobile Radio Communications (PIMRC)*, Aug. 2015, pp. 710-714.

[10] T. Morohashi, C.-H. Liao, A. Koizuka, M. Suzuki, and H. Morikawa, "Inter-user interference cancellation improvements for LTE-Advanced random access detector using dynamic thresholding mechanism," in *Proceedings of the 6th International Conference on Information and Communication Technology Convergence (ICTC)*, Oct. 2015, pp. 206-208.

ポスター，デモ発表，コンテスト（査読あり）

[11] C.-H. Liao, M. Suzuki, and H. Morikawa, "Toward Robust Concurrent Transmission for sub-GHz Non-DSSS Communication: Poster Abstract," in *Proceedings of the 14th ACM Conference on Embedded Networked Sensor Systems (SenSys)*, Nov. 2016, pp. 354-355.

[12] T. Sakdejayont, C.-H. Liao, M. Suzuki, and H. Morikawa, "Beating the Beat: RSSI-Based Packet Combining in Concurrent Transmission Sensor Networks: Poster Abstract," in *Proceedings of the 14th ACM Conference on Embedded Networked Sensor Systems (SenSys)*, Nov. 2016, pp. 356-357.

[13] M. Suzuki, C.-H. Liao, Y.i Katsumata, K. Jinno, and H. Morikawa, "Competition: Is Concurrent Transmission Flooding a Good Idea for Random Traffic?, "in *Proceedings of 2016 International Conference on Embedded Wireless Systems and Networks*, Nov. 2016, pp. 293-294.

[14] K. Awaki, C.-H. Liao, M. Suzuki, and H. Morikawa, "Speaker-less Sound-based 3D Localization with Centimeter-level Accuracy," in *Proceedings of the 2016 ACM International Joint Conference on Pervasive and Ubiquitous Computing (UbiComp)*, Sept. 2016, pp. 249-252.

研究会

[15] Y. Takeuchi, C.-H. Liao, M. Suzuki, and H. Morikawa, "Demodulation Method of LPWA (Chirp Spread Spectrum) Signals and Multi-hop Transmisson Method" , *IEICE Technical Report on Radio Communication System (RCS)*, vol. 117, no. 132, RCS2017-138, July 2017, pp. 233-238.

[16] G. Zhu, C.-H. Liao, M. Suzuki, Y. Narusue, and H. Morikawa, "Investigating the LoRa Receiver Performance under Mutual Interference," *IEICE Technical Report on Radio Communication System (RCS)*, vol. 117, no. 132, RCS2017-110, July 2017, pp. 103-108.

[17] C.-H. Liao, G. Zhu, D. Kuwabara, S. Ohara, M. Suzuki, and H. Morikawa, "Evaluating the Sub-GHz LoRa Receiver Performance under Synchronized Packet Collisions," *IEICE Technical Report on Radio Communication System (RCS)*, vol. 117, no. 11, RCS2017-27, Apr. 2016, pp. 143-148.

[18] C.-H. Liao, M. Suzuki, and H. Morikawa, "Level Crossing Rate and Average Fading Duration of Beating Signals under Concurrent Transmission," *IEICE Technical Reporton Radio Communication System (RCS)*, vol. 116, no. 383, RCS2016-222, Dec. 2016, pp. 75-80.

[19] T. Sakdejayont, C.-H. Liao, M. Suzuki, and Hiroyuki Morikawa, "Evaluation of Packet Combining using RSSI for Reliable Reception of Concurrent Transmission," *IEICE Technical Report on Radio Communication System (RCS)*, vol. 116, no. 383, RCS2016-223, Dec. 2016, pp. 81-86.

[20] C.-H. Liao, M. Suzuki, and H. Morikawa, "Simulating and Emulating the IEEE 802.15.4 Receiver Performance under Concurrent Transmission," *IEICE Technical Report on Radio Communication System (RCS)*, vol. 115, no. 472, RCS2015-382, Mar. 2016, pp. 285-290.

[21] T. Morohashi, C.-H. Liao, A. Koizuka, M. Suzuki, and H. Morikawa, "An Evaluation of LTE-Advanced Random Access with Non-orthogonal Preamble Interference Cancellation in M2M Environment," *IEICE Technical Report on Radio Communication System (RCS)*, vol. 115, no. 160, RCS2015-131, July 2015, pp. 181-186.

[22] T. Sakdejayont, C.-H. Liao, and H. Morikawa, " Evaluation of Subcarrier-Selected Short Preamble for OFDM Wireless Control Systems," *IEICE Technical Report on Radio Communication System (RCS)*, vol. 115, no. 160, RCS2015-130, July 2015, pp. 175-180.

[23] C.-H. Liao and H. Morikawa, "Non-linear Pre-coding for Non-Orthogonal Multiple Access in MU-MIMO System with Modulo-based Interference Cancellation," *IEICE Technical Report on Radio Communication System (RCS)*, vol. 114, no. 490, RCS2014-365, Mar. 2015, pp. 381-386.

全国大会

[24] G. Zhu, C.-H. Liao, T. Sakdejayont, Y. Narusue, and H. Morikawa "Enabling the Fast Flooding over Multi-hop LoRa Network using SF-pipeline," in *Proceedings 2017 IEICE Society Conference*, 12-15 Sept. 2017.

[25] C.-H. Liao, M. Suzuki, and H. Morikawa, "Evaluations of the Applicability of Concurrent Transmission on sub-GHz LoRa Receivers," in *Proceedings 2017 IEICE General Conference*, B-5-128, 22-25 Mar. 2017.

[26] C.-H. Liao, M. Suzuki, and H. Morikawa, "Evaluations of sub-GHz IEEE 802.15.4g Receiver Performance under Concurrent Transmission," in *Proceedings of 2016 IEICE Society Conference*, B-5-97, 20-23 Sept. 2016.

[27] K. Chutisemachai, T. Sakdejayont, C.-H. Liao, M. Suzuki, and H. Morikawa, "Distributed Antenna System Using Concurrent Transmission with Loose Carrier Frequency Control in Wireless Factory," in *Proceedings of 2016 IEICE Society Conference*, B-5-99, 20-23 Sept. 2016.

[28] C.-H. Liao, Y. Katsumata, T. Sakdejayont, R. Nakao, M. Suzuki, and H. Morikawa, "Evaluation of 802.15.4 Receiver Performance under Concurrent Transmission," in *Proceedings of 2016 IEICE General Conference*, B-5-84, 15-18 Mar. 2016.

[29] T. Sakdejayont, C.-H. Liao, M. Suzuki, and H. Morikawa, “Performance Evaluation of Real-Time Wireless Control System using Shortened Preambles,” in *Proceedings of 2016 IEICE General Conference*, B-5-151, 15-18 Mar. 2016.

[30] 勝間田 優樹, 廖 椿豪, 田代 諭拡, 鈴木 誠, 森川 博之, “同時送信における IEEE 802.15.4 のパケット到達率の実験評価,” in *Proceedings of 2016 IEICE General Conference*, B-5-85, 15-18 Mar. 2016.

[31] 中尾 亮太, Theerat Sakdejayont, 廖 椿豪, 鈴木 誠, 森川 博之, “同時送信技術におけるビート干渉抑制のための RSSI を用いたパケット合成手法”, in *Proceedings of 2016 IEICE General Conference*, B-5-155, 15-18 Mar. 2016.

[32] 粟木 一輝, 田代 諭拡, 恋塚 葵, 廖 椿豪, 鈴木 誠, 森川 博之, “可聴音を用いたセンサノードの高精度測位手法の省資源実装,” in *Proceedings of 2016 IEICE General Conference*, B-18-1, 15-18 Mar. 2016.

[33] T. Morohashi, C.-H. Liao, A. Koizuka, M. Suzuki, and H. Morikawa, ”On Improving the Inter-User Interference Cancellation for LTE RACH Preamble Detection in M2M Environment,” in *Proceedings of 2015 IEICE Society Conference*, B-5-4, 8-11 Sept. 2015.

[34] T. Sakdejayont, C.-H. Liao, M. Suzuki, and H. Morikawa, “Adaptive Channel Estimation for OFDM Wireless Control Systems using Subcarrier-Selected Short Preambles,” in *Proceedings of 2015 IEICE Society Conference*, B-5-116, 8-11 Sept. 2015.

[35] C.-H. Liao and H. Morikawa, “Non-linear Pre-coding for Non-Orthogonal Multiple Access in Downlink Multi-User MIMO System, ” in *Proceedings of 2015 IEICE General Conference*, B-5-83, 10-13 Mar. 2015.

[36] T. Sakdejayont, C.-H. Liao, and H. Morikawa, ” Short OFDM Preamble for Channel Estimation in Real-Time Wireless Control Systems,” in *Proceedings of 2015 IEICE General Conference*, B-5-156, 10-13 Mar. 2015.

特許出願

[37] 森川 博之, 廖 椿豪, 鈴木 誠, 大原 壮太郎, 朱 桂兵, ”通信装置及びプログラム” 出願予定 , July 2017.

[38] 竹内 嘉彦, 廖 椿豪, 鈴木 誠, 森川 博之, ”復調器及び復調方法,” 出願予定 , July 2017.

[39] 竹内 嘉彦, 廖 椿豪, 鈴木 誠, 森川 博之, ”通信システム及び通信方法,” 出願予定 , July 2017.